Harmonic Mitigation of Biomass-Fired Combined Heat and Power Plant

- In Collaboration with Aalborg Energie Technik A/S -

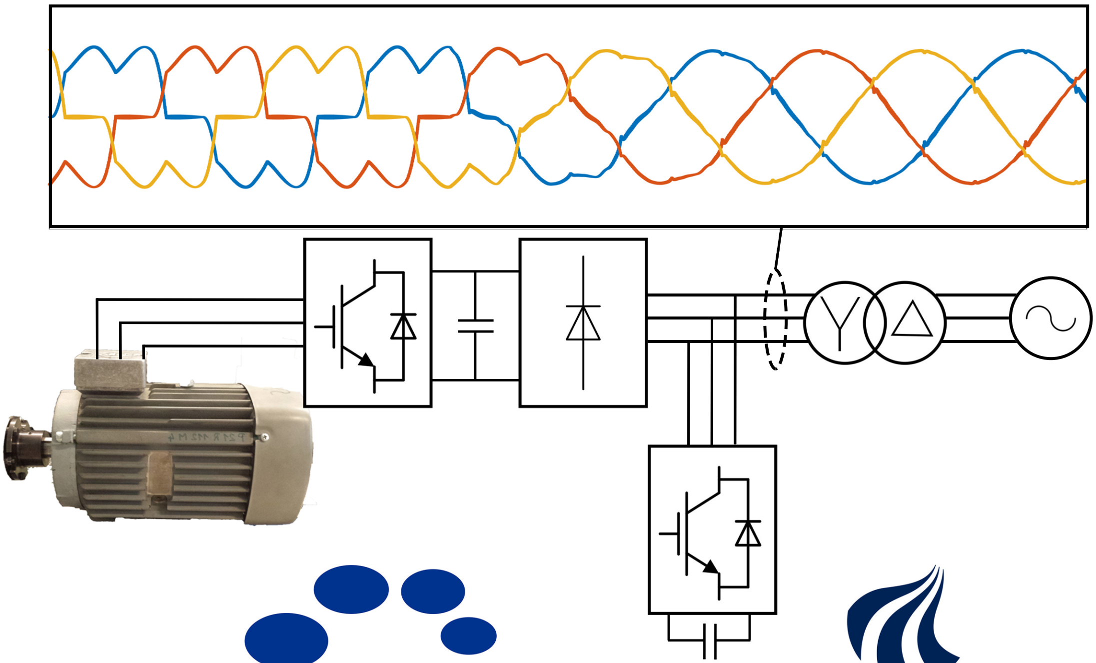

AALBORG UNIVERSITY
STUDENT REPORT

M.Sc. Thesis
by
Søren Lund Lorenzen & Alex Buus Nielsen

Aalborg University
Department of Energy Technology

Title:	Harmonic Mitigation of Biomass-Fired Combined Heat and Power Plant
Semester:	MSc. 4. Semester
Project period:	01.02.2017 to 01.06.2017
ECTS:	30
Supervisor:	Professor Frede Blaabjerg
Company Collaboration:	Aalborg Energie Technik
Company Contact:	Morten Sørensen
Project group:	PED4-1042

Alex Buus Nielsen

Søren Lund Lorenzen

No. of pages: 116
No. of appendices : 2
Finished: 01-06-2017

Synopsis:

The aim of this master thesis was to investigate the benefits of implementing an active filter in a biomass-fired power plant, in collaboration with Aalborg Energie Technik A/S.

For the active power filter different harmonic controllers were investigated where the repetitive controller was shown by experiments to achieve the best harmonic mitigation performance with a grid current THD of 6.4 %, however the PR controller was more flexible and had a lower settling time.

The benefits of installing an APF is reduced current THD losses at the PCC, reduced power ratings if reactive power compensation is employed, and a centralised solution is possible. To get a fast estimation of the required rating of an APF for a desired performance, sizing equations and the Danfoss harmonic toolbox was used which corresponded well to simulations, thus gives a good guideline when designing an APF.

By accepting the request from the fellow student who uploads the study group's project report in Digital Exam System, you confirm that all group members have participated in the project work, and thereby all members are collectively liable for the contents of the report. Furthermore, all group members confirm that the report does not include plagiarism.

Preface

This master thesis is the result of a collaboration between two "Power Electronics and Drives" students from the Department of Electrical Energy Technology at Aalborg University and Aalborg Energie Technike A/S (AET). AET is a company designing and building biomass-fire combined heat and power plants. This master thesis investigates the benefits of implementing an active power filter in a power plant through case study and experimental work.

The group would like to address a recognition to the following persons:

- Frede Blaabjerg, Professor at AAU for excellent supervisory support.
- Morten Sørensen, Electrical Engineer at Aalborg Energie Technik A/S, for technical assistance, data sheets, and support.
- Dapeng Lu, Ph.d. student at AAU for laboratory assistance.
- Yongheng Yang, Assistant Professor at AAU for correcting and commenting on the report.

Reading instructions

All sections, tables, equations and figures, are in chronological order according to the chapter number. Hence the first section, figure, table, or equation in chapter 4 is numbered 4.1, the second 4.2 and so on. Each figure and table contains a caption with a description of the figure or table.

The reference system used in this report is the IEEE Method. The IEEE Method show the references with the label [Number of Reference]. If the reference is placed before a full stop, the reference is for the specific sentence. If the reference is placed after a full stop, the reference is for the entire section. The complete list with the references is placed in the section called Bibliography, where the Author, Title and Year are shown. Internet websites are labelled as the other references, but they will also include the [URL].

The following software has been used in this project:

- MATLAB - Design of controllers and data processing
- Simulink - Simulation of controllers
- PLECS - Simulations of electrical circuits and controllers
- dSPACE - Control of laboratory setup

Resumé

Dette projekt er udarbejdet i samarbejde med Aalborg Energie Technik A/S (AET). AET er et dansk firma der designer og bygger biomasse kraftværker, der både kan levere fjernvarme og elektrisk energi. I projektet tages der udgangspunkt i biomasse kraftværket "Helius CoRDe" placeret i Skotland, der omdanner restproduktet af whiskey produktion og træflis blandt andet, til fjernvarme og el. For at drive kraftværkets mange pumper og blæsere der bruges til varme og el produktionen, bruges elektriske motorer som er styret ved hjælp af ensrettere og frekvensomformere. I kraftværket er den simple og relativt billige seks puls ensretter brugt. Ulempen ved brugen af denne type ensretter er at strømmen på tre-fase siden vil have et højt harmonisk indhold. Et højt harmonisk indhold i strømmen kan have en del ulemper f.eks. tab i ledninger og transformer, interferens i mellem komponenter og kontrol systemer, og det harmoniske indhold i spændingen kan stige. AET har tidligere undersøgt muligheden for at installere et aktive filter, som er en frekvensomformer parallel koblet til forsyningstransformeren hvor det der igennem er muligt at reducere det harmoiske indhold i strømmen. Fordelene for AET og kunden ved at installere et aktivt filter er: det kan installeres som en central løsning og ikke ved hver motor udgang, reaktiv effekt kan kompenseres og forbedre effekt kvaliteten, tabene i transformer og ledninger kan reduceres og derfor muligvis spare penge.

Udover at undersøge fordelene ved at installere et aktivt filter, undersøges forskellige kontrol løsninger til det aktive filter også. Det generelle kontrolsystem består af en ydre DC spændings controller og en indre strøm controller. I projektet sammenlignes og eksperimentielt verificeres to forskellige strøm-controllere til at reducere det harmoniske indhold i strømmen. Igennem simuleringer og eksperimentelt arbejde vises operationen af de forskellige controllere, og det konkluderes at den repetitive controller har en bedre harmonisk ophævelse end PR controlleren. PR controlleren foretrækkes dog da den har en større fleksibilitet.

For fremtidigt design af kraftværker for AET, er der lavet en analyse af hvordan man hurtigt kan få et estimat af hvilken størrelse aktivt filter der skal bruges, hvis man kender den ønskede ydelse i form af ønsket power factor og harmonisk indhold. Analysen konkluderer at man ved hjælp af simple ligninger og ved brugen af et Danfoss program, der beregner motor og aktive filter størrelser, hurtigt og simpelt kan få et godt estimat af den krævede størrelse på det aktive filter. Udover det vises det, i følge simuleringer og eksperimentielt arbejde, at man kan spare i omegnen af 5-9 % effekt for mellemspændings transformeren og tavlen ved brugen af et aktivt filter.

Nomenclature

Nomenclature

Symbol	Specification	Unit
S	Power	VA
Q	Reactive Power	VAr
P	Active Power	W
D	Distortion Power	VA
V	Voltage	V
I	Current	A
Z	Impedance	Ω
X	Reactance	Ω
R	Electrical resistance	Ω
L	Inductance	H
C	Capacitance	F
$cos(\phi)$	Power factor	-
ϕ_m	Phase margin	deg
ω_n	Natural Frequency	rad/s
ξ	Damping	-
τ	Time Constant	-
d	Duty Ratio	-
f	Frequency	Hz
T	Time Period	s
ω	Angular Frequency	rad/s
G	Transfer Function	-
α	Bandwidth	Hz
h	Harmonic Order	-

Acronyms

Acronym	Specification
RMS	Root Mean Square
PWM	Pulse Width Modulation
THD	Total Harmonic Distortion
PI	Proportional Integral
PR	Proportional Resonance
ASD	Adjustable Speed Drive
APF	Active Power Filter
CHP	Combined Heat and Power
PCC	Point of Common Coupling
UPS	Uninterrupted Power Source
HPF	High Pass Filter
LPF	Low Pass Filter
PF	Power Factor
KCL	Kirchhoff's Current Law
PLL	Phase Locked Loop

Table of Contents

Introduction 1

On the path to become solely dependent on renewable energy sources, not only wind and solar power, biomass-fired power plants are widely used to replace coal-fired power plants. A biomass-fired power plant can generate heat and electricity from biological waste products and wood chips. The procedure of using biomass to drive a power plant can be seen as recycling of carbon dioxide, because the emitted carbon dioxide is consumed, for example when trees and corn are growing. In this regard biomass-fired power plants are more environmentally friendly than traditional power plants, and in 2014, 14% of the total energy consumed globally was generated from biomass [1]. This project is done in collaboration with Aalborg Energie Technik (AET), a Danish company designing biomass-fired boilers and combined heat and power (CHP) plants. AET has designed and built the "Helius CoRDe" power plant in Scotland, which uses the waste product of whiskey production called draff [2]. The Helius CHP plant can be seen in Fig. 1.1.

Figure 1.1. Helius CoRDe power plant [2].

The draff is supplied by the nearby distilleries and is mixed with wood chips and used to heat up the boiler. The Helius power plant can generate 7.5 MVA, which is enough to supply electricity to 9000 homes [3]. In addition to a large turbine, pumps and fans are also installed in a the CHP in order to operate the power plant. In general, the Helius power plant consists of three voltage-level stages: a 400 V low-voltage stage (V_{low}), a 11 kV medium-voltage stage (V_{med}), and a 33 kV transmission-level voltage stage (V_{grid}). The turbine generator of the power plant is connected to the medium-voltage stage. The power generated by the generator is transferred to the grid and consumed by the loads of the power plant. The power consumed is an expense of the power plant, and if this could be reduced, it might be possible to save money. The loads connected to the low voltage bus bar are among others: pumps and fans connected by adjustable speed drives, uninterruptible power supplies (UPS), and fuel handling systems. Many of these systems are connected with a full-bridge diode rectifier and a three-phase two-level converter, which is used to control motors. Diode rectifiers can generate harmonics in the input current, which increases the power consumption due to extra losses [4]. A simplified overview of the electrical network of the Helius power plant can be seen in Fig. 1.2.

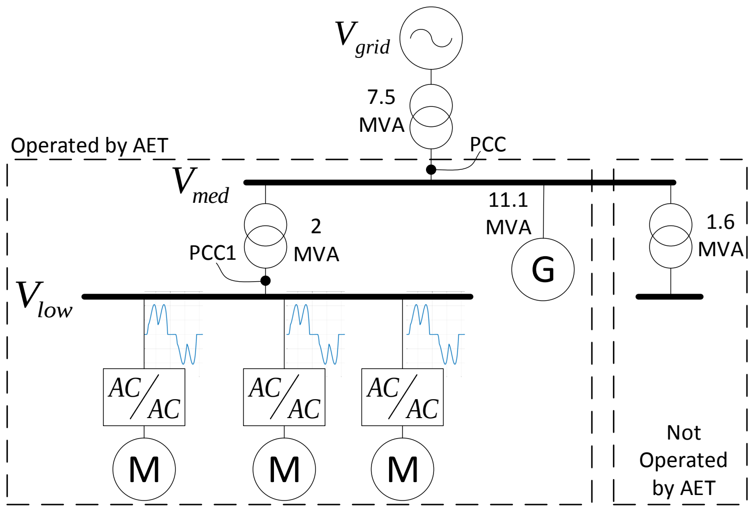

Figure 1.2. Simplified network of the Helius power plant, including turbine generator (G), and motor loads (M) connected using diode rectifiers and inverters (AC/AC).

In order to reduce the harmonics in the 2 MVA transformer current, AET has considered to implement an active power filter at the Point of Common Coupling (PCC) of the own consumption (PCC1 in Fig. 1.2). Doing so may help to reduce the power consumption thus save money while ensuring that the power quality is in compliance with relevant standards. However, from an economical aspect, Helius Energy and Rothes CoRD decided not to install an active filter [5]. Therefore Helius CHP is chosen as a case study in this project, because this contains one of AETs largest installations, and for future projects AET want to know the benefits of implementing an active filter.

1.1 Loads and Harmonics in Power Systems

Over the last three decades the number of electrical loads connected to the grid has increased. This includes both an increase in household loads like computers and other electronic equipment, but also an increase in larger industrial loads, e.g. electrical machines connected to the grid [6], [7]. The loads connected to the grid can be divided into two categories: linear loads and non-linear loads. The linear loads are characterized by a linear relationship between the voltage and the current or a constant impedance, thus if the voltage is pure sinusoidal, the current is also pure sinusoidal. Linear loads can both be resistive, inductive, or capacitive, thus can both attain a lagging or leading power factor. Examples of linear loads could be a direct grid-connected AC machine (unsaturated operation [8]), or incandescent lightning [6]. Voltage and current of a linear inductive (RL) load simulation are exemplified in Fig. 1.3(a). The non-linear loads have a non-linear relation between the voltage and current, and it can be seen as a non constant impedance. Therefore the current is not purely sinusoidal even if the voltage is purely sinusoidal. A simulation example of a non-linear load, with line inductor, is shown in Fig 1.3(b). The non-linear loads are commonly due to the use of diodes, e.g. a diode bridge rectifier [9]. Examples of non-linear loads can be switch-mode power supplies like computer chargers and LED lightning, and electrical machines using an adjustable speed drive system including diode rectifiers [6].

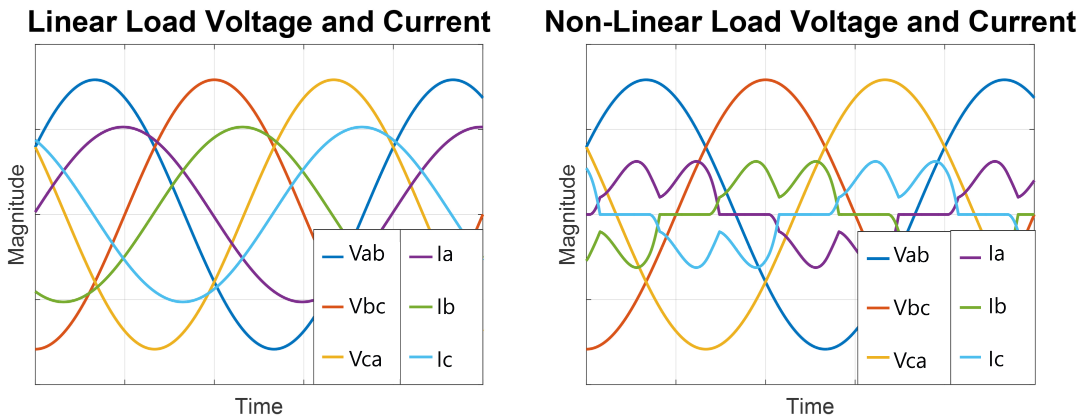

(a) (b)

Figure 1.3. Simulated examples of current and voltage for a) an inductive linear load b) a non-linear load using a six pulse diode rectifier.

Since a non-linear load generates non-sinusoidal currents, a measure of the harmonic content is necessary to examine the power quality. To calculate the harmonic content of a voltage or current drawn by a non linear load, the total harmonic distortion (THD) is used. The THD is given by:

$$\mathrm{THD} = \frac{\sqrt{\sum_{h=2}^{\infty} y_h^2}}{y_1} \cdot 100 \qquad [\%] \tag{1.1}$$

where y_1 is the magnitude of the fundamental frequency component, and y_h is the magnitude of the h^{th} harmonic component. The number of harmonic frequencies that should be considered when calculating the THD, depends on the specific standards or grid codes. In the standard "G5/4" which applies to the Helius CHP, the THD should be measured up to the 50^{th} harmonic component [10]. The Root Mean Square (RMS) current can also be written as a square sum of the harmonic frequency components and the fundamental frequency component [4]:

$$I_{\mathrm{RMS}} = \sqrt{I_1^2 + \sum_{h=2}^{\infty} I_h^2} \tag{1.2}$$

Therefore, the RMS current (I_{RMS}) increases when more or larger harmonic components appear in the current, as described by Eq. 1.2. This can be rewritten, according to [11], as:

$$I_{\mathrm{RMS}} = I_1 \cdot \sqrt{1 + \left(\frac{\mathrm{THD_i}}{100}\right)^2} \tag{1.3}$$

where $\mathrm{THD_i}$ is the total harmonic current distortion. Therefore, an increase in $\mathrm{THD_i}$ results in a larger RMS current and consequently increases the losses in the system. An increase in losses can have thermal side effects, which might induce reliability problems in terms of shorter lifetime or component damages [6], [12]. When a harmonic current is flowing through an impedance, it causes distortions to the voltage too. Current and voltage distortions can also introduce other problems in addition to power losses. For instance harmonics may cause noise and communication interference between different system components and control systems [12]. To limit the harmonic distortions there are different standards that should be followed when installing power plants. For the Helius CHP, the standard concerning allowable harmonic content is called "G5/4". The harmonic voltage limits in G5/4 are summarised in table 1.1.

Voltage at the PCC	Voltage THD Limit
400 V	5 %
6.6, 11 and 20 kV	4 %
22 kV to 400 kV	3 %

Table 1.1. Voltage harmonic limits in G5/4 [10].

The current emission limits in G5/4 are not specified as THD limits, but given in a table with the maximum current magnitude for each harmonic. Furthermore, the current magnitude limits are given for each load/equipment, and are not the limits at the PCC. The current emission limits, for equipment/loads rated for 16 − 75 A per phase, can be seen in Fig. 1.4.

Harmonic order, h	Emission current, I_h	Harmonic order, h	Emission current, I_h	Harmonic order, h	Emission current, I_h	Harmonic order, h	Emission current, I_h
2	28.9	15	1.4	28	1.0	41	1.8
3	48.1	16	1.8	29	3.1	42	0.3
4	9.0	17	13.6	30	0.5	43	1.6
5	28.9	18	0.8	31	2.8	44	0.7
6	3.0	19	9.1	32	0.9	45	0.3
7	41.2	20	1.4	33	0.4	46	0.6
8	7.2	21	0.7	34	0.8	47	1.4
9	9.6	22	1.3	35	2.3	48	0.3
10	5.8	23	7.5	36	0.4	49	1.3
11	39.4	24	0.6	37	2.1	50	0.6
12	1.2	25	4.0	38	0.8		
13	27.8	26	1.1	39	0.4		
14	2.1	27	0.5	40	0.7		

Figure 1.4. Current emission limits for different harmonics, in RMS ampere, for equipment and loads rated for 16 − 75 A per phase [10].

As seen in Fig. 1.4 the current limit is more stringent for higher currents up to 75 A, since the limits for each harmonic are constant for all current levels above 16 A. However in the Helius CHP all of the main loads are above 75 A. The load drawing most current in the Helius CHP, has a maximum capacity of 800 A. Above 75 A, there is no current THD restriction in G5/4. The main limit of G5/4 is therefore the voltage THD, but the voltage THD is satisfied in the Helius CHP. For example the voltage THD at PCC1 on a given day was measured to be 4.35 %.

In addition to the harmonic limits from standards that should be satisfied, it is also possible to save power by reducing the THD_i, because the RMS current increases with the THD_i as described in Eq. 1.3 and therefore also the power. The power saved from the attenuated harmonic frequencies, ΔS, can be calculated as:

$$\Delta S = 3 \cdot V_{\text{RMS}} \cdot (I_{tot_{\text{RMS}}} - I_{1_{\text{RMS}}}) \tag{1.4}$$

where V_{RMS} is the RMS voltage measured at the PCC1, $I_{tot_{RMS}}$ is the total RMS current including the harmonic content, and $I_{1_{\text{RMS}}}$ is the RMS current of the fundamental frequency without any harmonics. In [6], the power portion from the distorted current (or voltage) is defined as the distortion power, D. By this definition, the apparent power is given as:

$$S = \sqrt{P^2 + Q^2 + D^2} \tag{1.5}$$

The distortion power D cannot be directly identified as a real or imaginary part, and cannot directly be included as active or reactive power. If D is real, it is possible to save active power and therefore money.

If it is assumed that the CHP is almost running 24/7 a year, with only one to two weeks of downtime [5], then the money saved per year by reducing the THD_i (assuming D to include an active power component ΔP) can be calculated by:

$$\text{Savings} = \Delta P \cdot 24 \cdot 355 \cdot x_{price} \tag{1.6}$$

where x_{price} is the price per watt-hour, and the downtime per year is assumed to be 10 days. The power sale prices for the self consumption regarding the Helius CHP plant is $x_{price} = 0.03$ £/kWh (0.26 DKK/kWh) [5].

Additionally, AET is also interested in including reactive power compensation. In the Helius power plant there are directly connected AC machines which usually is driven at $50 - 70$ % of the rated power. Therefore, these AC machines consume a certain amount of reactive power, which decreases the power factor. For example, the active power of the self supply was 1.08 MW and the reactive power was 0.44 MVAr on a given day in the Helius CHP, which corresponds to a power factor of 0.927. Due to this reactive power, the apparent power at PCC1 increases. As a consequence AET has designed the components eg. the supply transformer with a large margin, thus over-sizing the components [5]. Therefore, money could be saved, by reducing component over-sizing, when designing the power plant if reactive power compensation is employed.

1.2 Harmonic Mitigation Solutions

To suppress harmonics caused by non-linear loads, different solutions can be applied. The choice of solution depends on a number of factors like: price, size, and filtering capability. Generally the solutions can be categorised into two groups: centralised solutions, and decentralised solutions. The centralised solutions means that the harmonics are attenuated at the PCC1, using a single installation for all loads. The decentralised solutions are achieved by installing a harmonic compensation solution at each load or at the loads with the highest pollution. Some of the solutions are listed in table 1.2.

Solution Type	Centralised Option	Decentralised Option
Passive Filtering	✓	✓
Transformer Filtering	✓	✓
Rectifier Types	-	✓
Active Front End Converters	-	✓
Active Filtering	✓	✓

Table 1.2. Centralised and decentralised harmonic mitigation solutions.

One option to suppress harmonic currents is by using passive filters. Passive filters only consist of passive components, primarily inductors and capacitors but also resistors. Passive filters are based on the nature of a frequency dependent reactance, and therefore impedance of inductors and capacitors. The combination of inductors and capacitors creates frequencies of resonance, where the impedance theoretically is either zero or infinite depending on how the inductors and capacitors are configured. This can be used to sink or block currents/voltages at different frequencies. For instance multiple shunt passive filters are used to sink harmonic currents from a non-linear load as shown in Fig. 1.5.

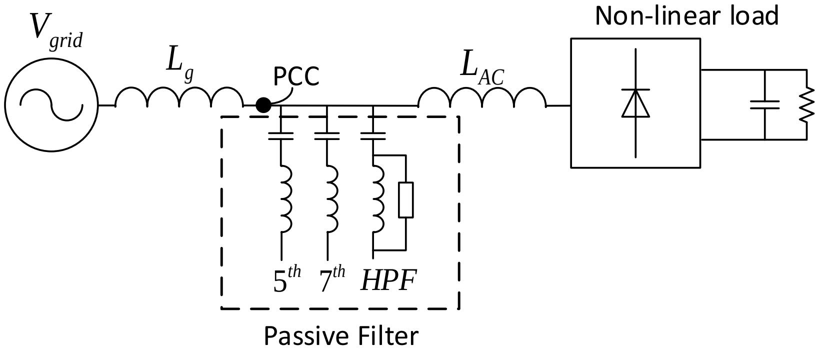

Figure 1.5. Shunt passive filter with specific harmonic attenuation and a high pass filter (HPF) to reduce harmonic currents.

Different shunt passive filters are tuned to sink harmonic currents at specified frequencies, thus low impedance paths at the specific harmonic currents. Furthermore, a high pass filter (HPF) can be used for high frequency harmonics, since these have smaller magnitudes [6]. The passive filter shown in Fig. 1.5 uses simple second order filters for each harmonic, but it can also be realized with higher order filters [7]. In those cases, passive damping (e.g., using resistors) may be required to dampen the resonance to ensure system stability. The advantages of passive filters are: a simple circuit form requiring no control loops, and the capacitors can also be used for reactive power compensation [11]. The disadvantages of passive filters are: lack of flexibility when the filters are designed and installed [13], parallel resonance can occur between the filter components and other system components e.g. the grid inductance [7], if there exist background distortion in the grid this might flow through the passive filters and could cause overloading of the filters [11], and for high power the passive filter can be large and bulky [13].

Instead of using passive filters it is possible to use a transformer as a harmonic filter. Due to the leakage inductance, the transformer behaves like a first order filter, which suppresses the current harmonics [14]. However, the leakage inductance is usually limited to $5 - 6$ % in power transformers to limit the losses [14]. Another possibility for transformer harmonic filtering is to use a phase shifting transformer to mitigate harmonic currents [15], [16]. The transformer phase shifting is, as an example, used in the higher order pulse rectifiers in order to cancel the current harmonics.

Another solution to mitigate harmonics instead of using a six pulse diode rectifier, is to use higher order diode rectifiers, like a twelve or eighteen pulse rectifier. In twelve pulse rectifiers the harmonic orders of the current are $12n \pm 1$, and in eighteen pulse rectifiers the harmonic orders are $18n \pm 1$, thus contains lower harmonic currents than the six pulse rectifier [4]. For the higher order rectifiers, the harmonic cancellation is achieved by using transformers to phase shift the inputs between each six pulse rectifier. For example the twelve pulse rectifier consists of two six pulse rectifiers, where one rectifier is phase shifted by 30° by using a wye-delta transformer [4]. The twelve pulse rectifier is shown in Fig. 1.6.

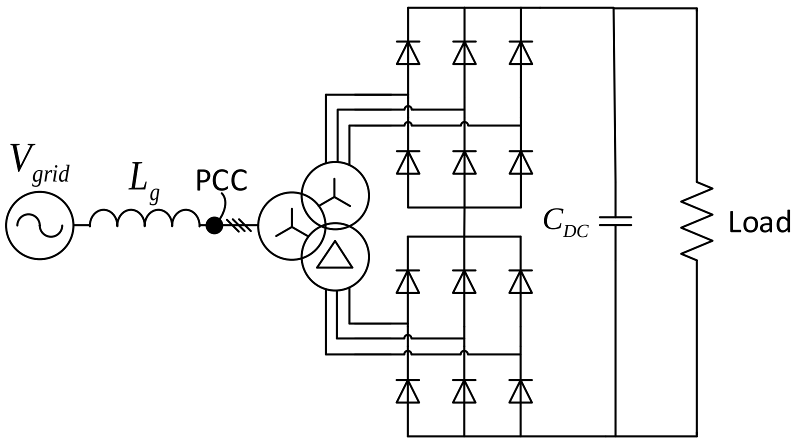

Figure 1.6. Twelve pulse rectifier circuit using wye-wye and wye-delta transformers.

Compared to the six pulse rectifier the higher order rectifiers have the disadvantages that additional six pulse rectifiers and phase shift transformers have to be introduced to the circuit, which increases both cost and size, but might also decrease reliability due to the increased redundancy. Furthermore, for a large power plant like the Helius CHP, there are many non-linear loads, which will require a large amount of higher order rectifiers, since a centralised solution is not possible.

The diodes used in rectifiers can also be replaced by switches, thus use active front end converters. By doing so, it is possible to directly control the current, and therefore reduce the generated harmonics, in theory only to contain the switching frequency harmonics due to the switching action. Compared with diode rectifiers, the active front end converters require a feedback control system, which increases the complexity. Like the higher order rectifiers, the active front end solution also requires a high amount of installed converters for a large power plant.

The last solution presented, which is the solution AET previously has investigated, is to install active power filters to mitigate current harmonics. The active power filter is an active three phase converter connected in series or parallel to the location where the harmonics are desired to be attenuated, as shown in Fig. 1.7.

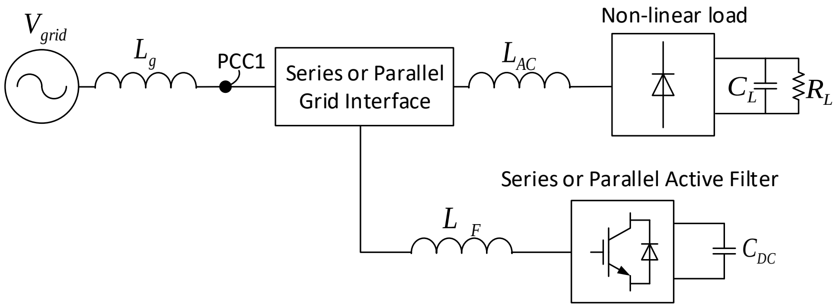

Figure 1.7. Simplified circuit of a parallel or series active filter connected at the PCC1.

The concept of counter-phase operation of the active filter, is to generate a current or voltage, which is equal but of opposite direction to that of the non-linear load harmonic current or voltage. Thereby the harmonic current or voltage is cancelled, so only the fundamental component is present at the grid. The advantages of using an active power filter compared with passive filters are higher flexibility, better filtering performance, smaller size, and ageing effects can be compensated [13]. The main advantage of using the active power filter instead of installing higher order rectifiers or active front end converters in each non-linear load, is that it is possible to connect a single active power filter close to the PCC1 as a centralised solution.

The harmonic mitigation performance in terms of the resultant grid current THD and energy efficiency, made by Danfoss, can be seen in Fig. 1.8.

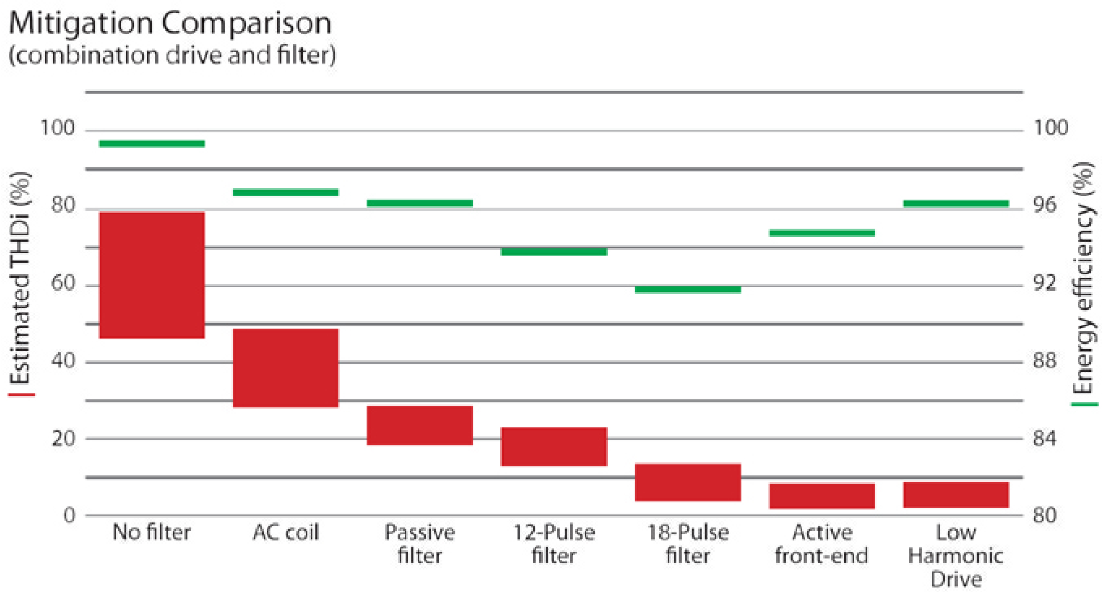

Figure 1.8. Comparison of harmonic mitigation solutions in terms of current THD and energy efficiency [17].

In Fig. 1.8 the "Low Harmonic Drive" is a shunt active power filter, and the "No Filter" option is a standard six pulse rectifier without a DC or AC filter. The energy efficiency and THD performance comparison is for a single harmonic load, thus centralised solutions are not considered. The converter solutions have better harmonic performance than the passive filter solutions, but similar energy efficiency. Although the higher order rectifiers have better harmonic performance compared to traditional six pulse rectifier, the efficiency is also worse. An active front end and active power filter solution can achieve a similar low THD, but the active filter can achieve a slightly higher efficiency.

Problem Statement 2

As described in the introduction, AET has considered to install an active power filter in the Helius CHP system, due to the harmonic mitigation performance and reactive power compensation option. However, they cannot justify the active power filter addition to their customers for economic reasons. By introducing an active power filter, it might be possible to reduce losses in the system and power ratings, thus potentially save money, and avoid side effects of a higher harmonic content. The problem statement of this project is therefore:

What are the benefits of implementing an active power filter in the Helius CHP plant, how is it controlled, and which considerations has to be made when choosing an active power filter?

This statement includes a generalized model and simulation of the Helius power plant without the active power filter which consists of: the medium voltage bus, a step down transformer, and low voltage non-linear loads. The problem statement also includes insight into which parts of the system that affects the harmonic pollution. When the model matches the power plant, an active power filter is implemented in the model. This is to investigate the harmonic mitigation and the influence of different control methods on the active power filters performance. This will also be verified through simulations and experiments on a down scaled laboratory setup. Finally, an analysis of adding an active power filter to the Helius power plant, seen from AET and its customers point of view will be performed. This will include guidelines for AET when considering an active power filter.

The electrical specifications of the Helius CHP plant can be seen in table 2.

Parameter	Value
Medium voltage	11 kV
Low voltage	400 V
Generation	8.3 MVA (PF = 0.99)
Consumption	1.1 MVA
Power Factor (PCC1)	0.927
Export	7.5 MVA

Table 2.1. Specifications of the Helius CHP plant.

In the Helius CHP, the converters used to drive the pumps and machines are Danfoss FC302 converters for different power levels.

Limitations of this project are:

- The CHP plant model is limited to a fraction of the actual non linear loads, nevertheless including the larger power consuming loads.
- The medium voltage grid is assumed to be an ideal and symmetrical voltage source.

System Analysis of Helius Power Plant 3

In order to understand the system and identify the specification of the active power filter and the controller, the Helius power plant is modelled. As stated in the introduction, the Helius power plant consists of different components. All the loads are modelled as non linear loads connected through a transformer to the medium voltage network. The objective using non linear loads is to match the power consumed by the power plant, thereby matching the values of the Helius power plant. Before simulating the power plant, the theory of the components are presented and then validated in a laboratory setup. Lastly the results of simulating the Helius power plant model will be presented.

3.1 Adjustable Speed Drive

One of the most common non linear loads, which induces harmonic current are the adjustable speed drive (ASD) loads. A typical ASD, as shown in Fig. 3.1, consists of a diode bridge rectifier, a DC link connection, a three phase inverter, and an electrical motor.

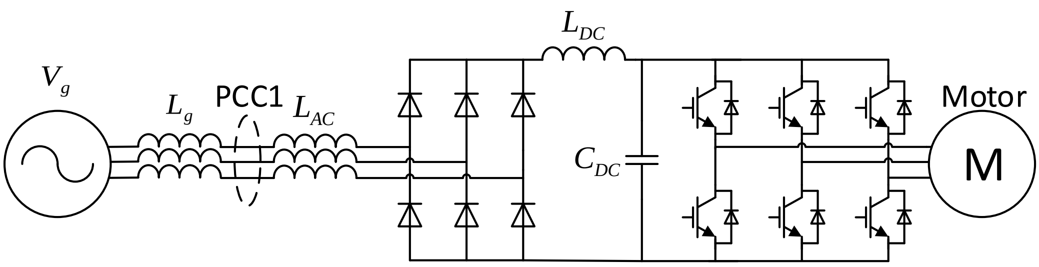

Figure 3.1. Typical ASD circuit diagram, which is also used in the Helius CHP.

In the Helius CHP, the rectifiers are six pulse diode rectifiers, which are selected due to lower price and lower size compared to higher order rectifiers, like the twelve or eighteen pulse rectifiers. However, this choice of rectifier topology have the side effect that the current drawn has a significant harmonic content. The current of a six pulse rectifier contains harmonics of the order $6n \pm 1$ of the fundamental frequency, where n is an integer [6]. Fig. 3.2 shows an example of phase-A current waveform of a six-pulse rectifier, and its harmonic distribution is presented in Fig. 3.3.

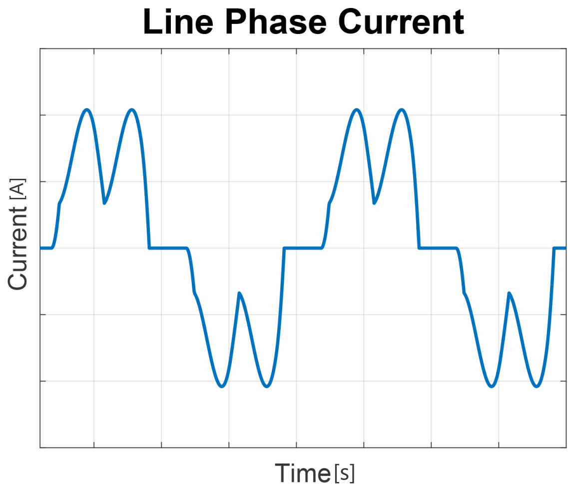

Figure 3.2. Simulated AC side current from a single ASD as shown in Fig. 3.1.

For the simulation case the DC link inductor $L_{DC} = 14.9$ %, the line impedance $L_{AC} = 3.0$ %, and the DC link capacitor $C_{DC} = 66.1$ %, which results in a highly distorted current [7]. The per unit values given are calculated based on the following equations:

$$Z_B = \frac{V_B^2}{S_B}$$
$$L_B = \frac{Z_B}{2\pi \cdot 50}$$
$$C_B = \frac{1}{Z_B \cdot 2\pi \cdot 50}$$

where S_B is the base power, V_B is the base voltage, Z_B is the base impedance, L_B is the base inductance, and C_B is the base capacitance.

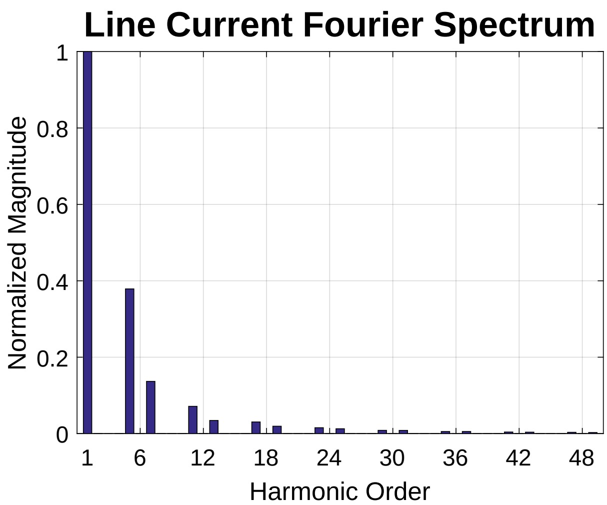

Figure 3.3. Fourier spectrum of grid side current illustrated in Fig. 3.2.

As seen in Fig. 3.3, the current contains $6th$ harmonic pairs like $5th$ and $7th$, and $11th$ and $13th$ harmonics etc. The THD of the current in Fig. 3.3 is 41.3 %. The current THD is affected by the line impedance, the DC link inductor, the DC link capacitor, and also the machine parameters. However, if the DC link capacitor is designed to ensure a smooth DC link voltage, it acts as a decoupling between the grid side and the machine side, thus any harmonic distortion from the machine side will not be in the grid side [18]. However, the DC link inductance and the line inductance has a higher influence on the current THD.

By assuming that the DC link capacitor is designed to ensure decoupling of harmonics, then the inverter and motor can be modelled as a variable resistor and capacitor in parallel, as shown in Fig. 3.4.

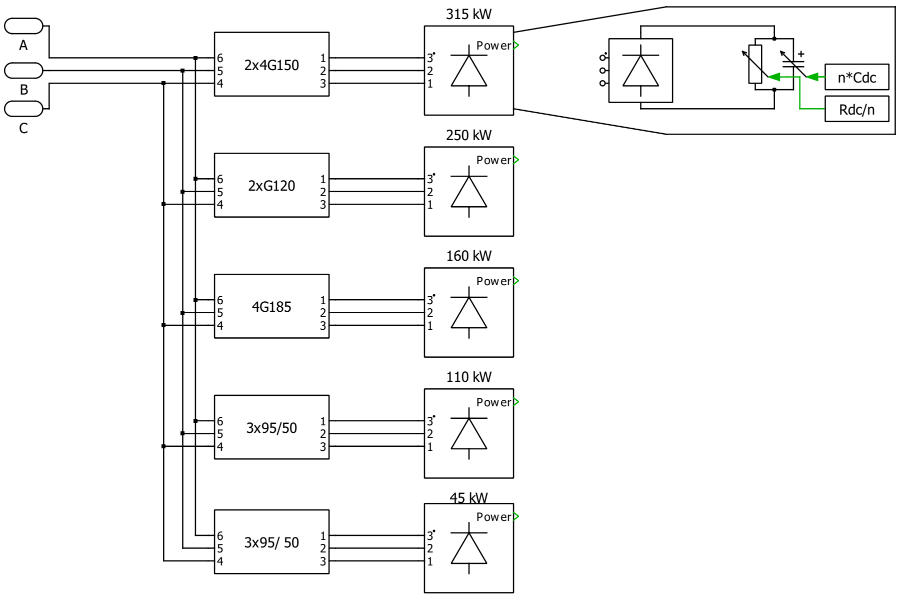

Figure 3.4. Simplified model of an ASD with a load.

In the Helius CHP the non-linear loads are all operating at constant power. Therefore, if the voltage increases the current decreases, which can be modelled as a negative resistor represented by a variable resistor. Because of the six pulse rectifier, the DC link voltage is not completely constant and therefore the variable resistor is used to keep the power constant. The resistance can be calculated by:

$$R_{load} \simeq \frac{V_{DC}^2}{P_{ref}} \tag{3.1}$$

where R_{load} is the variable resistance, and P_{ref} is the constant power reference. For a six pulse rectifier the average DC link voltage is given by:

$$V_{DC} = \frac{3 \cdot \sqrt{2}}{\pi} \cdot V_{LL_{\mathrm{RMS}}} \tag{3.2}$$

where $V_{LL_{\mathrm{RMS}}}$ is the RMS line to line input voltage of the rectifier.

Effect of Inductances and Load Power on THD

To investigate the effect of variation in the line side inductance, DC link inductance, and the power level of the ASD a simulation is conducted. The simulation is performed for a single ASD rated at 7.5 kW. The first two simulations are carried out by keeping the load power constant at 7.5 kW, and either keeping L_{ac} or L_{DC} constant at a per unit value of 5 % while the other inductance is varied. The simulation results are shown in Fig. 3.5(a) and Fig. 3.5(b).

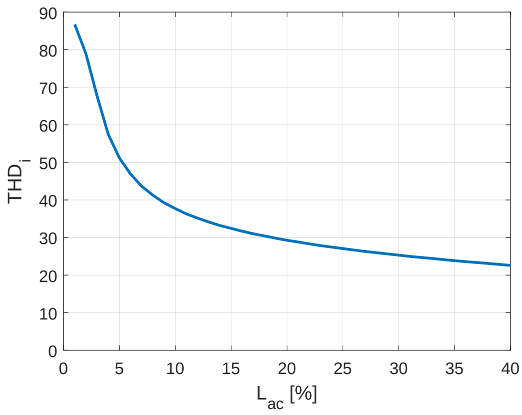

(a)

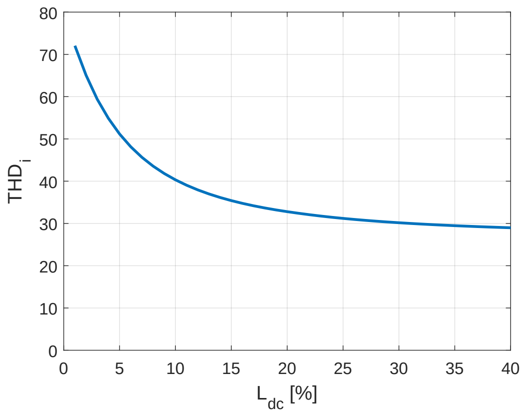

(b)

Figure 3.5. Simulated results for a single ASD load when a) the line side inductance is varied, with $L_{DC} = 5\%$ b) the DC link inductance is varied, with $L_{AC} = 5\%$.

As seen the tendency of the THD when varying one inductance while the other is constant, is similar. The THD is high for low values of inductance with a steep slope, while the THD is almost constant for higher values of inductance. When the inductances and load power is small, the current can enter discontinuous mode, where the current will be zero for certain periods. An example of the load current in the case of discontinuous mode is shown in Fig 3.6.

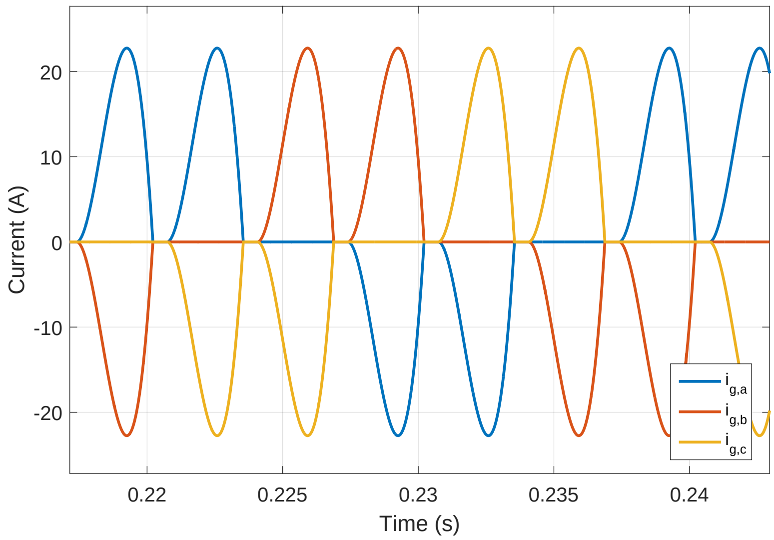

Figure 3.6. Simulation results of single ASD load in discontinuous mode.

To further analyse the effect of both inductors, a simulation ,where the THD is a function of both inductors, is performed. The result is seen in Fig. 3.7.

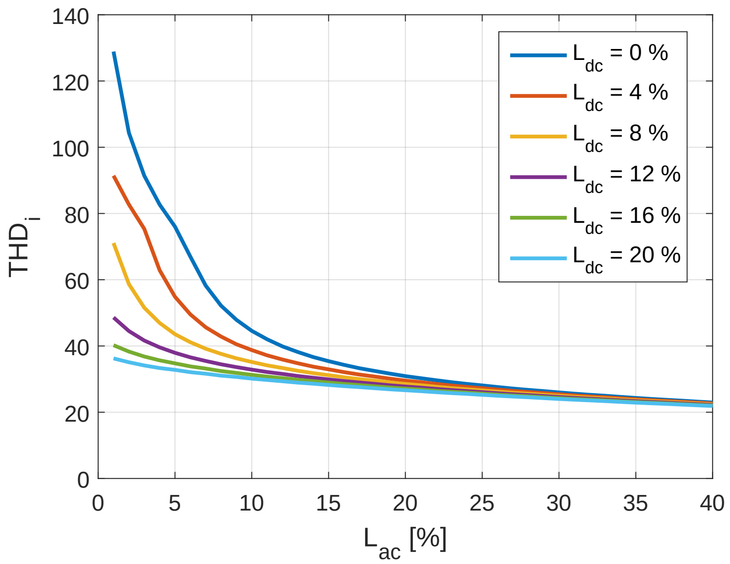

Figure 3.7. Simulated grd current THD as a function of L_{ac} and L_{DC} using a 7.5 kW ASD load.

From Fig. 3.7 it is seen that the DC link inductor has more influence on the THD at lower values of the line side inductor. In contrast the THD is almost not depending on the DC link inductance for higher values of the line side inductor.

The current THD also depends on the power level of the ASD load. This is shown in Fig. 3.8, where the THD, for the ASD load rated at 7.5 kW, is shown for different power levels, with a constant line side inductor and a constant DC link inductor.

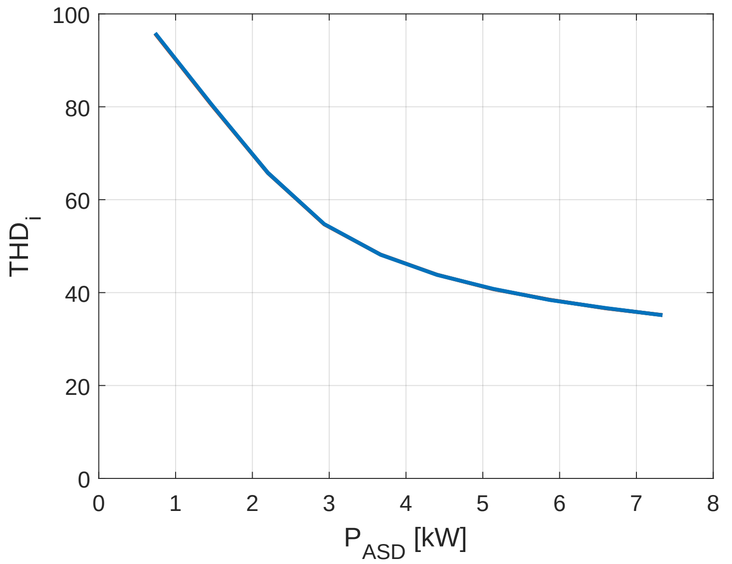

Figure 3.8. Simulated THD as a function of the ASD load power level.

The THD of the line side current is shown to be dependent on the ASD load power level. Even though the ASD load is rated at 7.5 kW, it might have worse harmonic performance, if the machine is not driven at the rated conditions. In the Helius CHP the load machines are often driven at $50-70$ % of the rated load power, thus this may cause a higher current THD. To compare the THD of the 7.5 kW to the 315 kW ASD load, which is the largest ASD load in the Helius CHP, a similar simulation is conducted. The THD as a function of the load power level is shown in Fig. 3.9.

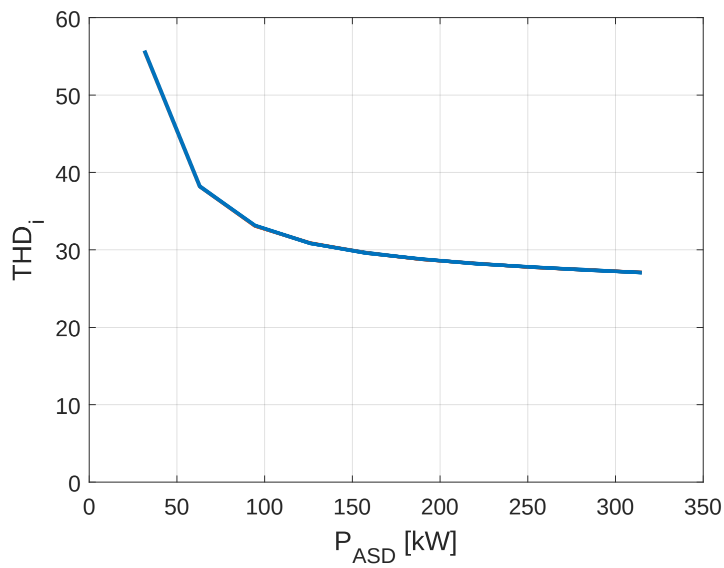

Figure 3.9. Simulated THD as a function the ASD load power level, for a 315 kW rated ASD load, with $L_{AC} = 6\%$ and $L_{DC} = 6\%$.

As observed in Fig. 3.9 it has the same tendency as the low power ASD simulation, however the slope of the curve is smaller, thus the harmonic performance at 50 % load does not change the current THD significantly. The effect of varying the inductances is also studied for the 315 kW ASD load, which is seen in Fig. 3.10.

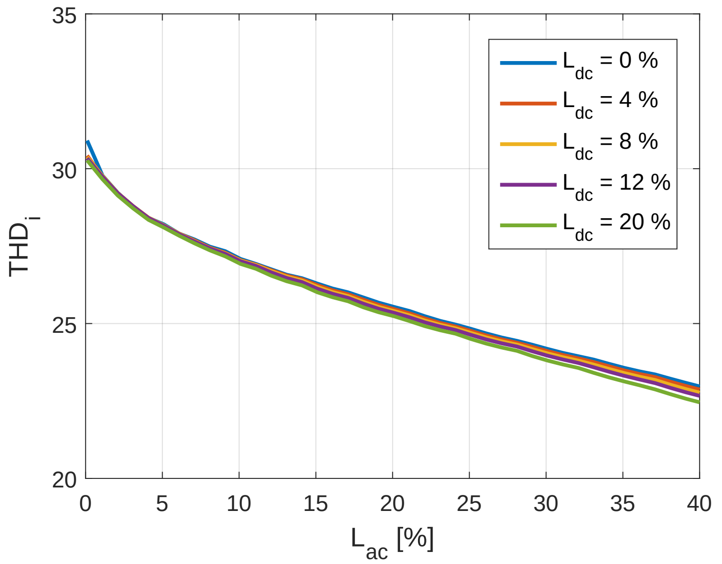

Figure 3.10. Simulated THD as a function of L_{ac} and L_{DC} using a 315 kW ASD load.

In this case, when the current is much higher, the DC link inductor has a negligible influence on the current THD. The line side inductor has a certain influence, but still lower influence than on the lower power ASD load.

3.2 Transformer

Transformers are used to scale different voltage levels of the system from the 33 kV to 11 kV and 11 kV to 400 V. In the Helius power plant two delta-wye transformers are used. One connects the 11 kV of the medium voltage bus bar in the power plant to the grid, this is the step up transformer, and another generates 400 V on the low voltage bus bar, which is the supply transformer, from the medium voltage bus bar. Furthermore, transformers also add isolation between the different voltage levels. The data of the transformers used in the Helius power plant can be seen in table 3.1.

Parameter	Step up transformer	Supply transformer
Rated Power	7.5 MVA	2 MVA
Rated Voltages	[33 kV,11 kV]	[11 kV;400 V]
Rated impedance	8 %	6 %
Vector Group	DYN11	DYN11

Table 3.1. Helius transformer data.

The losses in a transformer are core losses and ohmic or parasitic losses. The core losses are generated by hysteresis and eddy currents in the core, while the parasitic losses are generated by the cables of the transformer, such as resistive losses, proximity effect, and skin effect. The parasitic losses can be modelled as leakage inductance connected with a resistor and the core losses can be modelled as an inductor connected with a resistor, as seen in Fig. 3.11.

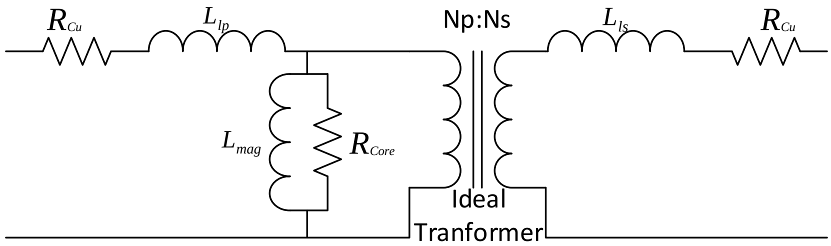

Figure 3.11. Single phase transformer model used for case study [4].

The harmonic components will increase the losses of the transformer. The resistive losses increases by $\mathrm{THD}_{\mathrm{i}}^2$, while the increase in eddy current losses for both core and windings are given by Eq. 3.3, [14].

$$P_e = \sum_{h=1}^{\infty} h^2 \left(\frac{I_h}{I_1}\right)^2 \cdot P_{e1} \tag{3.3}$$

P_{e1} is the eddy current loss at the fundamental frequency. From Eq. 3.3 reducing the magnitude of the harmonic components will reduce the loss of the transformer.

The magnetization inductance and core losses are not given by the supplier and therefore these are neglected. The three phase transformers used in the Helius CHP plant are delta-wye transformers, which can be seen in Fig. 3.12.

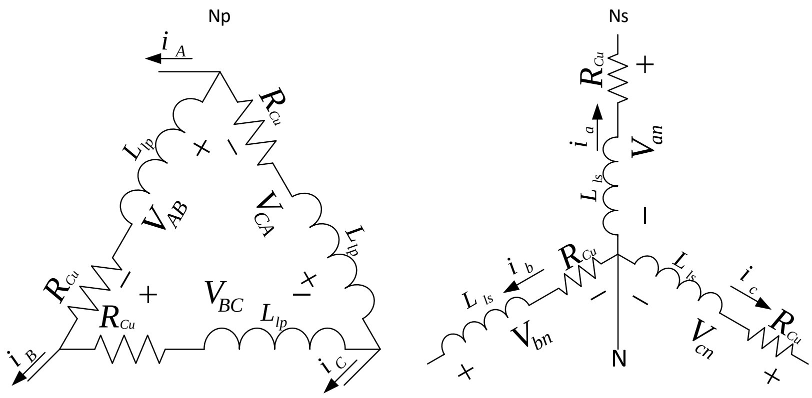

Figure 3.12. Three phase delta-wye transformer model.

This transforms the phase voltage of the wye side to the line voltage on the delta side. Thus, with a turns ratio of $1 : \sqrt{3}$ the voltages are:

$$V_{AB} = V_{an} \tag{3.4}$$

Furthermore, the delta wye connection has a 30 degree voltage phase-shift between the wye voltage and the delta voltage with the standard connection [14]. The line current of the delta side is calculated by:

$$i_A = (i_a - i_b)\,\frac{N_s}{N_p} \tag{3.5}$$

This will reshape the current waveform containing harmonic components, but not eliminate them. This can be seen in Fig. 3.13, where a delta-wye transformer is used for non linear loads.

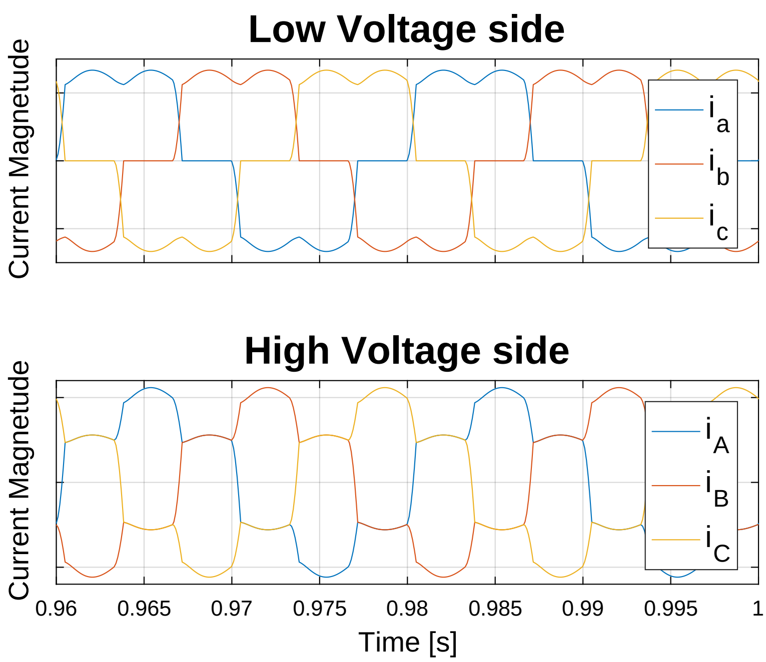

Figure 3.13. Currents of a delta-wye transformer connected to non linear load top) wye side current, bottom) delta side current.

As mentioned the line currents of a non linear load contain $6n \pm 1$ harmonics, and the delta side line currents contains the same harmonic components as the wye side, even though the current shape changes [14]. This can be seen in the Fast Fourier Transforms (FFT) of the wye and delta side currents of the transformer in Fig. 3.14.

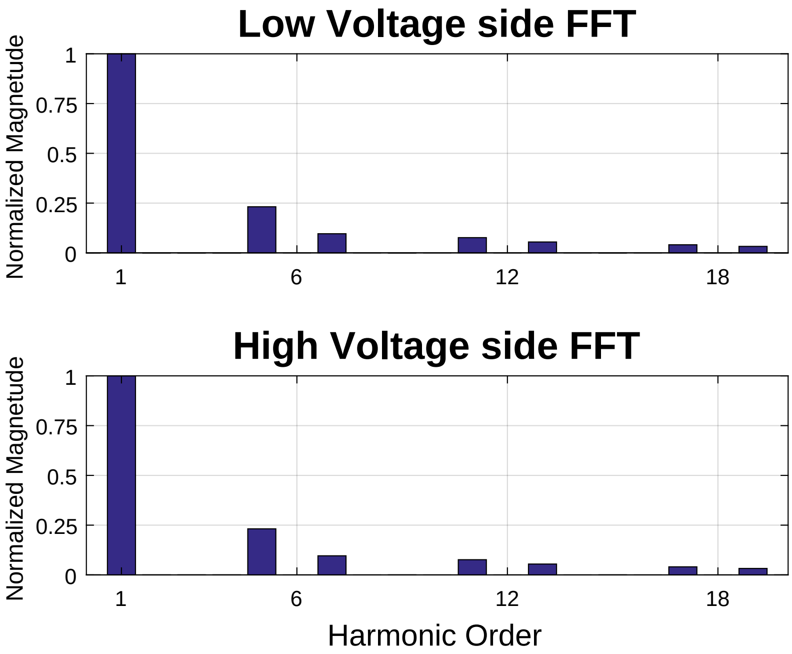

Figure 3.14. FFT of the currents of a delta-wye transformer connected to non linear load top) wye side current FFT, bottom) delta side current FFT.

As seen the magnitude of the harmonics are almost the same. The THD of the wye side is 28.2 % and the delta side is 27.1%. Therefore, the filtering effect of the transformer is the same as an inductor. Another feature of the delta-wye transformer is the elimination of the 3^{rd} order harmonics. In the delta connection 3^{rd} order harmonics are trapped in the magnetization currents of the transformer, which circulates within the windings, while they flow into the ground connection of the wye connection [14].

3.3 Validation of the Transformer and ASD Models

With a simple test setup the models of the ASD and the transformer are validated. In this test a 7 kVA, DYN11, delta wye transformer with a turn ratio of $1:\sqrt{3}$, is connected to a diode bridge with a 51 μF DC capacitor, 1.2 mH DC inductor and 51.2 Ω resistor as the load. The line current with the harmonics generated by the ASD can be seen in Fig. 3.15.

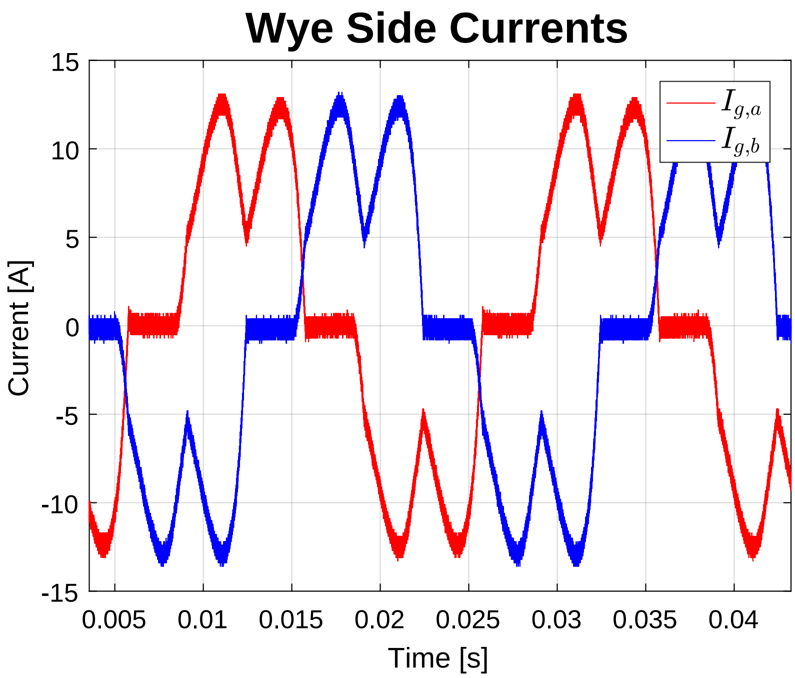

Figure 3.15. Measured line current of ASD.

The line current can be seen to match the simulated line current shown in Fig. 3.2, which also contains the 5^{th}, 7^{th}, 11^{th} and 13^{th} order harmonics. As stated the transformer changes the shape of the current. The delta side current of the test can be seen in Fig. 3.16.

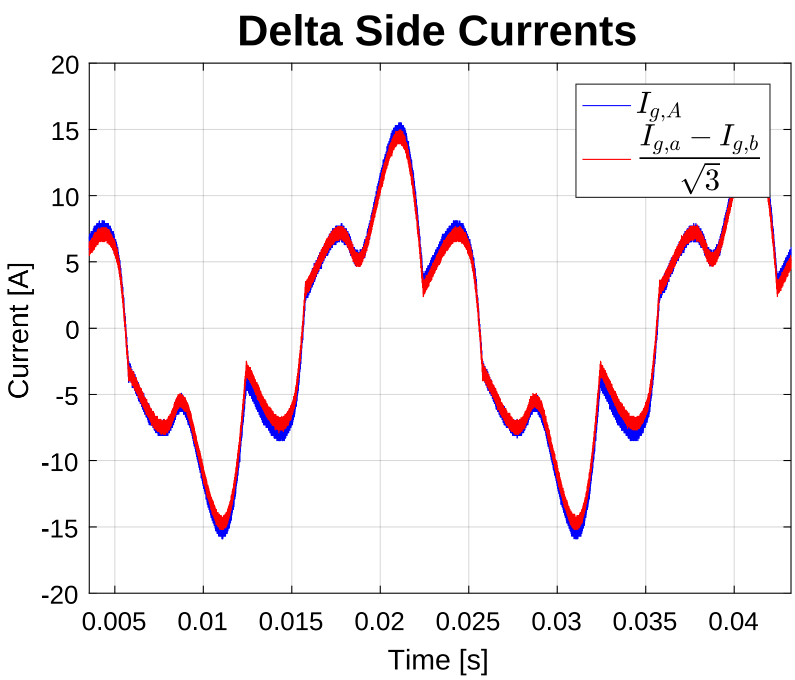

Figure 3.16. Measured and calculated delta side current.

As seen n Fig. 3.16 the current calculated from the wye side, in Fig. 3.15 using Eq. 3.5, matches the measured phase current on the delta side of the transformer, and matches the simulation in Fig. 3.13. Furthermore, a FFT analysis shows the harmonic content of the currents on each side of the transformer. This can be seen in Fig. 3.17.

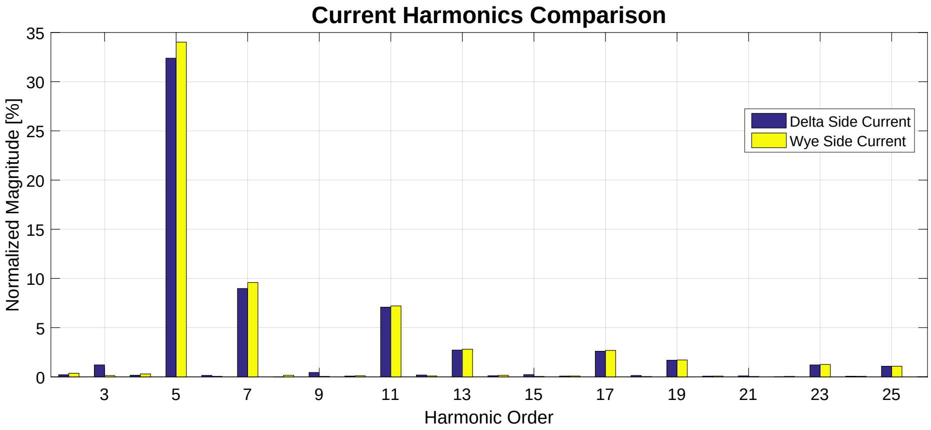

Figure 3.17. Comparison of measured harmonic content of the delta side current and the wye side current.

It is shown in Fig. 3.17 that the harmonic components of each side of the transformer are almost identical, and the delta side harmonics are slightly lower than the wye side due to the filtering effect of the leakage inductance. The THD of the delta side is 34.7% and 36.5% for the wye side.

3.4 Modelling of the Helius Power Plant

As mentioned in the introduction, the network of the Helius power plant consists of three voltage levels connected with transformers, which is shown in Fig. 1.2. The model of the power plant focusses on the supply of the power plant. This is presented in Fig. 3.18.

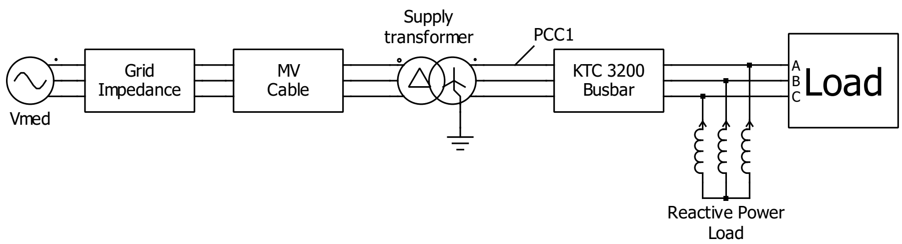

Figure 3.18. Overview of the Helius PLECS model.

The values of the cables in the Helius CHP plant, which can be seen in Fig. 3.19, are provided by AET [5], and the data can be found in App. A.1. The grid impedance is the medium voltage side of the step up transformer, which has an impedance of 8% and the impedance of the supply transformer is 6%.

In order to match the simulation and reality of the power plant, AET [5] has provided data from the Helius Power Plant. During normal production the values of the self consumption can be seen in table 3.2.

Parameter	Value
P	1.088 MW
Q	0.442 MVAr
$\mathrm{THD_i}$	25.88%
$\mathrm{THD_v}$	4.3 %

Table 3.2. Electrical data from the Helius CHP.

Reference [19] proposes when working with multiple ASD loads of the same power level, that these can be simulated as one load where the load is scaled by:

$$R_{tot} = \frac{R_{DC}}{n} \tag{3.6}$$

Where R_{DC} is the load resistance for one ASD load and n is the number of loads with the same power level. Furthermore the DC capacitance is scaled by:

$$C_{tot} = n \cdot C_{DC} \tag{3.7}$$

This is used to model the Helius power plant and merge loads of the same power levels together. This can be seen in Fig 3.19, where the resistor is a variable resistor parallel connected with a variable capacitor.

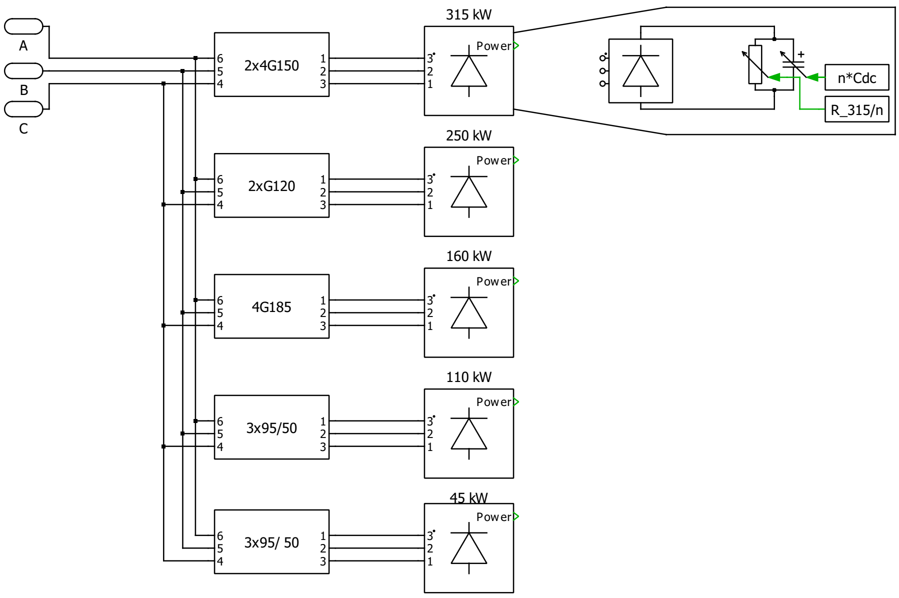

Figure 3.19. Model of different loads in the Helius power plant.

The loads of the Helius power plant consists of two 250 kW loads (120 kW nominal), one 315 kW load (240 kW nominal), one 160 kW load (145 kW nominal), three 110 kW loads (90 kW nominal), and three 45 kW loads (40 kW nominal). The non-linear load consumes some reactive power, but in order to reach the same value in table 3.2, a linear load of inductors is used instead of modelling the direct connected machines. The currents and voltages of the supply of Helius, can be seen in Fig. 3.20(c), Fig. 3.20(b), and Fig. 3.20(a).

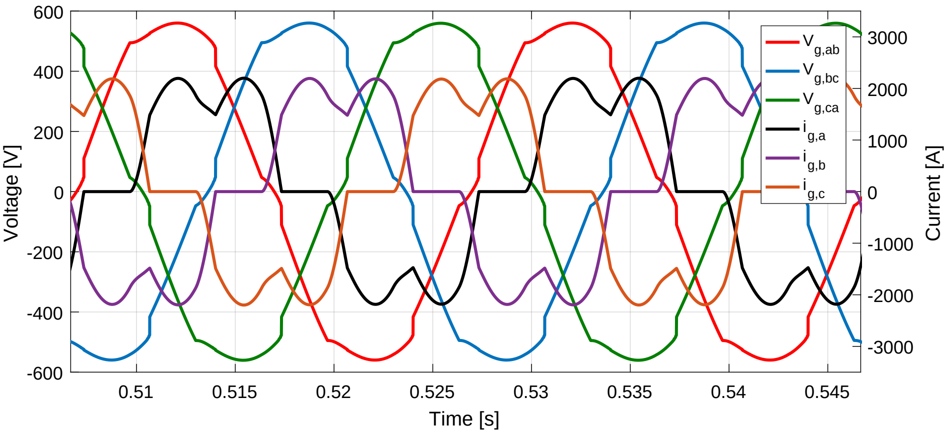

(a)

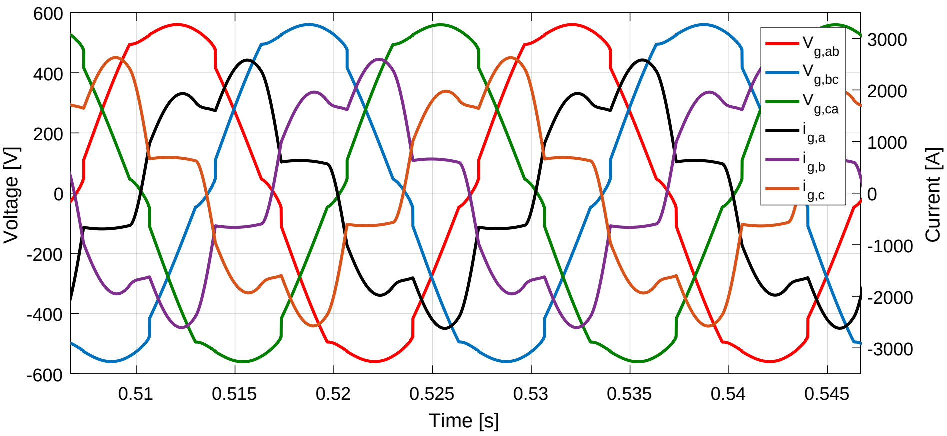

(b)

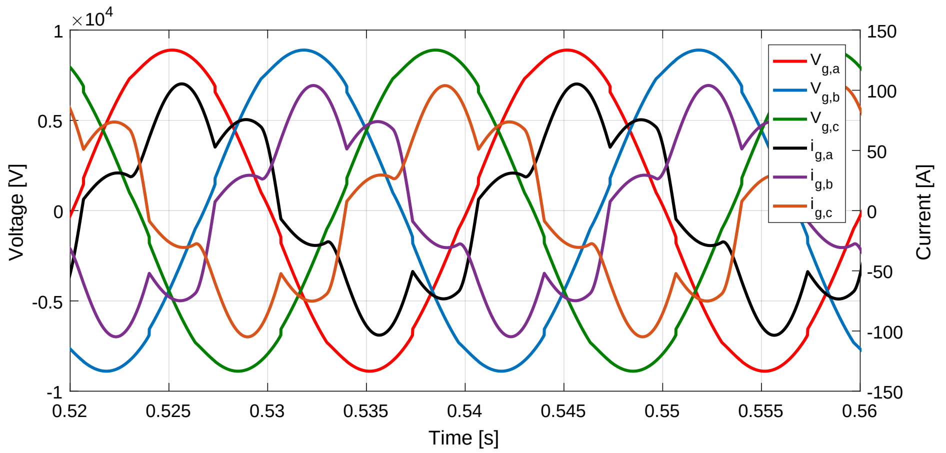

(c)

Figure 3.20. Simulated current and voltage in the Helius power plant at a) aggregate ASD load side b) PCC1 c) transformer delta side.

As seen the loads of the power plant distorts the line current and voltage. At PCC1 the RMS values are:

$$V_{ll_{\mathrm{RMS}}} = 405\ \mathrm{V}$$
$$I_{L_{\mathrm{RMS}}} = 1638\ \mathrm{A}$$

The harmonic content of the phase A current can be seen in the FFT analysis in Fig. 3.21.

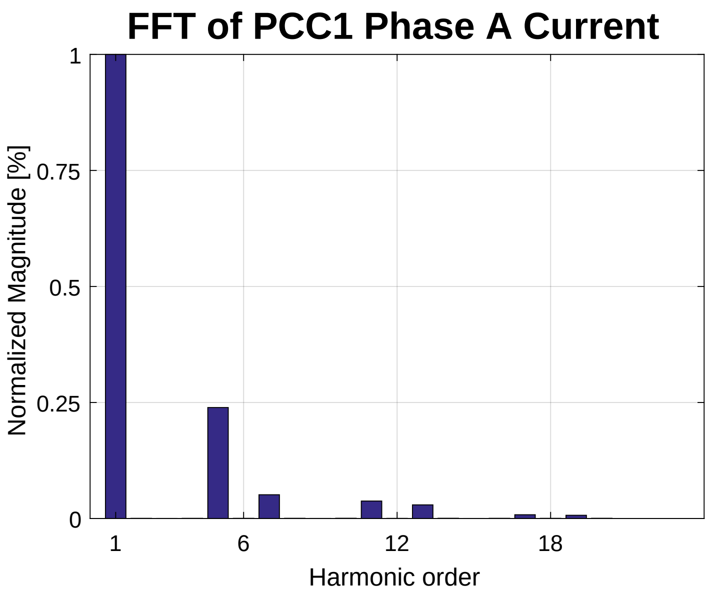

Figure 3.21. FFT analysis of the phase A current.

As seen the PCC1 current contains the $6n \pm 1$ order harmonic. The values measured in the simulation, at PCC1 can be seen in table 3.3.

P	1.106 MW
Q	0.450 MVAr
PF	0.925
$\mathrm{THD_v}$	5.75%
$\mathrm{THD_i}$	25.17%

Table 3.3. Simulation results of the Helius power plant model.

Comparing with the data of the Helius power plant provided by AET [5], the values from the simulation matches the real life data well.

As stated in Sec. 1.1, cancelling harmonics decreases the power rating of the supply of the power plant. Reference [7] states that the shunt active power filter can reduce the current THD to $5 - 10$ %, thus in this case remove 20.17 %. These simulated values will be used as design values for the shunt active power filter and controller design.

3.5 Active Power Filters

The general operation of an active power filter (APF) is to cancel or attenuate current or voltage harmonics generated by the loads on the grid side current or voltage. However, compared with passive filters the APF uses a three phase converter instead of passive components to draw the undesirable harmonic currents.

The active filters can be categorised into three topologies, the shunt (parallel) active filters, the series active filters, and the hybrid active filters. The shunt active filter topology is shown in Fig. 3.22.

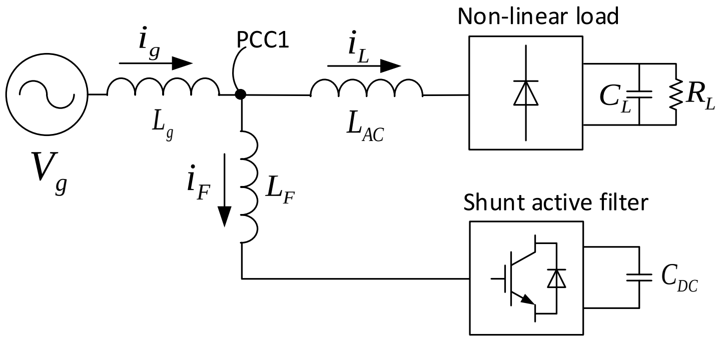

Figure 3.22. Simplified circuit of a shunt active filter.

The general operation and control strategy for the shunt active filter is firstly to measure the load side current, i_L, from the harmonic polluting load. The harmonic currents from the load current, i_{Lh}, is then extracted and used as a current reference in the active filter control system. According to Kirchhoff's Current Law (KCL) the grid current is given by:

$$i_g = i_{L1} + i_{Lh} + i_F \tag{3.8}$$

where i_g is the grid current, i_{L1} is the fundamental line current, and i_F is the current drawn by the active filter. If $i_F = -i_{Lh}$ the grid current will be equal to the fundamental frequency load current, thus the harmonics are cancelled in the grid current. To generate the harmonic current in the shunt active filter, it uses a boost inductor L_f to convert the voltage source inverter to a current source operated converter.

The series active filter configuration can be seen in Fig. 3.23.

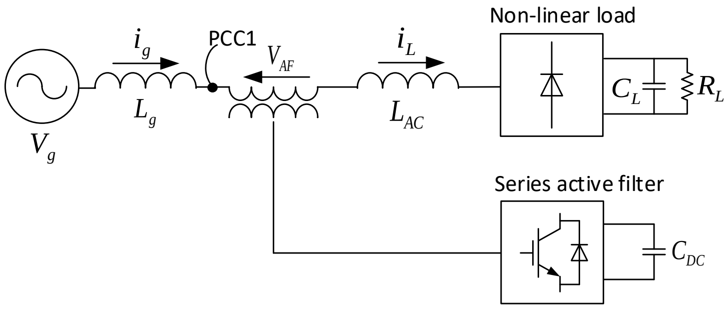

Figure 3.23. Simplified circuit of a series active filter.

The series active filter is connected to the grid by using a transformer coupling, to enable a series voltage generation. Compared with the shunt active filter the series active filter generates a voltage, V_{AF}, across the transformer coupling point. By doing so the voltage harmonics in the load can be cancelled in the grid side voltage. Furthermore, since a series voltage is induced in the line, it is possible to compensate for voltage sags and voltage unbalance [13]. However, in this project the series active filter is not included since the voltage THD of the Helius CHP is below the standard limits.

Another option is to combine an active filter and a passive filter, which is called a hybrid active filter. A hybrid active filter solution is shown in Fig. 3.24.

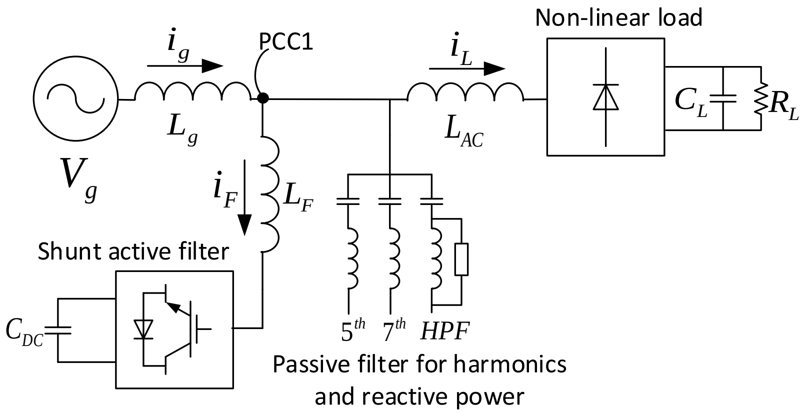

Figure 3.24. Simplified circuit of a hybrid active filter with a shunt active filter and a passive filter.

For this topology it is possible to reduce the required power rating of the active filter, by using a passive filter to compensate specific harmonics. Or alternatively use the passive filter for reactive power compensation, which also reduces the power rating of the active filter. Although it may be able to reduce the rating of the active filter, the hybrid filter has the same drawbacks as the passive filter, and therefore resonance damping is required, the flexibility after installation is limited, and size/volume of passive components. Therefore, this project is focused on a shunt active power filter.

3.6 Summary

In the Helius CHP a large amount of the non-linear loads, are the adjustable speed drive loads using diode rectifiers. Even though this is a simple and cheap solution, it introduces a highly distorted line current with harmonic currents of order $6n \cdot 50$Hz. To model the ASD's the motors are replaced with variable resistors, which is used to keep the power on the machine side constant. The machine side is modelled as a variable resistor, since the harmonics are not passed from the machine side if the DC capacitor of the ASD acts as a decoupling, by ensuring a constant DC voltage. The THD is though dependent on the DC and AC side inductors, where the DC inductor has more influence at lower values of inductance for a low power system, while the influence of the DC inductor is not significant for a high power ASD compared to the AC side inductor. The transformer was shown to have a small influence on the current THD. However, the losses of the transformer increases with an increasing current THD. Based on the ASD and the transformer model a simulation model was created to analyse the performance of the Helius CHP.

Control Strategy for Active Power Filter 4

This chapter presents different current control strategies used in an APF. As stated the objective of the shunt active power filter is to remove harmonic components in a current by generating a current which contains the same harmonic component with the same magnitude but with reverse polarity, and therefore cancelling the harmonic components in the total line current. The general control structure of the APF can be seen in Fig. 4.1.

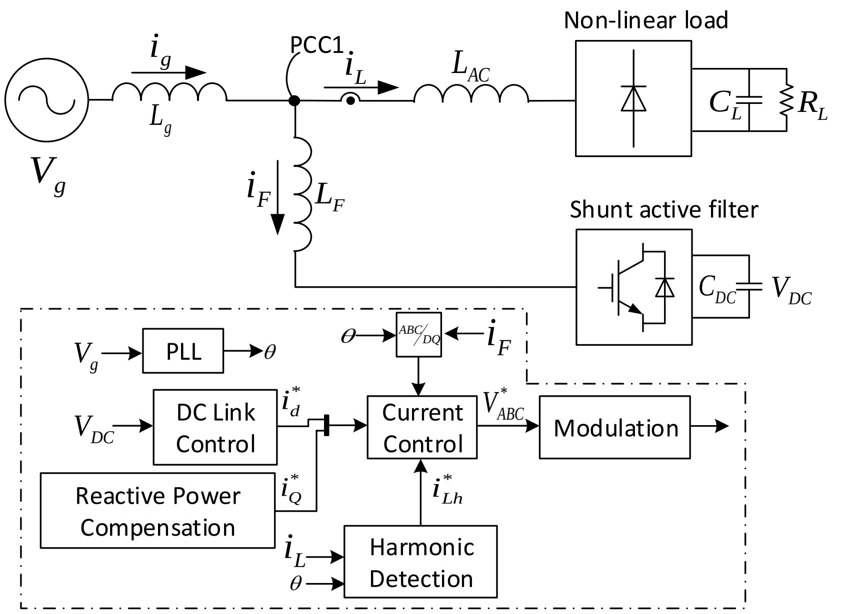

Figure 4.1. Overview of APF control system.

In addition to the standard control of a grid connected converter, the control consists of harmonic detection and harmonic current controllers. The harmonic detection selects the harmonic components in the line current and passes this signal through a filter and then uses it as the reference for the harmonic current controller. Different control solutions for harmonic compensation can be seen in Fig. 4.2.

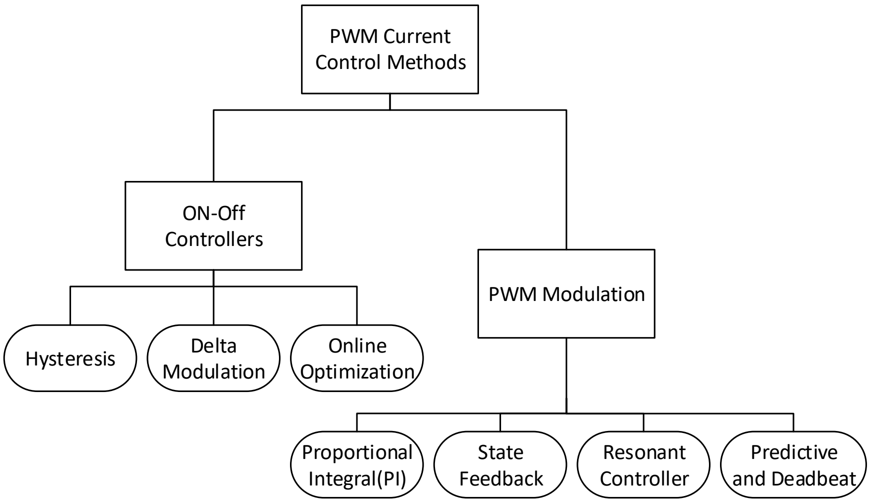

Figure 4.2. Overview of applicable current controllers of APF [7].

As seen different controllers can be used to compensate for harmonic components in the load current. The difference between the on/off controllers and the PWM modulated controllers is, that on/off controllers control the state of the switches directly, while the PWM modulated controllers generate a voltage reference from which a modulation method, such as space vector modulation, is used. Besides the harmonic current controllers, another specification of the APF is to be able to handle reactive power compensation simultaneous with the harmonic mitigation.

4.1 Control of Grid Connected Voltage Source Converters

The connection and power flow of the active power filter converter at PCC1 can be simplified to the schematic shown in Fig. 4.3. Where Z_{eq} is the equivalent impedance of any line and filter impedance, between the converter and the PCC1.

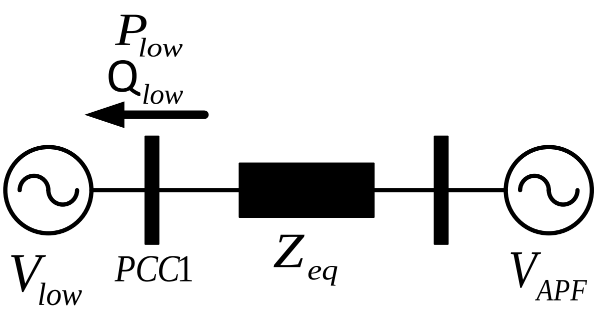

Figure 4.3. Simplified diagram of the active power filter and PCC1 connection.

Assuming that the impedance, Z_{eq}, is inductive such that $X_{L,eq} >> R_{eq}$ and the filter capacitors (if any) are restricted in reactive power consumption [20], then the active and reactive power flow is given by:

$$P_{low} = \frac{V_{APF} \cdot V_{low}}{X_{L,eq}} sin(\phi) \tag{4.1}$$

$$Q_{low} = \frac{V_{APF}}{X_{L,eq}} \left(V_{APF} \cdot cos(\phi) - V_{low}\right) \tag{4.2}$$

where ϕ is the angle between the voltages V_{APF} and V_{low} [20],[21]. When ϕ is small, $sin(\phi) \approx \phi$ and $cos(\phi) \approx 1$, thus the power flow equations are simplified to:

$$P_{low} \approx \frac{V_{APF} \cdot V_{low}}{X_{L,eq}} \phi \tag{4.3}$$

$$Q_{low} \approx \frac{V_{low}}{X_{L,eq}} \left(V_{APF} - V_{low}\right) \tag{4.4}$$

From these equations the active power flow is seen to be dependent on the phase angle between the two voltage sources, while the reactive power flow is dependent on the voltage magnitude between the two sources.

Instead of directly specifying the voltage magnitude and phase angle, it is possible to indirectly control the voltage by using current control. In the synchronous reference frame the instantaneous active and reactive power is given by:

$$P = \frac{3}{2} \left(V_d i_d + V_q i_q\right) \tag{4.5}$$

$$Q = \frac{3}{2} \left(V_q i_d - V_d i_q\right) \tag{4.6}$$

To enable the control, a Phase Locked Loop (PLL) is used to synchronize the control operation to the grid voltage phase and frequency, which is used to do the park transformations. The block diagram of the PLL is shown in Fig. 4.4.

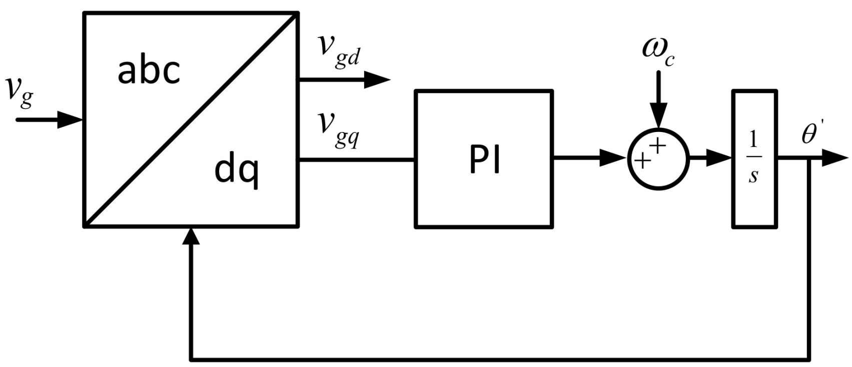

Figure 4.4. Block diagram of the PLL in the dq reference frame [20].

In the PLL the grid voltage q component, V_{gq}, is controlled to be zero using a PI controller, thus V_{gd} is equal to the magnitude of the grid phase voltage and aligned with phase-A. The grid frequency and therefore the phase can be extracted by integrating the output of the PI controller [20]. Since V_q is zero by using the PLL, the active and reactive instantaneous power from Eq. 4.5 and Eq. 4.6 can be reduced to:

$$P = \frac{3}{2}\left(V_d i_d\right) \tag{4.7}$$

$$Q = \frac{3}{2}\left(-V_d i_q\right) \tag{4.8}$$

which implies that the active power can be controlled by i_d, and the reactive power can be controlled by i_q. The basic circuit to control the current can be seen in Fig. 4.5.

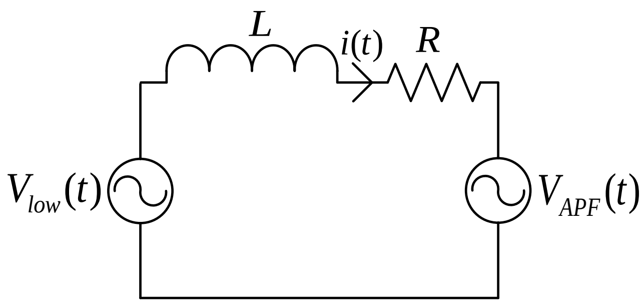

Figure 4.5. Simplified circuit of the active power filter at the PCC1 connection.

From Fig. 4.5 the governing voltage equation can be derived:

$$V_{APF}(t) = R \cdot i(t) + L\frac{di(t)}{dt} + V_{low}(t) \tag{4.9}$$

where L is the equivalent inductance of the line and any filter inductance, and R is the equivalent resistance. Instead of employing the control system in the natural three phase frame, Eq. 4.9 can be transformed into the synchronous frame using the park transformation [20], which yields:

$$V_{APF,d} = R \cdot i_d + L\frac{di_d}{dt} - \omega L i_q + V_{low,d} \tag{4.10}$$

$$V_{APF,q} = R \cdot i_q + L\frac{di_q}{dt} + \omega L i_d + V_{low,q} \tag{4.11}$$

To enable the current control from the governing voltage equations, PI controllers are used to generate the voltage references, V_d and V_q, to the PWM modulation. The PI controllers are therefore tuned according to the plant:

$$G_i(s) = \frac{V_d}{i_d}(s) = \frac{V_q}{i_q}(s) = \frac{1}{L_F \cdot s + R_F} \tag{4.12}$$

However, from the voltage equations it is seen that there are cross couplings between the d-axis and q-axis governing equations. To eliminate the cross couplings these terms are added as feed forward signals. Furthermore, the low voltage stage voltages ($V_{low,d}$ and $V_{low,q}$) are added as feed forward signals as well. The current control diagram with PI controllers, cross coupling feed forward terms, and grid voltage feed forward terms are shown in Fig. 4.6.

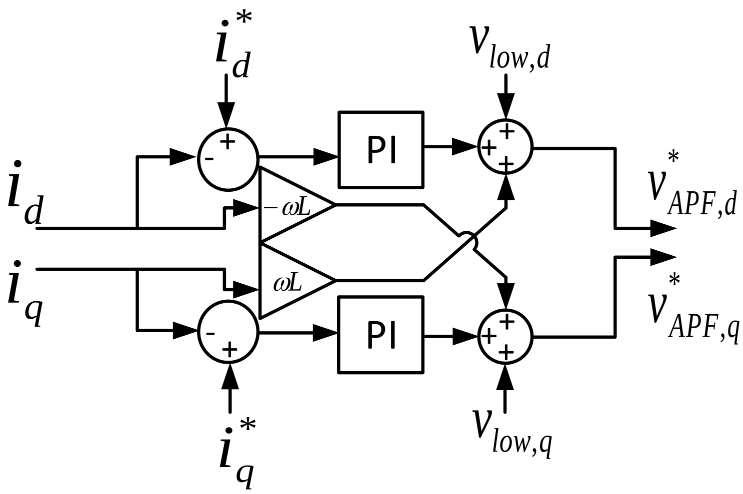

Figure 4.6. Current control diagram with cross coupling and voltage feed forward terms [20].

Besides the PI controller and the plant, the addition of a first order digital delay approximation can be used to compensate for the delay in the digital controller, which includes time delays due to PWM generation, sampling and calculation. According to [20], the first order time delay approximation is given by:

$$G_{Delay} = \frac{1}{1.5 \cdot T_s \cdot s + 1} \tag{4.13}$$

where T_s is the sampling time of the digital controller. The current loop block diagram to design the current controller and investigate the stability is shown in Fig. 4.7.

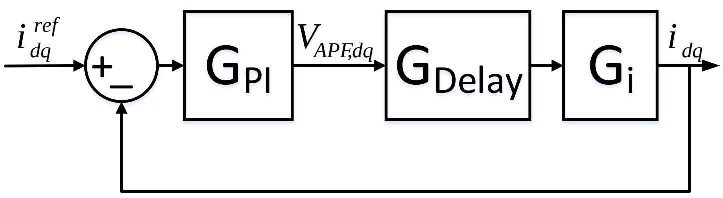

Figure 4.7. Current control block diagram including digital time delay transfer function.

The open loop transfer function of Fig. 4.7 is given by:

$$G_{ol} = \frac{K_i}{R} \frac{\frac{K_p}{K_i} s + 1}{s\,(1.5 \cdot T_s \cdot s + 1)\left(\frac{L}{R} s + 1\right)} \tag{4.14}$$

To design the PI controller one strategy is to choose $\frac{K_p}{K_i} = \frac{L}{R}$. The advantage of this choice is that the dominant pole of the current loop plant is cancelled thus increasing the bandwidth of the closed loop system, and it reduces the open loop transfer function to a second order transfer function instead of a third order transfer function. The proportional gain K_p can be chosen based on achieving a damping ratio of 0.707, which yields [22]:

$$K_p = \frac{L}{3T_s} \tag{4.15}$$

Then K_i can be calculated from the relation $\frac{K_p}{K_i} = \frac{L}{R}$.

The practical implementation of the grid connected converter is often to use an LCL filter instead of a single L filter at the converter output. This is due to the better harmonic attenuation for the switching frequencies and side-bands, since the LCL filter in theory have 60 $^{dB}/_{decade}$ attenuation after the resonance frequency compared with the 20 $^{dB}/_{decade}$ attenuation of the single L filter. Therefore, the single L filter can be large and bulky compared to an LCL filter, which can use smaller components [20]. The PI controller design of this section can still be used, even though an LCL filter is installed, since the LCL and L filter have the same frequency response before the resonance frequency of the LCL filter as shown in Fig. 4.8.

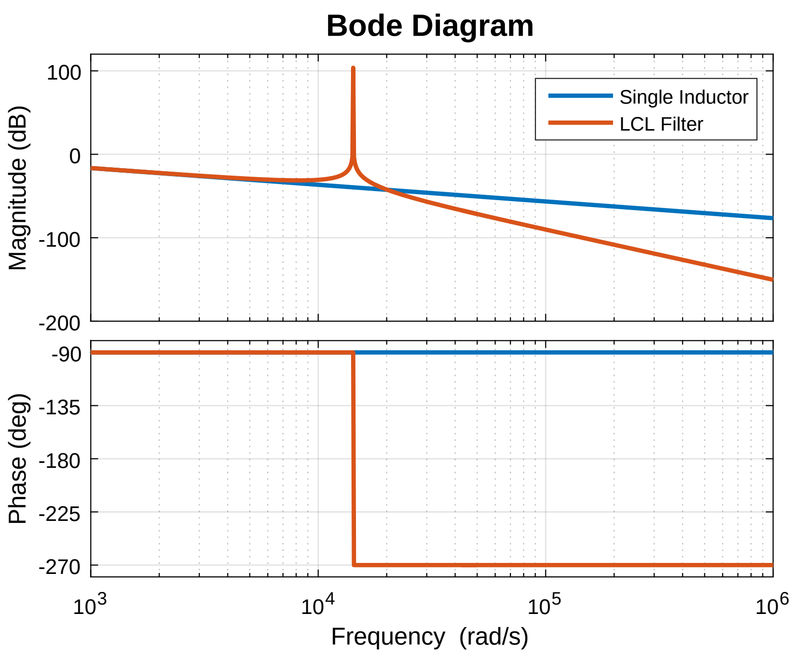

Figure 4.8. Frequency response comparison of a single inductor and an LCL filter.

The single inductor is chosen as the total inductance of the LCL filter, and the LCL filter is designed according to [20]. The stability should however be re-evaluated using the LCL filter transfer function after designing the PI controller, because of the response of the LCL filter at and above the resonance frequency, although the resonance is damped either passively or actively.

4.2 Active Power Filter Control

The most common control strategy used for the APF control [7], is shown in Fig. 4.9.

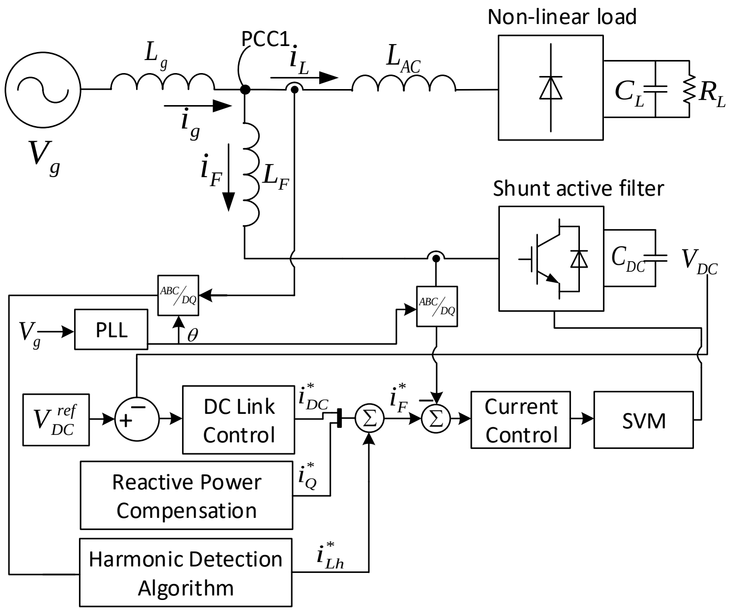

Figure 4.9. Simplified control diagram of an APF.

The DC link capacitor is usually charged by drawing current from the grid [7], which saves the need of an auxiliary DC link charger, but requires a DC link voltage control loop. Therefore, the control strategy consists of an outer DC link voltage loop, which keeps the DC link voltage constant. Since the DC link capacitor can be charged by drawing more active power to the capacitor, the output of the DC link voltage controller is the active power current reference, required to maintain the DC link voltage constant. Normally a PI controller is used for the DC link loop, due to the constant voltage reference [7].

To draw the current harmonics generated by the non-linear loads, a harmonic detection algorithm is used to generate the harmonic current reference. The operation of the harmonic detection algorithm is to extract the harmonic current components from the load side current, and discard the fundamental component. The harmonic detection method will be proven in a later section.

Another option of the APF control is to enable reactive power compensation. This also adds to the current reference, and needs a reactive power current reference generation to track the reactive power to be compensated for. This could be an interesting option for the Helius CHP, due to the directly connected AC machines which have a poor power factor as described in Sec. 1.1. If reactive power compensation is applied and the harmonic mitigation is unchanged, the current drawn by the APF will increase, which in turn increases the required power rating of the APF. Another option could be to limit the harmonic mitigation, and use the rest of the available power for reactive power compensation. Reactive power compensation can be a viable option for the Helius CHP since the current distortion limits are not very stringent.

When the reference current is generated, depending on the DC link capacitor charging, the reactive power compensation, and the harmonic current detection, an inner current loop is used to track the current reference. Compared to other grid connected voltage source converters, the inner current controller of the APF is challenged by the shape of the current reference, since it contains the harmonic current components and not only the fundamental component. The PI controller is not very efficient to track the harmonic reference current [20]. As a simulation example a PI controller with $K_p = 10$ and $K_i = 1000$ is used to track a 250 Hz sinusoidal signal, for a LR plant. The controller performance after reaching steady state is shown in Fig. 4.10(a) and Fig. 4.10(b) respectively.

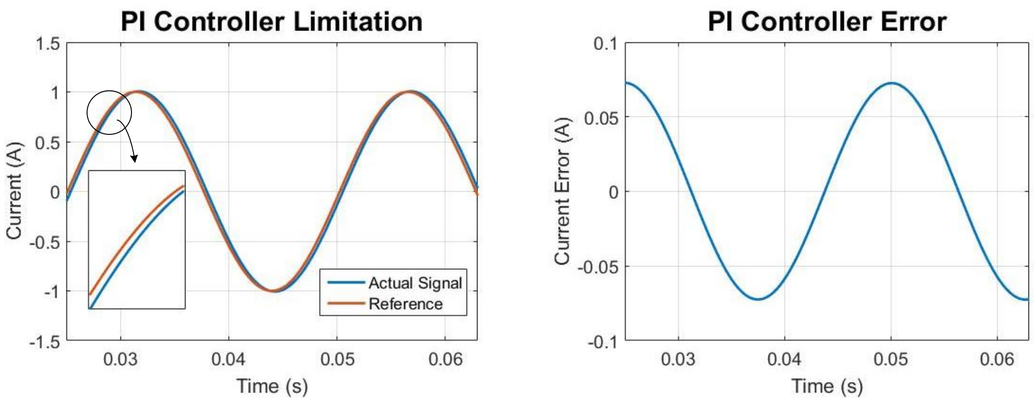

(a) (b)

Figure 4.10. Simulated PI controller tracking a 250 Hz sinusoidal waveform where a) is the reference and actual output b) is the error signal fed to the PI controller.

As seen the PI controller has a steady state error, which is not eliminated. The controller gains could be increased however, the steady state error can only be minimised and not removed, and furthermore it might decrease stability and reach the bandwidth limit for a discrete system. Even though the PI controller cannot track the harmonic reference without an error, the PI controller can still be used to control the fundamental component and therefore the active and reactive power flow. Therefore the analysis and design from Sec. 4.1 sill applies for these PI controllers. To track the harmonic current reference there are different controller types which can be used, some of them are shown in Fig. 4.11.

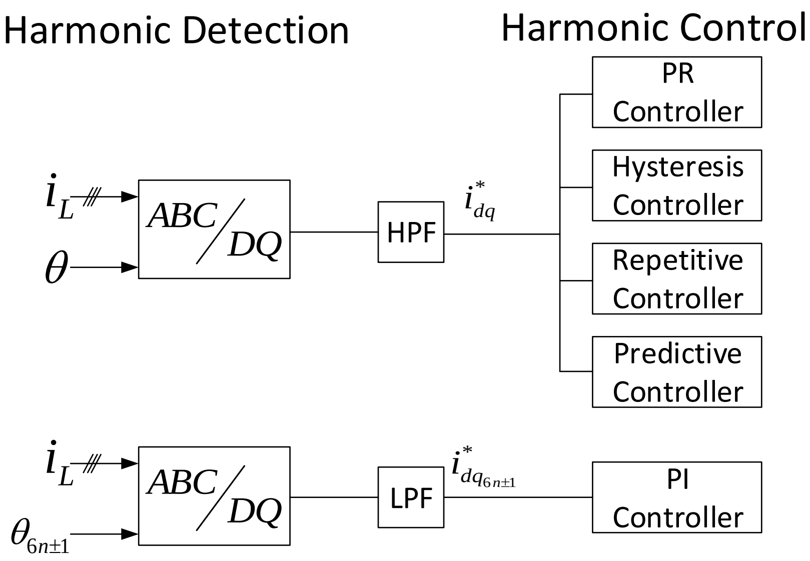

Figure 4.11. Overview of different control methods of harmonic detection and control.

Hysteresis control is a control strategy where a hysteresis band limits the maximum ripple allowed on the current/voltage desired to control. If the reference current/voltage rises very rapidly, then the switching frequency for that moment will increase and the switching frequency will not be constant. A non constant switching frequency is not preferable since it might create timing issues since the sampling frequency is normally kept constant. Furthermore, loss modelling and estimation of switching losses are complicated by a non constant switching frequency. Therefore, the hysteresis controller is not included in this project.

Predictive control is based on predicting the current or voltage ahead in time, and in this way use the prediction to control the plant output. The predictive control method is usually based on the governing equations of the plant, and using approximations of derivatives to calculate the predictions. Since predictive control is based on the governing equations of the plant, an issue that arises is the parameter sensitivity and being able to estimate the plant parameters with a high accuracy. Another drawback of predictive control is that the controller is based on optimization algorithms, which increases the complexity of the control system. For these reasons the predictive controller is not investigated in this project.

So in this project the proportional resonant controller, repetitive controller, and high frequency PI controller will be further studied.

4.2.1 DC Capacitor Voltage Control

To control and maintain a constant DC voltage, an outer control loop is used as shown in Fig. 4.9. Since the capacitor can be charged by drawing active power to the capacitor from the grid, the DC voltage can be controlled using the d-axis current, i_d [20]. The DC link circuit is shown in Fig. 4.12.

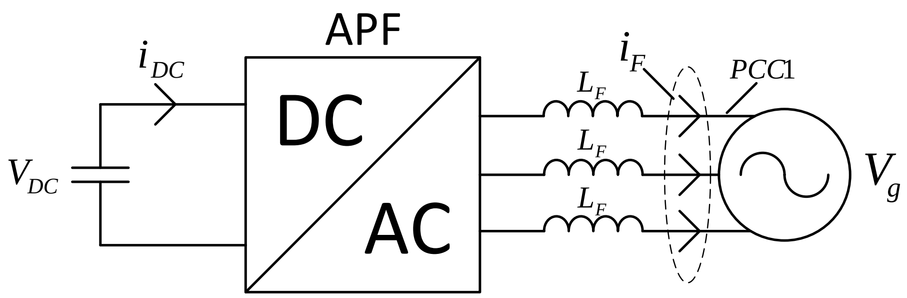

Figure 4.12. Circuit diagram of DC capacitor and grid connection.

The inductance L_f in the figure is the filter inductance of the APF. The instantaneous power relation through the converter, without considering any losses, is given by:

$$\frac{3}{2}\left(v_{gd}i_{fd} + v_{gq}i_{fq}\right) = v_{DC} \cdot C\frac{dv_{DC}}{dt} \tag{4.16}$$

To model the control dynamics, the small signal linearisation theory is used for Eq. 4.16. The small signal linearisation is employed by defining each variable with a constant DC value and a small signal perturbation as:

$$x = X + \hat{x} \tag{4.17}$$

where x is the original variable, X is the DC part of x, and $\hat{x}$ is the small signal perturbation. Using this for Eq. 4.16, the result is:

$$\frac{3}{2}\left[\left(V_{gd} + \hat{v}_{gd}\right)\left(I_{fd} + \hat{i}_{fd}\right) + \left(V_{gq} + \hat{v}_{gq}\right)\left(I_{fq} + \hat{i}_{fq}\right)\right] = \left(V_{DC} + \hat{v}_{DC}\right)C\frac{d\left(V_{DC} + \hat{v}_{DC}\right)}{dt} \tag{4.18}$$

Since the transfer function desired is the d-axis current relation to the DC voltage thus $\frac{\hat{v}_{DC}}{\hat{i}_{fd}}$, the other small signal perturbations are therefore assumed to be zero. Furthermore the second order small signal perturbations are neglected [20]. By applying these assumptions the AC part of Eq. 4.18 can be reduced to:

$$\frac{3}{2}V_{gd}\hat{i}_{fd} = V_{DC} \cdot C\frac{\hat{v}_{DC}}{dt} \tag{4.19}$$

This equation can be written in the Laplace domain as:

$$\frac{3}{2}V_{gd}\hat{i}_{fd} = \hat{v}_{DC} \cdot V_{DC} \cdot Cs \tag{4.20}$$

The choice of DC capacitor voltage is based on the grid voltage at the connection of the converter. To ensure the correct power flow, and therefore enable current control the DC capacitor voltage should follow $V_{gd} \cdot \sqrt{3} < V_{DC}$. Furthermore, a too large DC capacitor voltage increases the losses of the switches in the converter. Thus for this analysis it is assumed that $V_{DC} = V_{gd} \cdot \sqrt{3} \Leftrightarrow V_{gd} = \frac{V_{DC}}{\sqrt{3}}$ [20]. Using this to replace V_{gd} in Eq. 4.20 the result is:

$$\frac{\sqrt{3}}{2}\hat{i}_{fd} = \hat{v}_{DC} \cdot Cs \tag{4.21}$$

Now the transfer function $\frac{\hat{v}_{DC}}{\hat{i}_{fd}}$ can be found:

$$\frac{\hat{v}_{DC}}{\hat{i}_{fd}} = \frac{\sqrt{3}}{2}\frac{1}{Cs} \tag{4.22}$$

The control loop of the DC capacitor voltage can therefore be seen in Fig. 4.13.

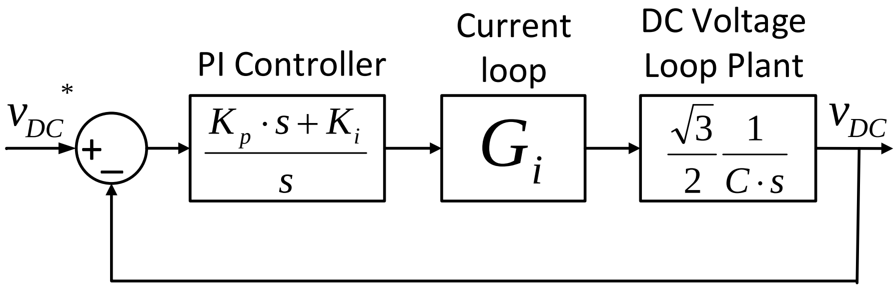

Figure 4.13. DC capacitor voltage control loop diagram.

The current loop is the fundamental current control loop of i_d with the PI controllers, since the output of the DC voltage controller is the i_d reference. Instead of using the full transfer function of the current loop as shown in Sec. 4.1, [20] suggests to approximate the current loop with a first order system using the bandwidth of the current loop. According to [20] the bandwidth of the current loop when the PI controller is tuned to cancel the dominant pole, is given by $\omega_{Bi} \approx \frac{1}{3T_s}$ thus the current control loop approximation is given by:

$$G_i \approx \frac{1}{3T_s s + 1} \tag{4.23}$$

The open loop transfer function of the DC voltage loop, to design the PI controller from, is therefore given by:

$$G_{DC} = \frac{\sqrt{3}}{2}\frac{K_p s + K_i}{C\,(3T_s s + 1)\,s^2} \tag{4.24}$$

4.2.2 Harmonic Detection of Load Current

To generate the harmonic current reference for the harmonic current controller, a harmonic detection method of the ASD load current is necessary. The objective of the harmonic detection method is to extract all the harmonic current content of the ASD load current and discard the fundamental current component. In [7] it was shown that the effectiveness of the harmonic mitigation in an active filter, depends on the choice and accuracy of the harmonic detection method. It was concluded, in [7], using a harmonic detection comparison that transforming the load current to the dq-reference frame and using a high pass filter (HPF) to attenuate the 50 Hz fundamental DC component have the best performance. The transfer function of the second order high pass filter is shown in Eq. 4.25.

$$G_{HPF} = \frac{s^2}{s^2 + 2\zeta\omega_n s + \omega_n^2} \tag{4.25}$$

Using a cut-off frequency of $\omega_n = 300$ rad/s and a damping coefficient of $\zeta = 0.8$, the frequency response can be seen in Fig. 4.14.

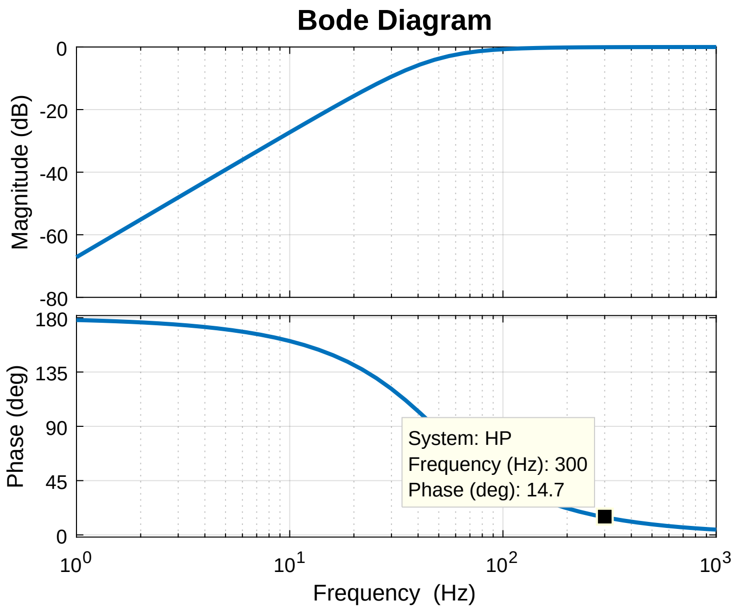

Figure 4.14. Frequency response of a standard second order high pass filter from Eq. 4.25 with $\omega_n = 300$ rad/s, and $\zeta = 0.8$.

As seen in Fig. 4.14 the high pass filter attenuates below 300 rad/s. A problem with the high pass filter is that it has a phase angle different from zero degree (14.7°) at 300 Hz, corresponding to the 5^{th} and 7^{th} harmonic, as indicated in Fig. 4.14. This may create a phase shift in the generated active filter current compared to the load current. One solution can be to decrease the damping coefficient, however this also increases the magnitude peak at the cut off frequency. Another solution to this problem is to implement the high pass filter by using a low pass filter (LPF), by using:

$$HPF = 1 - LPF \tag{4.26}$$

suggested by [7]. The frequency response of Eq. 4.26 and the frequency response of a 1st order high pass filter compared to the high pass filter in Fig. 4.14 is shown in Fig. 4.15.

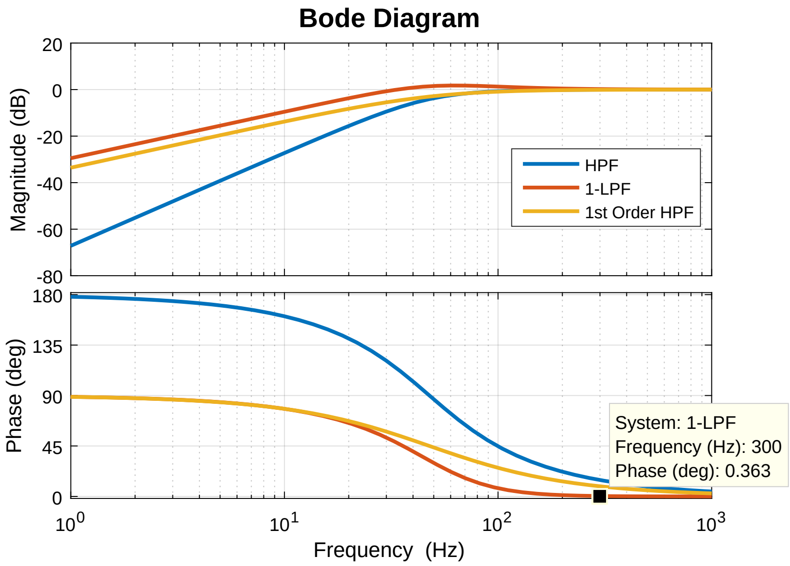

Figure 4.15. Frequency response comparison of different high pass filter implementations.

As seen the phase shift at 300 Hz is minimised to 0.363°. Eq. 4.26 does not give the standard second order high pass filter, when the low pass filter used is the standard second order low pass filter, as shown in Eq. 4.27.

$$\frac{s^2}{s^2 + 2\zeta\omega_n s + \omega_n^2} \neq 1 - \frac{\omega_n^2}{s^2 + 2\zeta\omega_n s + \omega_n^2} \tag{4.27}$$

This is only true for the first order filters, and not for higher order filters. Therefore some zeros are included in the HPF when using the implementation of Eq. 4.26, which has the disadvantage that it decreases the attenuation before the cut off frequency, which is seen in Fig. 4.15. The transfer function of the high pass filter using Eq. 4.26 is given by:

$$\frac{s^2 + 480s}{s^2 + 480s + 90000} \tag{4.28}$$

The high pass filter implementations will be experimentally verified in the experimental chapter.

4.2.3 Resonant Controllers

The controller solution using resonant controllers is actually a combination of PI controllers and resonant controllers. The solution can be realised in the dq-reference frame where two

PI controllers are regulating the required active power current to maintain a constant DC link voltage, and regulating the corresponding reactive power current to enable reactive power compensation. To track the harmonic load currents, resonant controllers are used for each desired harmonic to be mitigated. The combined solution using PI and resonant controllers is shown in Fig. 4.16.

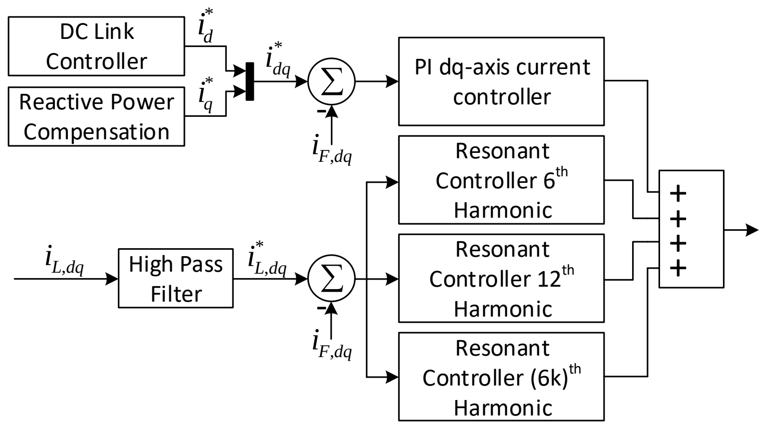

Figure 4.16. Resonant current control diagram using the dq reference frame.

An advantage of using the dq reference frame is that the harmonic pair 5^{th} and 7^{th} translates to the 6^{th} harmonic, the 11^{th} and 13^{th} translates to the 12^{th} harmonic, and so on. Therefore, it is possible to use a single resonant controller to compensate for each harmonic pairs.

The principle of resonant controllers is to attenuate or amplify only at a specific resonant frequency or at multiple resonant frequencies. In theory it is possible to have an infinite gain at the resonant frequency, as shown in Fig. 4.17, which can remove or amplify the resonance frequency for a given input signal. In the active filter current controller this principle can be used to track the harmonic current components of the load current. To ensure a constant DC link voltage and reactive power compensation, PI controllers can be used. Therefore, the output of the combined current controller is the sum of the required active and reactive power and the required harmonic current to attenuate the load side current harmonics. A type of resonant controller used in grid connected converters is the proportional resonant (PR) controller. The transfer function of the PR controller is given by:

$$G_{PR}(s) = K_p + K_i \frac{s}{s^2 + \omega_{res}^2} \tag{4.29}$$

where K_p is the proportional gain, K_i is the integral gain, and ω_{res} is the resonant frequency. The gain at the resonant frequency is infinite, which can be seen from the denominator:

$$s^2 + \omega_{res}^2 = (j\omega_{res})^2 + \omega_{res}^2 = -\omega_{res}^2 + \omega_{res}^2 = 0 \tag{4.30}$$

With a denominator of zero the gain is infinite. The PR is similar to the PI controller, however the PR uses a generalized integrator, which only integrates close to the resonant frequency thus only introducing phase shift at or close to the resonant frequency. Therefore, there is no attenuation/amplification on both sides of the resonant frequency. A Bode diagram of a PR controller with controller gains of 1 and a resonant frequency of 50 Hz is shown in Fig 4.17.

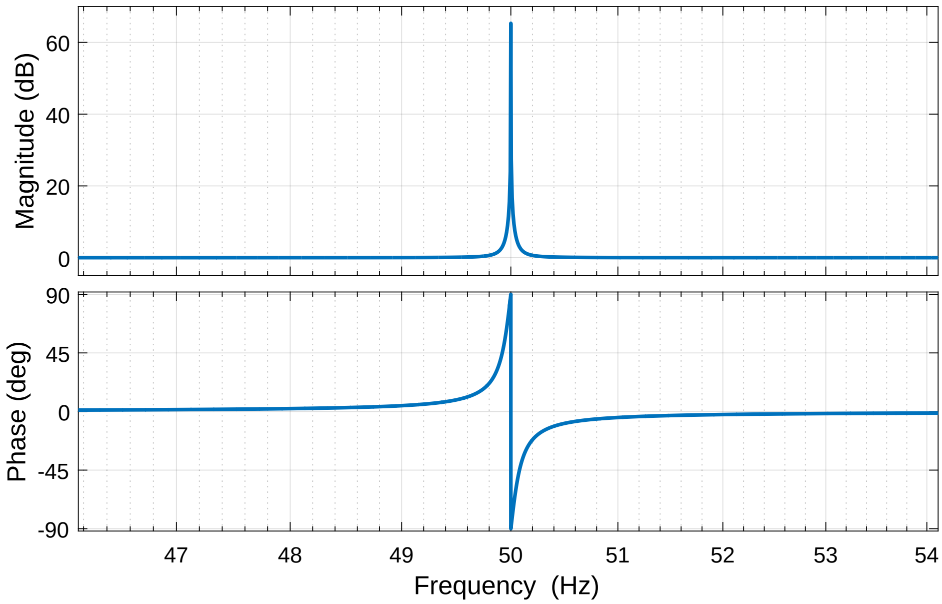

Figure 4.17. Resonant controller with controller gains of $K_p = K_i = 1$ with resonant frequency at 50 Hz.

Before designing the controller the effect of the controller gains is analysed. The effect of the proportional gain can be seen in Fig. 4.18.

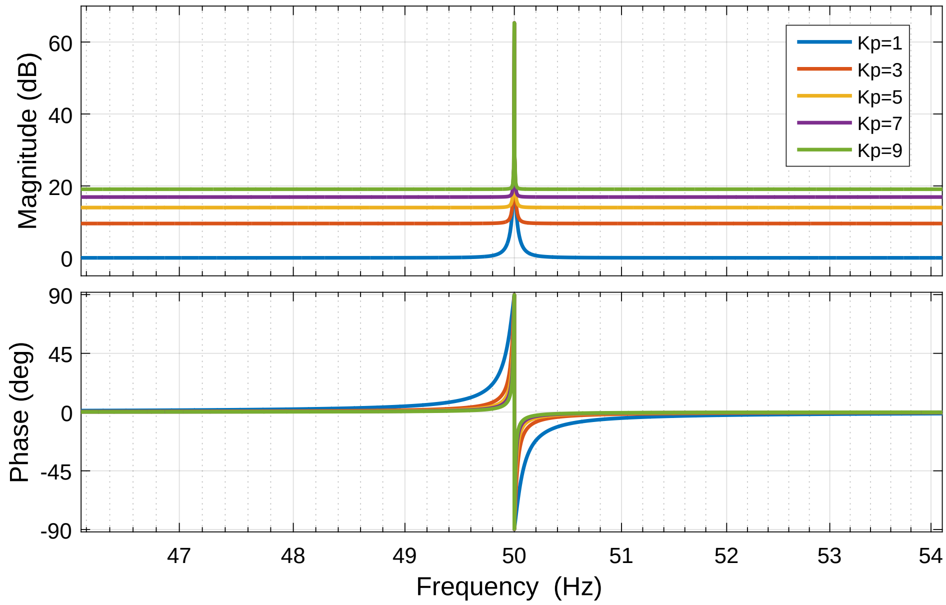

Figure 4.18. Resonant controller with a proportional gain of $K_p = [1:9]$ at resonant frequency at 50 Hz.

As stated for all other frequencies, the controller acts as a proportional gain, thereby the gain of the controller is increased with the proportional gain. When changing K_i and keeping K_p constant the effect on the controller can be seen in Fig. 4.19.

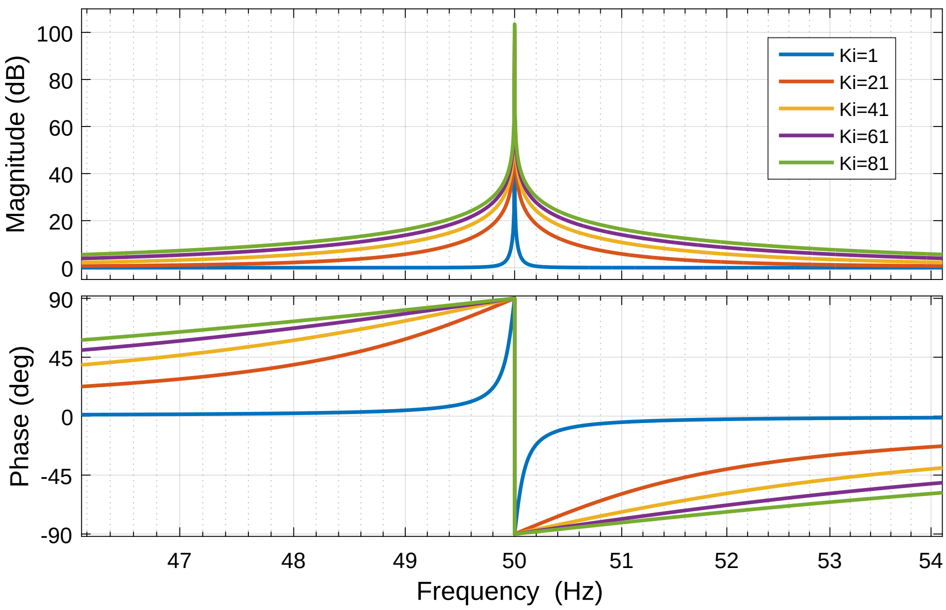

Figure 4.19. Resonant controller with a resonant gain of $K_i = [1:81]$ at resonant frequency at 50 Hz.

As seen in Fig. 4.19, K_i controls how narrow the magnitude and phase response is around the resonant frequency.

4.2.4 Repetitive Controller

Another controller type, which is based on a principle called "The internal model principle", is the repetitive controller. The internal model principle states that to track or reject a given input signal with zero steady state error, a generator (or model) of the input signal must be included in the control loop [23], [24]. In the classical control theory, this principle is used to determine the type of controller necessary to track a given reference signal. As an example to track a step input, which is described as $\frac{1}{s}$ in the Laplace domain, the open loop transfer function must include a free integrator. For periodic input signals, the reference generator to be included in the control loop is called a repetitive controller. The basic transfer function of the repetitive controller [23], [24], G_r, is given by:

$$G_r(s) = \frac{e^{-T_p \cdot s}}{1 - e^{-T_p \cdot s}} \tag{4.31}$$

where T_p is the period of the periodic signal. The transfer function of Eq. 4.31 can be represented as a positive feedback loop as shown in Fig. 4.20.

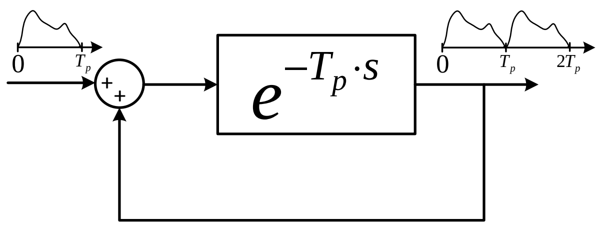

Figure 4.20. Basic repetitive controller for tracking/rejecting periodic signals where T_d represents the periodic signal.

The magnitude response of Eq. 4.31 has infinite gain at the frequencies ${}^{n}/_{T_p}$, where $n = 1, 2, 3...\infty$, and therefore also poles at $s \pm j\frac{n}{T_p}$ [23]. When assuming the closed loop system is stable, the steady state error is zero at these frequencies. A frequency response example using a 50 Hz periodic repetitive controller is shown in Fig. 4.21.

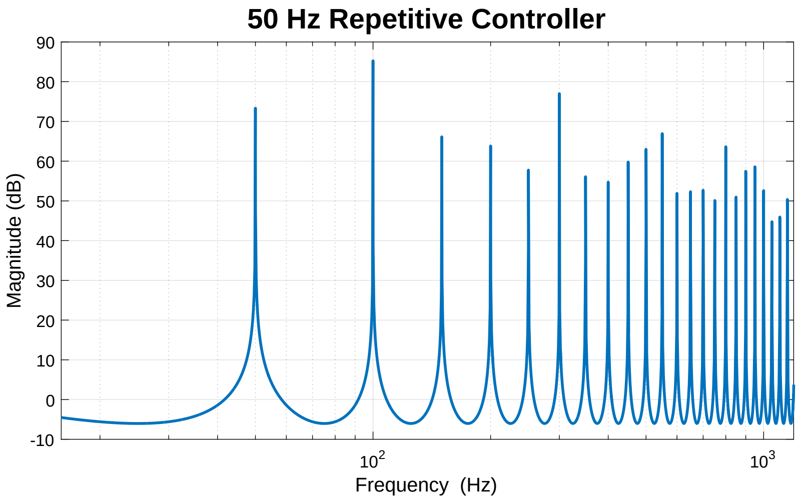

Figure 4.21. Magnitude plot for a 50 Hz repetitive controller.

As seen the gain is large (theoretically infinite) at each 50 Hz harmonic component. The delay terms $e^{-T_p \cdot s}$ however, complicates the analysis of the controller and interaction with the plant, due to the non rational form. In discrete time the analysis is simpler, if the sampling frequency is an integer of the periodic signal frequency. If that is true then the delay term is given by z^{-N}. Therefore, in the discrete time domain, the repetitive controller is given by [24]:

$$G_r(z) = \frac{z^{-N}}{1 - z^{-N}} \tag{4.32}$$

where $N = {}^{T_p}/_{T_s}$, and T_s is the sampling time. Besides the desire of choosing T_s, such that N becomes an integer, it should also be noted that the discrete repetitive controller only can track/reject frequencies below the Nyquist frequency. The problem of ensuring N to be an integer will be discussed later.

Since the harmonic load current frequencies to be tracked are known to be $6 \cdot 50 \cdot n$ Hz, then the repetitive controller can be simplified to:

$$G_r(z) = \frac{z^{-\frac{N}{6}}}{1 - z^{-\frac{N}{6}}} \tag{4.33}$$

which also reduces the calculations. The frequency response of the fast repetitive controller in Eq. 4.33 tracking a $300n$ Hz signals is shown in Fig. 4.22.

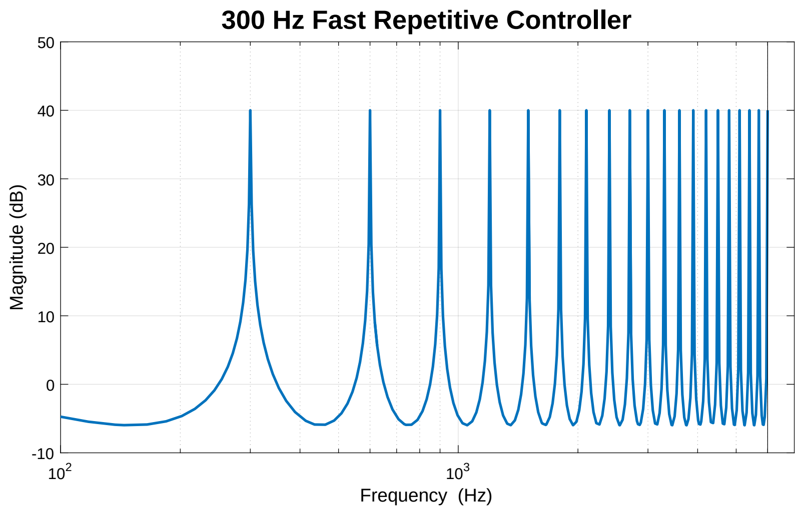

Figure 4.22. Magnitude plot for a 300 Hz fast repetitive controller.

As seen it only has high gains at multiples of 300 Hz. Although the time delay is reduced to $^1/_6$ of the conventional repetitive controller, the dynamic performance and stability is still challenged by the time delay terms included in the repetitive controller. Therefore one solution is to aid the repetitive controller by using a PI controller, which is designed for a dynamic response and to ensure stability. This type of cascaded control using a repetitive controller is referred to as a "plug-in repetitive controller" [25]. The concept of the plug-in repetitive controller is shown in Fig. 4.23.

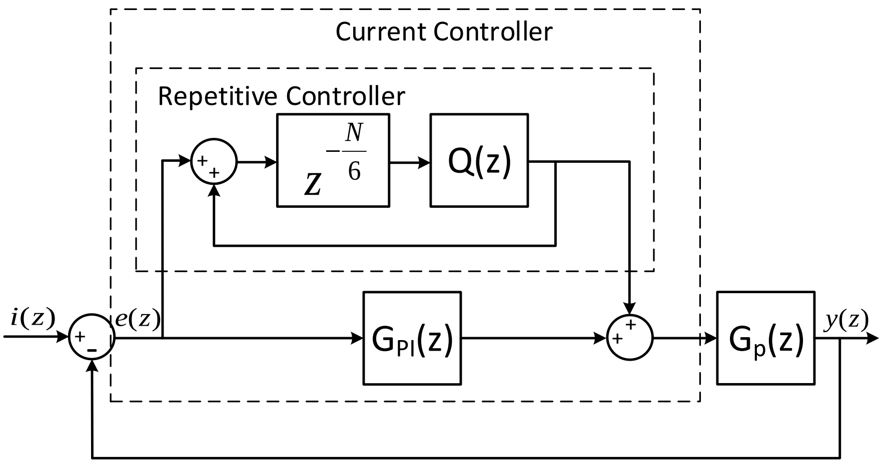

Figure 4.23. A fast discrete repetitive controller used as a plug-in controller, with a PI controller.

Compared with the discrete repetitive controller of Eq. 4.33, the plug-in repetitive controller uses a low pass filter $Q(z)$ to increase the stability of the control loop [24], [25]. Without the low pass filter ($Q(z) = 1$), all the open loop poles of the repetitive controller are located on the unit circle.

To ensure stability of the closed loop system shown in Fig. 4.23, there are two stability criteria, which should be satisfied [23], [24]:

1) The closed loop system, G_{cl}, given by:

$$G_{cl}(z) = \frac{G_{PI}(z)G_p(z)}{1 + G_{PI}(z)G_p(z)} \tag{4.34}$$

excluding the repetitive controller, but including the PI controller should be stable. Where $G_p(z)$ is the plant transfer function in the discrete time domain.

2) The following condition is satisfied:

$$\big|H(z)\big| = \big|Q(z) - Q(z)G_{cl}(z)\big| < 1 \tag{4.35}$$

A benefit of the repetitive controller is that it is only a single controller which has to be inserted in the control loop, to compensate all harmonics below the Nyquist frequency. The major drawback of the repetitive controller however, is that it is based on a time delay implementation using $z^{-\frac{N}{6}}$. As described earlier this is simple if $\frac{N}{6}$ is an integer, but there might be situations where this is not possible. As an example, if the sampling frequency is chosen to be 10 kHz, then $\frac{N}{6} = \frac{10000/50}{6} = 33.3$, thus not an integer. For $\frac{N}{6}$ to be an integer it is also assumed that the grid frequency is constant, however as reported in [26], this is not always true. In this situation $\frac{N}{6}$ might be an integer for the designed grid frequency, and if the grid frequency changes $\frac{N}{6}$ might not be an integer any more. A non integer $\frac{N}{6}$ can be compensated using discrete approximations of the discrete time delay term $z^{-\frac{N}{6}}$ as reported in [26]. The approximation used in [26] has the drawback that it increases implementation complexity, and that the harmonic mitigation performance with a non integer $\frac{N}{6}$ is worse than with an integer.

4.2.5 High Frequency PI Controller

Instead of using a PR or repetitive controller and a high pass filter to compensate the harmonic components in the line current, a PI controller with fast rotating reference frames can be used. The block diagram of the high frequency PI controller can be seen in Fig. 4.24.

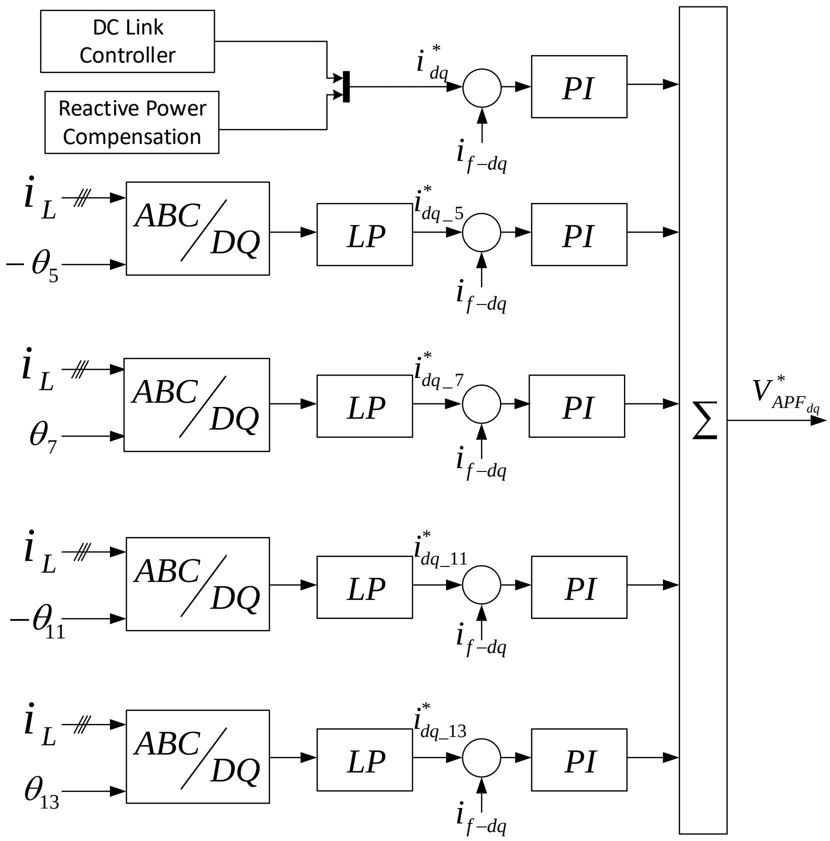

Figure 4.24. Harmonics controller using high frequency PI controllers.

As seen the output for each reference frame transformation is passed through a low pass filter (LPF), this is to remove higher order harmonics, leaving the specific harmonic component as a DC value, thus used as harmonic detection. Designing the PI controllers is done using the same method as the PI controllers in the current control of the converter. This can be done since the plant is the same and the inputs of the high frequency controllers are DC. Furthermore, the 5^{th} and 11^{th} harmonic receive the negative angular velocity of the harmonic component. This is from the rotational direction of all $6n-1$ harmonic components. When investigating the current components of the 5^{th} and 7^{th} harmonics, the rotational direction can be found as:

5^{th} harmonic component	7^{th} harmonic component
$i_{A_5} = sin\,(5 \cdot (\omega \cdot t))$	$i_{A_7} = sin\,(7 \cdot (\omega \cdot t))$
$i_{B_5} = sin\,(5 \cdot (\omega \cdot t + 120°))$	$i_{B_7} = sin\,(7 \cdot (\omega \cdot t + 120°))$
$= sin\,(5 \cdot \omega \cdot t + 600°)$	$= sin\,(7 \cdot \omega \cdot t + 840°)$
$= sin\,(5 \cdot \omega \cdot t - 120°)$	$= sin\,(7 \cdot \omega \cdot t + 120°)$
$i_{C_5} = sin\,(5 \cdot (\omega \cdot t - 120°))$	$i_{C_7} = sin\,(7 \cdot (\omega \cdot t - 120°))$
$= sin\,(5 \cdot \omega \cdot t - 600°)$	$= sin\,(7 \cdot \omega \cdot t - 840°)$
$= sin\,(5 \cdot \omega \cdot t + 120°)$	$= sin\,(7 \cdot \omega \cdot t - 120°)$

Table 4.1. Phase sequence of current for 5^{th} and 7^{th} harmonics.

As seen the phase angles of phase B and C are switched, therefore the 5^{th} harmonic is rotating in the reverse direction compared with the fundamental component. While phase B and C are not reversed for the 7^{th} harmonic component, but is rotating the same direction as the fundamental component. All harmonic components with order of $(6n-1)$ are rotating with the negative angular velocity compared to the fundamental component. Therefore, the reference frame transformation used for harmonic detection for $(6n-1)$ order harmonics receives the negative angle generated by the PLL. As mentioned this control method uses the reference frames for each harmonic component and the angular velocities are generated from the output of the PLL. This can be seen in Fig 4.25.

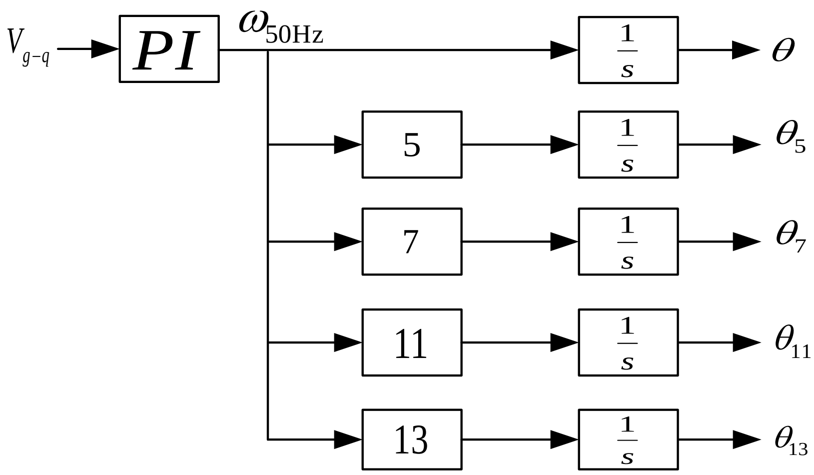

Figure 4.25. PLL for a high frequency controller.

Overall this control method uses more controllers than the PR and repetitive controller, since each harmonic component of interest requires a reference frame transformation and PI controllers for the d and q component. Furthermore, it also uses more filters, for the harmonic detection, since a low pass filter is needed for all harmonics to be mitigated. As an example if the the goal is to cancel harmonics up to the 19^{th} harmonic, the high frequency PI solution requires 12 controllers, 6 reference frame transformations, and 12 low pass filters.

4.2.6 Harmonic Controller Comparison

In terms of the frequency response, the PR with multiple resonant points and the repetitive controller are quite similar. The PR controller has the benefit that it is possible to directly select the desired frequencies to be tracked/rejected, which is not possible with the repetitive controller due to the repetitive nature. Instead the low pass filter in the plug-in repetitive controller can be used to limit the frequencies tracked up to the Nyquist frequency, depending on the cut off frequency of the low pass filter. The high frequency PI controller solution also has the benefit of being able to choose the specific harmonics to be cancelled.

Compared to the PR and the high frequency PI controller solutions, it is not possible to influence the closed loop stability using the plug-in repetitive controller, which is possible for other two solutions due to the K_p and K_i gains of these controllers. This gives an added flexibility in the tuning of the controllers to aid the closed loop stability, but might also introduce coupling between the fundamental PI controller and the harmonic tracking controllers. Alternatively it could be possible to change the closed bandwidth by using the repetitive controller if a gain like K_p of the PR controller is introduced.

As described in Sec 4.2.4, the repetitive controller performance might be limited if the combination of the grid frequency and sampling frequency is not equal to an integer. This is not a problem for the PR and high frequency PI solutions since these are based on the measured/calculated grid angle from the PLL, and not include any delay terms.

When comparing the control complexity, the repetitive controller only requires a single controller and a single high pass filter for the harmonic detection. The PR controller requires also only a single high pass filter, but needs a controller for each harmonic desired to track. The high frequency PI, as described, requires many low pass filters for the harmonic detection, lots of reference frame transformations, and many PI controllers. For these reasons the high frequency PI controller will not be tested further, but the PR and repetitive controller will be designed and tested through simulations and experimental work.

4.3 Summary

To control both the harmonic current mitigation and the reactive power compensation, the APF control system consists of an outer DC voltage loop and an inner current loop with fundamental PI controllers to control the fundamental frequency components, and harmonic controllers to track the harmonic ASD load currents. To generate the harmonic current reference from the measured ASD load current, a harmonic detection algorithm is needed. It is the key for the harmonic mitigation, that the harmonic detection method is accurate in both magnitude and phase, to cancel the current harmonics. The harmonic detection method chosen is a high pass filter implementation by using low pass filters, on the form $HPF = 1 - LPF$. To track the harmonic current reference there are different controller topologies, which can be used. In this project it was concluded to use and compare the PR and repetitive controllers.

Design of Active Filter Controllers and its Components 5

In this chapter the APF passive components and the APF controllers will be designed based on chapter 4, to be able to do simulations and experimental work. Firstly the APF filter components will be designed, and afterwards these designed values will be used to design the PLL, fundamental PI controllers, DC voltage controller, and harmonic controllers. The chapter will ended in a simulation where the controllers performance is shown, and the harmonic controllers are compared.

5.1 Active Power Filter Design

Before designing the active power filter controllers, the passive components (C_{dc} and L_F) should be designed. The APF is designed for two cases, the laboratory setup and the Helius power plant. The rated parameters of these can be seen in table 5.1.

Parameter	Laboratory Value	Helius Value
S_{load}	2.89 kVA	1.18 MVA
$\mathrm{THD_i}$	30 %	25.9 %
S_{APF}	1.39 kVA	566.28 kVA
V_{LL}	400 V	400 V
V_{DC}	620 V	750
$i_{L(\mathrm{RMS})}$	4.24 A	1.71 kA
$i_{L(pk)}$	6 A	2.42 kA
Δi_{max}	0.4 A	164.1 A

Table 5.1. Active filter design values for laboratory and Helius power plant.

The power rating of the APF depends on the amount of harmonics in the line current, and the reactive power that should be to compensated. The power rating of the APF is calculated by Eq. 5.1 according to [7].

$$S_{APF} = \sqrt{(\mathrm{THD_i} \cdot S_{load})^2 + Q_{APF}^2} \tag{5.1}$$

Reference [27] proposes a method of designing the passive components for the APF. The inductor is designed to limit the current ripple of the APF to 10%, using $V_L = L\frac{di_L}{dt}$. At the zero crossing of the phase A voltage, the current ripple is the largest due to the active switching states of the space vector modulation (SVM). Here the total time of the active states is $0.433 \cdot T_s$ [27]. Using this as dt, the current ripple equation becomes:

$$L_f = \frac{2 \cdot V_{dc} \cdot 0.433}{3 \cdot f_s \cdot \Delta i_{max}} \tag{5.2}$$

Calculating the filter inductance for the laboratory setup yields 37.3 mH, while calculating the inductance for the APF to be implemented in the Helius power plant results in 110 μH. In the laboratory the closest achievable value is 10.8 mH and this will therefore be used for the design of the controller in the laboratory. The capacitance of the DC-link capacitor is found by:

$$C_{dc} = \frac{2 \cdot I_{dc}}{4 \cdot \Delta V_{max} \cdot f_s} \tag{5.3}$$

where I_{dc} is the mean capacitor current, that can be estimated from $^{S_{APF}}/_{V_{dc}}$. Calculating the power of the APF using Eq. 5.1, according to [27], the DC-link capacitor can be found by:

$$C_{dc} = \frac{2 \cdot {}^{S_{APF}}/_{V_{dc}}}{4 \cdot \Delta V_{dc} \cdot f_s} \tag{5.4}$$

From this, the capacitance required for 1% voltage ripple is 15 µF. The converter used in the laboratory is a DANFOSS FC302 7.5kVA converter, which has a 300 µF DC-link capacitor. Thereby the 1% voltage ripple is achieved. By calculating the capacitance using the rated values of the Helius power plant, the DC-link capacitor needed for 1% ripple is 4.2 mF. The design values are summarized in table 5.2.

Parameter	Laboratory Value	Helius Value
L_f	10.8 mH	109 µH
C_{DC}	300 µF	4.2 mF

Table 5.2. Design values of the active power filter.

The values of the passive components of the APF are used when designing the controllers to regulate the harmonic cancellation, and reactive power compensation.

5.2 Phase Locked Loop Design

As stated in Sec 4.1, the objective of the PLL is to align the d-axis of the reference frame with phase A, and rotate the reference frame with the same angular velocity as the three phase voltages. The closed loop transfer function of the PLL is given from [20] by:

$$H_\theta(s) = \frac{\theta'(s)}{\theta(s)} = \frac{K_p s + \frac{K_p}{T_i}}{s^2 + K_p s + \frac{K_p}{T_i}} \tag{5.5}$$

By approximating Eq. 5.5 to a normalized second order transfer function [20], the damping coefficient, ξ, and the natural frequency, ω_n, are given by:

$$\omega_n = \sqrt{\frac{K_p}{T_i}} \qquad \xi = \frac{\sqrt{K_p T_i}}{2} \tag{5.6}$$

The PLL is designed by setting the settling time, t_{set}. From the settling time estimation for a second order system with a damping coefficient of $\frac{1}{\sqrt{2}}$:

$$t_{set} = 4.6 \cdot \tau \tag{5.7}$$

where $\tau = \frac{1}{\xi\omega_n}$. This relation can be used to choose K_p and T_i:

$$K_p = 2\xi\omega_n = \frac{9.2}{t_{set}} \tag{5.8}$$

$$T_i = \frac{2\xi}{\omega_n} = \frac{t_{set}\xi^2}{2.3} \tag{5.9}$$

The PI controller is designed with a damping coefficient of $\frac{1}{\sqrt{2}}$, and settling time of 100 ms. This results in controller values of:

$$K_p = 92$$
$$K_i = 1058$$

The step response of the PLL can be seen in Fig. 5.1.

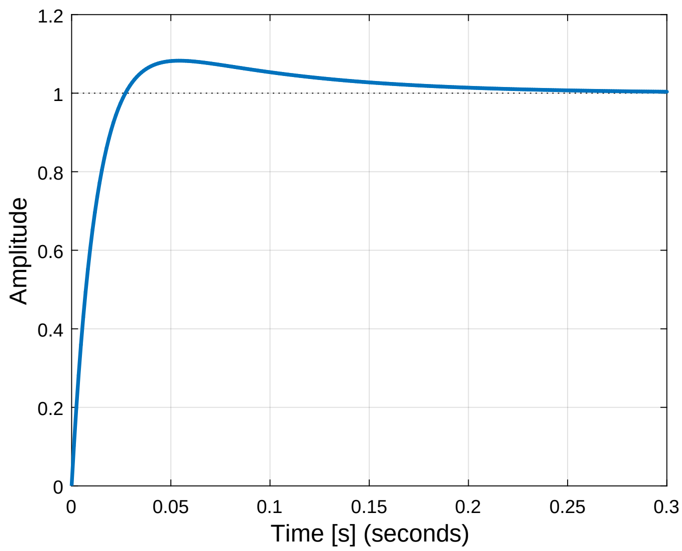

Figure 5.1. PLL response for a step input.

As seen the controller has a settling time of more than the 100 ms the controller is designed for. This is because the closed loop transfer function contains the term $k_p \cdot s$ in the numerator, which introduces an error compared to the standard second order transfer function. For the real system a slower PLL is acceptable because the PLL is always running, even before the controller is enabled. Simulating the synchronization of the PLL to the grid voltage, the angle generated can be seen to follow the phase A voltage.

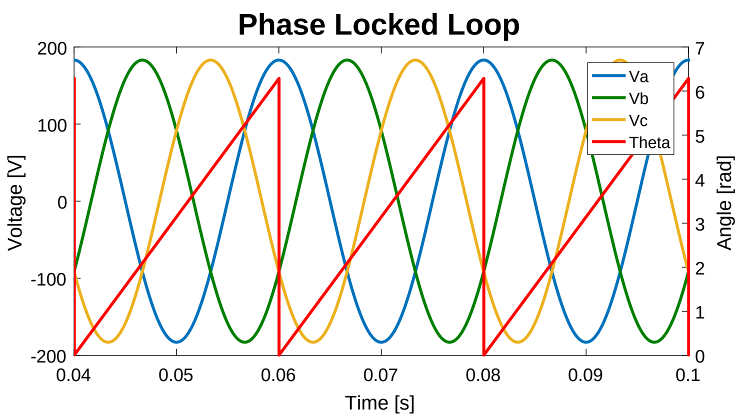

Figure 5.2. Simulation of the designed PLL synchronization to the grid voltage.

Fig. 5.2 shows that the angle is zero at the peak of phase A voltage, and the angle increases with the rotation of phase A voltage.

5.3 Controller Design

In this section the different controllers will be designed. This both includes the fundamental PI current controllers, the harmonic mitigation controllers, and the DC link voltage controller. All the controllers will be designed based on the laboratory setup, since the design of the controllers for the Helius power plant follows the same procedures. The relevant parameters of the controller designs are shown in table 5.3.

Parameter	Value
L_f	1.5 mH
R_f	0.3 Ω
C_{DC}	300 µF
f_s	12 kHz
T_s	$\frac{1}{f_s}$

Table 5.3. Design parameter values for the laboratory APF.

These parameters will be used for all the controller designs. The controller designs will be based on the theory presented in Sec. 4.2. When implementing the controllers, they are all restricted by the discrete control limitations. First of all the discrete controllers can only track a given reference signal if the signal is below the Nyquist frequency, which is half of the sampling frequency. Furthermore, aliasing issues might occur if the frequency of the reference signal to be tracked is less than or approximately 10 times of the sampling frequency, suggested by [28]. Therefore, the effectiveness of the active filter for cancelling current harmonics also depends on the sampling frequency chosen. In this case it means that since $f_s = 12$ kHz then aliasing issues can occur for frequencies larger than 1.2 kHz, which approximately is the 23^{th} and 25^{th} harmonic pair.

From Ch. 3, the APF should be able to reduce the THD_i at the grid to approximately 5% and compenste the power factor at PCC1 to be between 0.95 and 1. Furthermore, for the APF transient speed is not the main design specification, since there are no standards for how fast it should be. Therefore stability is preferred over fast settling times.

5.3.1 Fundamental PI Controller

To design the PI controllers that controls the fundamental 50 Hz i_{dq} current components, the controller design presented in Sec. 4.1 is used. Using the parameters of table 5.3 the PI controller gains can be calculated as:

$$K_p = \frac{L_f}{3T_s} = 6$$

$$K_i = \frac{K_p}{{L_f}/{R_f}} = 1200$$

The root locus of the closed loop system is shown in Fig. 5.3.

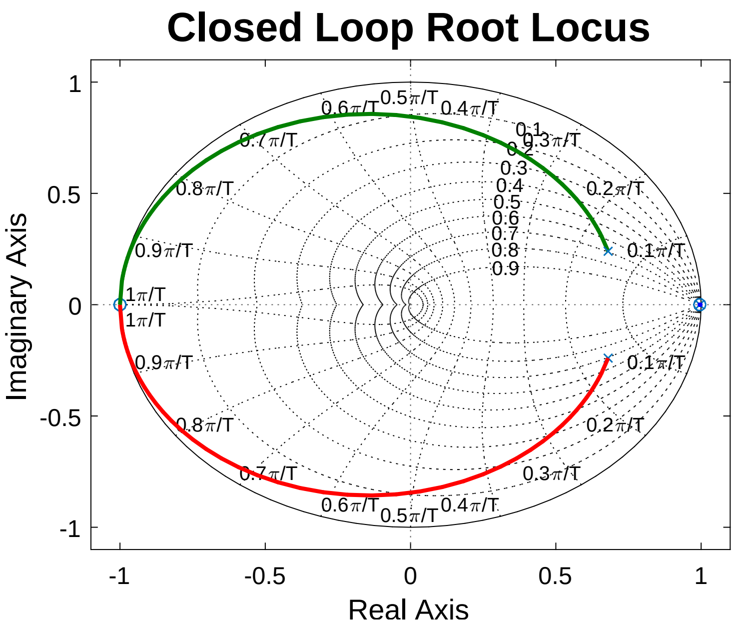

Figure 5.3. Closed loop root locus using the designed PI controller.

As seen the closed loop complex pole pair is placed approximately with a damping of 0.7, as it is designed for. For a damping factor of 0.7 the overshoot of the step response should be limited. To prove the limited overshoot and stability margins of the open loop system, the discrete time domain step response and open loop bode diagram is shown in Fig. 5.4(a) and Fig. 5.4(b).

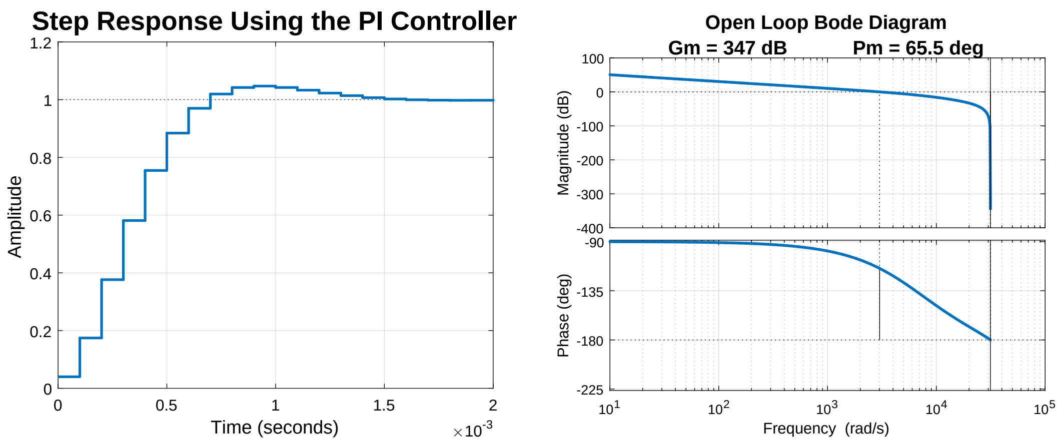

(a) (b)

Figure 5.4. The step response and open loop frequency response with the designed PI controller.

From Fig. 5.4(a) it is seen that the overshoot is limited to approximately 5 % and that the settling time is around 1.75 ms. Since the fundamental PI current controllers should ensure stability of the system without the harmonic mitigation controllers, the stability margins should be high. As shown in Fig. 5.4(b) the gain margin is very high, only limited by the gain at the Nyquist frequency, since this is where it reaches a phase of $-180°$. The phase margin is also well above 45° as suggested by [28]. The bandwidth of the closed loop system is 736 Hz.

5.3.2 DC Voltage Controller Design

The design of the DC voltage PI controller is based on that the output of the PI controller is the active power current reference, i_d, to the current controller, thus the outer control loop. Therefore, the DC voltage PI controller is designed so that the outer loop is slower than the inner current loop to decouple the two loops, thus having a lower bandwidth. To achieve this, the desired outer loop bandwidth is approximately 10 times lower than the bandwidth of the inner current loop. Furthermore the outer loop is tuned to ensure stability by having high enough stability margins.

To tune the DC voltage PI controller the controller design tool "SISOTOOL" from Matlab is used. SISOTOOL is a controller tuning application, which is able to handle controller designs of single-input single-output control systems, based on different controller requirements. In this case a desired bandwidth of 74 Hz, and at least 45° phase margin. Using these requirements the PI controller gains are $K_p = 0.1$ and $K_i = 12$. The open loop bode plot with the gain and phase stability margins is seen in Fig. 5.5.

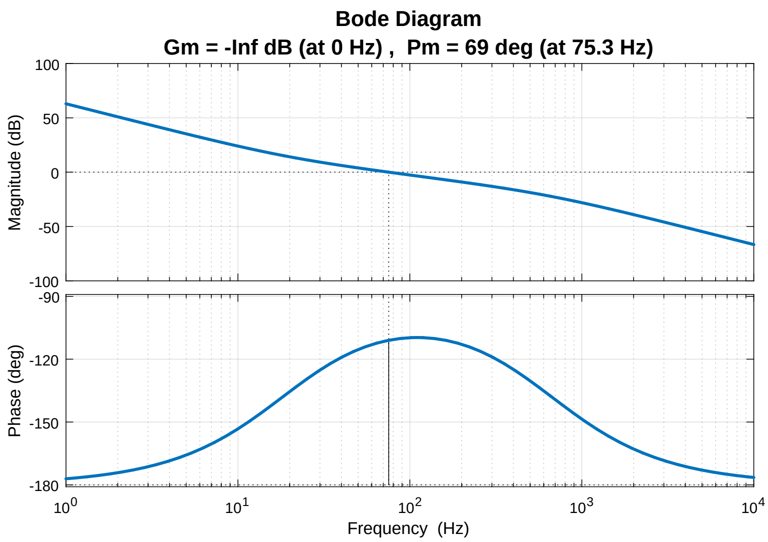

Figure 5.5. Open loop bode plot with indicated stability margins.

As seen the phase margin is 69°, which indicates a stable closed loop system. The step response of the closed loop system is shown in Fig. 5.6.

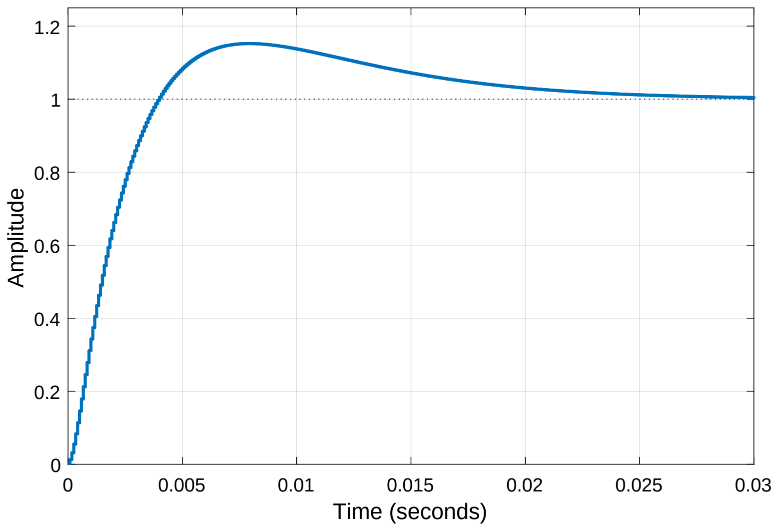

Figure 5.6. Step response of the closed loop DC voltage loop.

The overshoot of the step response is 15 %. However, for normal operation the DC voltage should be kept constant, thus the overshoot is only experienced during start-up of the system. The bandwidth of the closed loop system is 84 Hz, which is approximately 10 times lower than the bandwidth of the inner current control loop. Normally the DC voltage is kept constant, thereby disturbance rejection is an important aspect of the DC voltage loop. This will be tested in simulations later.

5.3.3 PR Controllers

The design of the PR controller is based on [29], where the controller is designed to comply with a specific closed loop bandwidth. As seen in Fig. 4.17 in Sec. 4.2.3, for all other frequencies than the resonant frequency the controller acts as a proportional gain. Thereby the closed loop transfer function for a purely inductive plant can be reduced to:

$$G_{cl} = \frac{K_p}{sL_f + K_p} \tag{5.10}$$

where K_p is the proportional gain of the PR controller and L_f is the inductance of the output filter. By multiplying Eq. 5.10 with $\left(\frac{1}{L}/\frac{1}{L}\right)$, s is isolated and the bandwidth of this first order system is:

$$\alpha_c = \frac{K_p}{L_f} \tag{5.11}$$

The resonant controller is designed by choosing the bandwidth of the closed loop system and calculating the controller gains. The desired bandwidth is chosen based on the sampling frequency by:

$$\alpha_c = 2 \cdot \pi \cdot \frac{f_s}{x} \tag{5.12}$$

where a_c is the closed loop bandwidth, f_s is the sampling frequency and x is a scaling factor of the sampling frequency. As a criterion the closed loop bandwidth has to be smaller than the Nyquist frequency $\left(\frac{f_s}{2}\right)$. For this design the bandwidth is set to $\frac{f_s}{5}$ and the proportional gain is calculated to:

$$K_p = \alpha_c \cdot L_f \tag{5.13}$$

The resonant gain is also determined by the filter inductor and the bandwidth, which can be simplified to the proportional gain of the controller:

$$K_i = 2 \cdot \alpha_h \cdot \alpha_c \cdot L_f = 2 \cdot \alpha_h \cdot K_p \tag{5.14}$$

where α_h is the resonant bandwidth, which has to respect $\alpha_h \ll \alpha_c$ and $\alpha_h < \omega_1$ [20]. As shown in Fig. 4.18 in Sec. 4.2.3 increasing K_p increases the magnitude gain for all frequencies. Since the fundamental PI controllers are used for stability control, a gain close to 0 dB for all but the resonant frequency is desired. Therefore K_p is set to 1 and $\alpha_h = 150$ rad/s.

When K_p is set, K_i is calculated as:

$$K_i = \frac{K_p \cdot 2 \cdot 150}{L} = 32.23 \tag{5.15}$$

Using these controller values for three resonant controllers with resonant frequency at 6^{th}, 12^{th}, and 18^{th} order harmonics, the frequency response of the combined PR controller can be seen in Fig. 5.7.

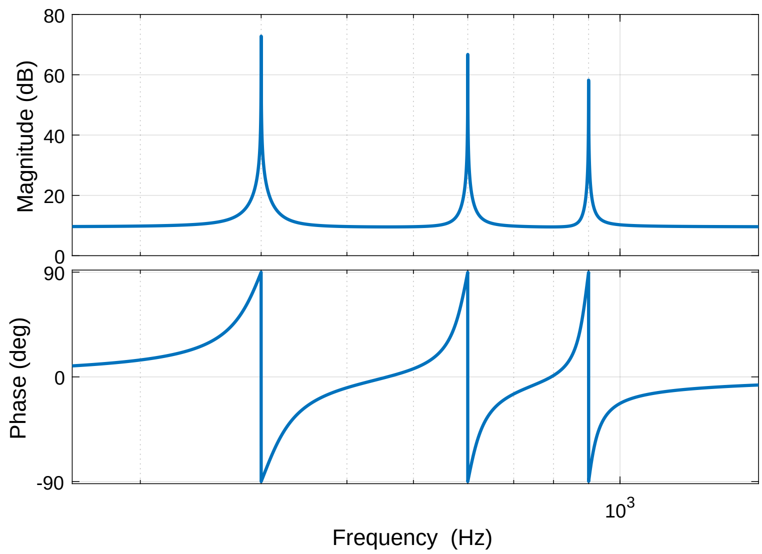

Figure 5.7. Bode plot of the PR controller used in APF.

As stated the fundamental PI controls the stability of the APF, while the PR controllers compensate the harmonics. By investigating the closed loop bode plot, as seen in Fig 5.8, the resonant controllers only change the bandwidth by 1.6 Hz. Thereby the objective of the resonant controllers, only working for the harmonics, is true.

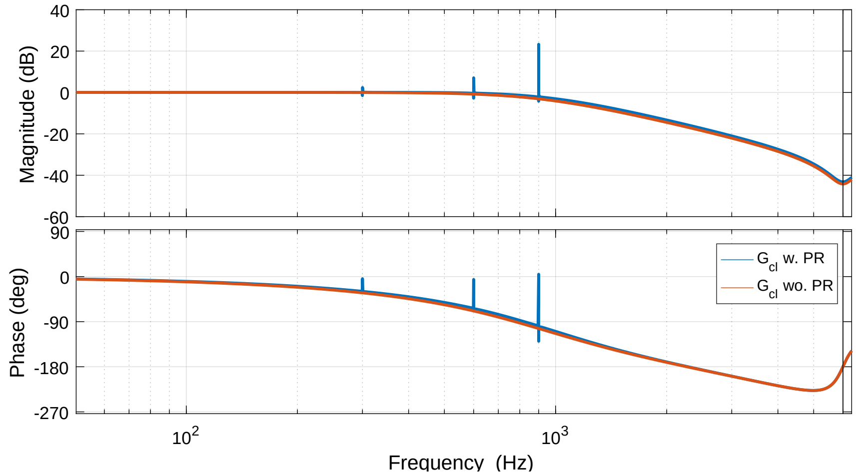

Figure 5.8. Closed loop bode plot with and without resonant controller.

Furthermore when investigating the step response of the closed loop system, the addition of the PR controller decreases the step response settling time by 0.1 ms and increases the overshoot with 2 %. This can be seen in Fig. 5.9.

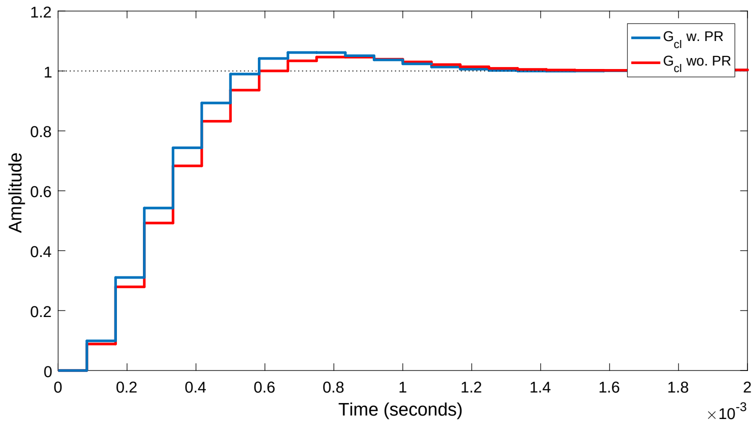

Figure 5.9. Step response of the closed loop system with and without resonant controller.

Thus the fundamental PI controllers primarily control the stability and dynamics, while the PR controllers ensure tracking of the harmonic currents.

5.3.4 Repetitive Controllers

As described in the Sec. 4.2.4, there are two stability conditions which should be satisfied for the plug-in repetitive controller. But before these are considered the low pass filter $Q(z)$ has to be chosen. To increase the stability, $Q(z)$ is designed to move the poles inside the unit circle. The drawback of including $Q(z)$ is that the tracking accuracy is decreased, as shown in Fig. 5.10.

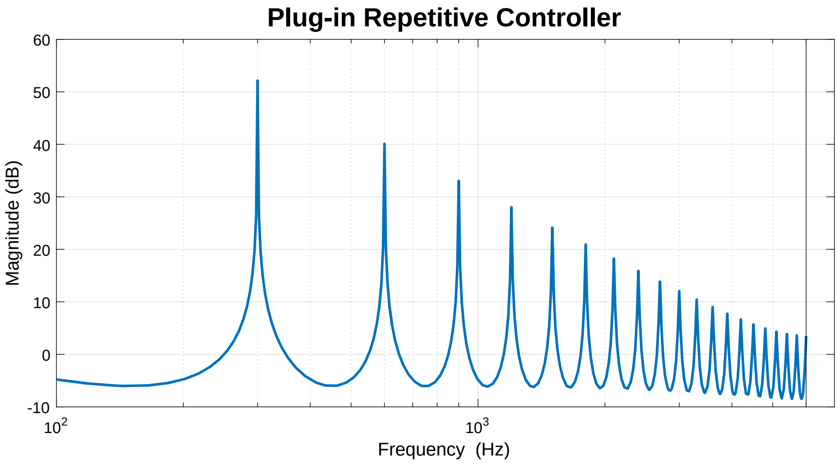

Figure 5.10. Magnitude plot for a 300 Hz plug-in fast repetitive controller with a low pass filter.

To increase the stability by moving the open loop repetitive controller poles inside the unit circle a low pass filter with zero phase shift, proposed in [25], can be used. The chosen low pass filter is given by:

$$Q(z) = \frac{z^2 + 8z + 1}{10z} \tag{5.16}$$

The frequency response of the low pass filter $Q(z)$ is seen in Fig. 5.11.

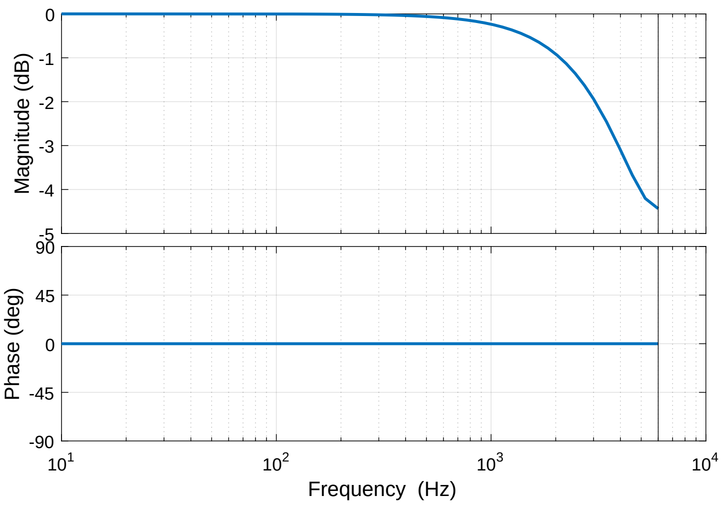

Figure 5.11. Frequency response of the low pass filter Q(z).

The filter has no phase shift due to the improper form, and a cut off frequency at approximately 1 kHz. The pole zero map with and without the low pass filter is shown in Fig. 5.12. Only half of the unit circle is shown since the other half is the mirrored version.

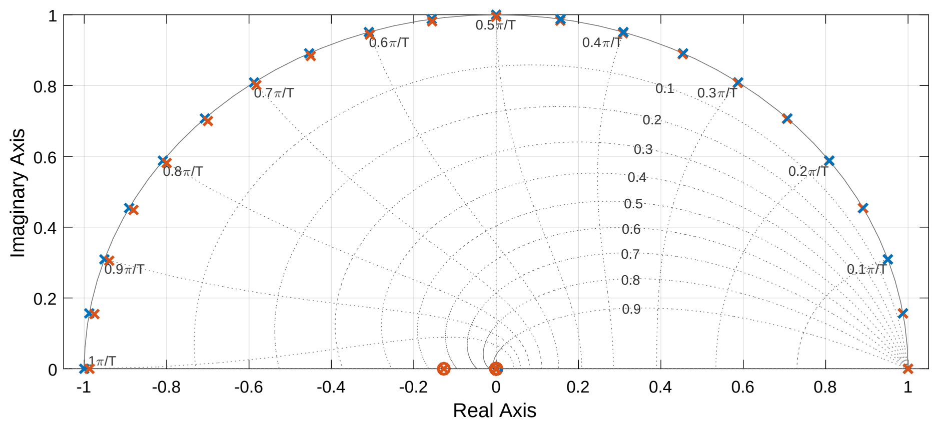

Figure 5.12. Pole zero map with low pass filter (red) and without low pass filter (blue).

As seen the low pass filter moves the poles slightly inside the unit circle, and dampens the higher frequency poles more. Although the low pass filter of Eq. 5.16 is an improper transfer function, meaning that there are more zeroes than poles, it is not an issue since $Q(z)$ is cascaded with a high order discrete time delay term.

The first stability condition from Sec. 4.2.4 is satisfied through the PI controller design of Sec. 5.3.1, since it is designed with high stability margins. The second stability condition can be verified using the Nyquist diagram of H(z), as shown in Fig. 5.13.

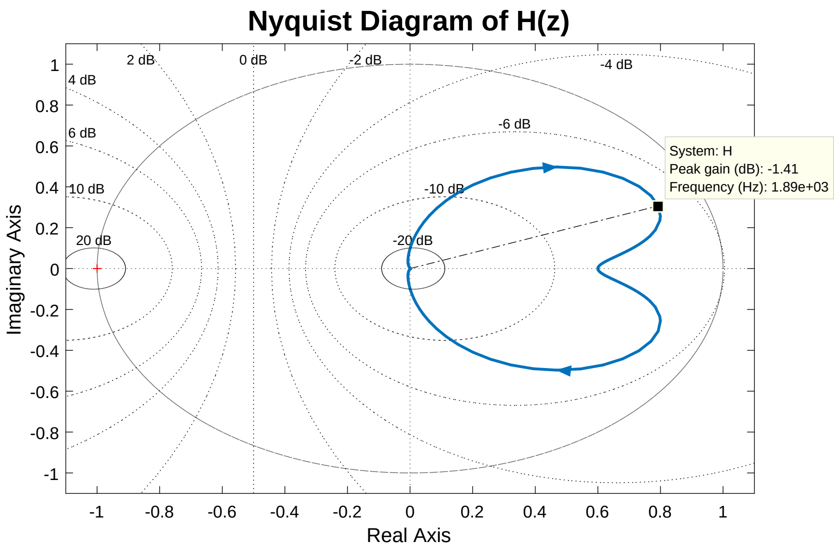

Figure 5.13. Nyquist diagram of H(z) with the peak gain and minimum stability (unit circle) indicated.

As seen the entire locus of H(z) is inside the unit circle and therefore there are no encircles of the point (-1,0), and furthermore the peak gain is -1.41 dB, which is equal to $10^{\frac{-1.41}{20}} = 0.85$ in the standard gain, thus the second stability condition is satisfied.

The closed loop frequency response with and without the repetitive controller is shown in Fig. 5.14.

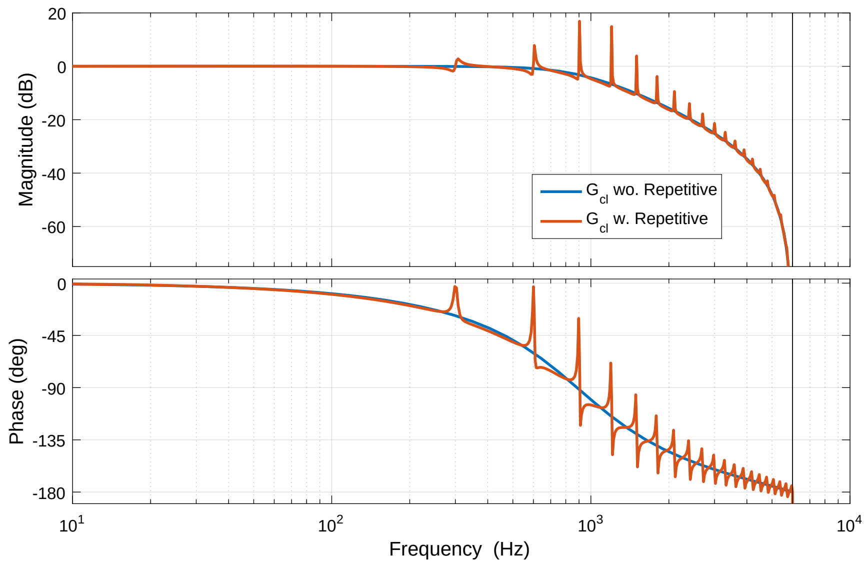

Figure 5.14. Closed loop frequency response with and without the repetitive controller.

As seen the repetitive controller does not change the bandwidth of the closed loop transfer function, but only ensures tracking of the desired harmonics, leaving the PI controller to ensure stability. The step response of the closed loop transfer function with and without the repetitive controller is seen in Fig. 5.15.

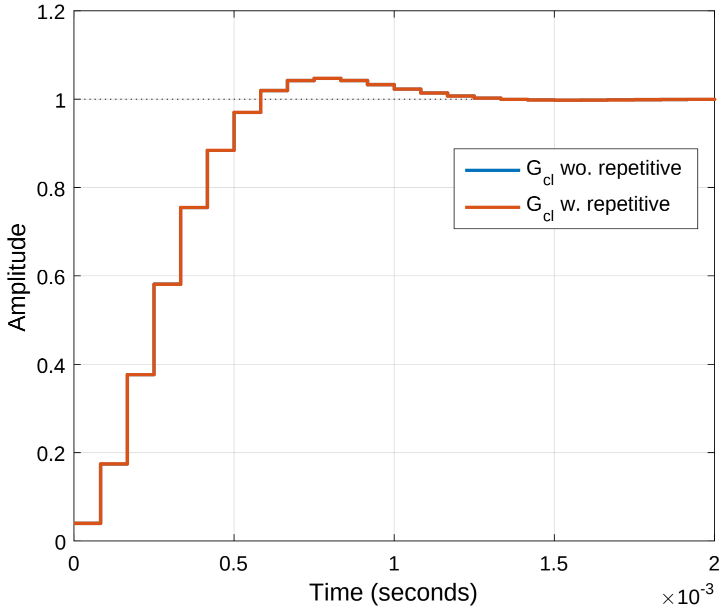

Figure 5.15. Step response of the closed loop system with and without the repetitive controller.

As seen the step responses with and without the repetitive controller are exactly identical, thus the repetitive controller does not alter the dynamics of the closed loop system.

5.4 Simulated Controller Performance and Controller Comparison

In this section the designed controllers performance are evaluated through a simulation of the laboratory setup. The performance of the PR controller and the repetitive controller are also compared in terms of harmonic mitigation effectiveness.

The simulation tools used are Plecs, which is used for the electrical simulation, and Simulink/Matlab which is used for the control/calculation parts. The electrical simulation schematic is shown in Fig. 5.16.

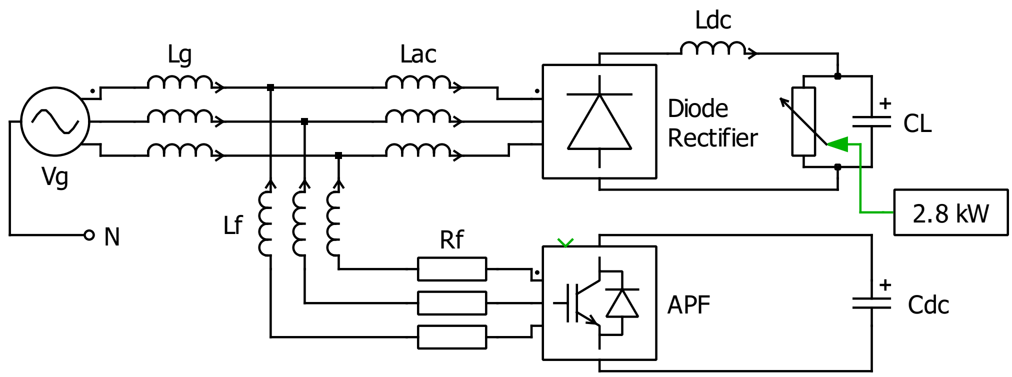

Figure 5.16. Plecs schematic of the electrical part used for the simulations.

To emulate the discrete laboratory implementation in dSPACE, all the control and calculations are performed in a "triggered subsystem", which has a sampling time of 12 kHz. Using this, the control is executed each $\frac{1}{12\text{kHz}}$, just as the dSPACE system is operated. The parameters used for the simulation are summarised in table 5.4.

Component	Name in Fig. 5.16	Value
APF filter inductance	L_f	10.8 mH
APF filter resistance	R_f	0.3 Ω
Load DC inductance	L_{DC}	2.4 mH (8 %)
APF DC capacitance	C_{DC}	300 µF
Load line inductance	L_{ac}	3 mH (10 %)
Load DC capacitance	C_L	325 µF
Grid inductance	L_g	1.8 mH (6 %)
APF switching frequency	f_s	12 kHz
APF switching time period	T_s	83.33 μs

Table 5.4. Simulation parameter values for the laboratory APF.

where L_g is chosen as the 6 % transformer impedance. The DC voltage reference is chosen to ensure controllability of the power flow to the APF. Therefore, the minimum theoretical DC voltage reference is $V_{DC}(min) = 230 \cdot \sqrt{3} \cdot \sqrt{2} = 563.4$ V, however to compensate for the voltage drop across the APF output filter a safety margin of 10 % of the minimum DC voltage reference is chosen, thus the DC voltage reference is set to 620 V.

The grid current without any harmonic mitigation or reactive power compensation, for a 2.8 kW ASD load used for all simulations in this section, is shown in Fig. 5.17.

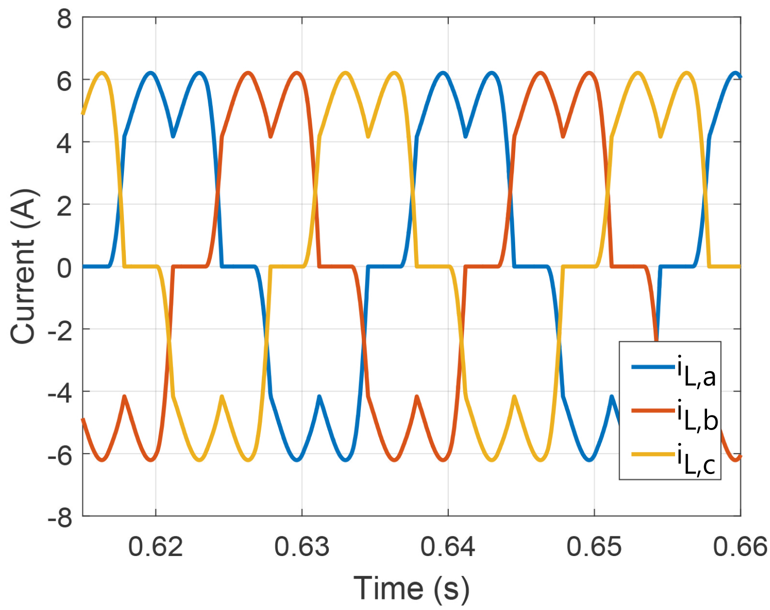

Figure 5.17. Simulated grid current without any harmonic mitigation or reactive power compensation.

The THD of the grid current without the APF is 26.6 %.

5.4.1 DC Voltage Tracking and Disturbance Rejection

To evaluate the DC voltage controller a step in the DC voltage reference from 580 V to 660 V is conducted. The test is performed with harmonic current compensation in the APF, which will be proven later in this section. The step response result is shown in Fig. 5.18.

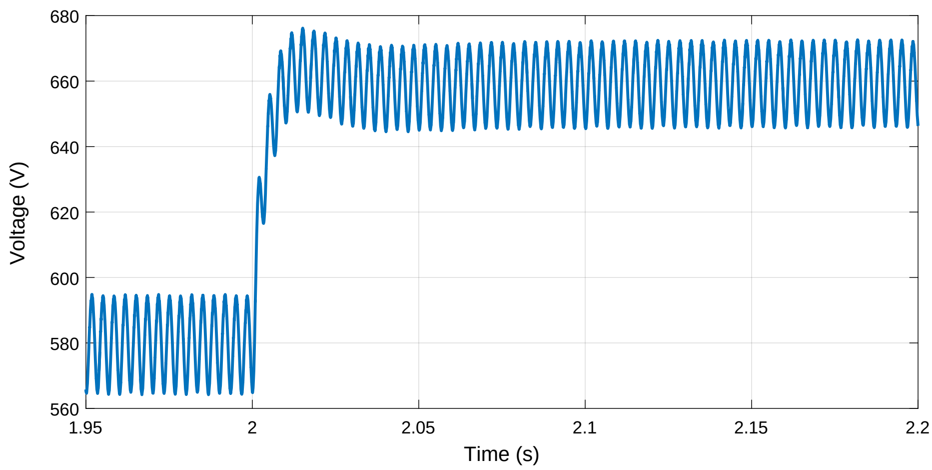

Figure 5.18. Simulated DC voltage step from 580 V to 660 V.

As seen the DC voltage controller can track a step change in the DC voltage, with an overshoot of approximately 10 % and a settling time of approximately 0.05 s. Since the capacitor is charged by drawing active power from the grid, the grid current should increase at this instance. The grid current for the DC voltage step is shown in Fig. 5.19.

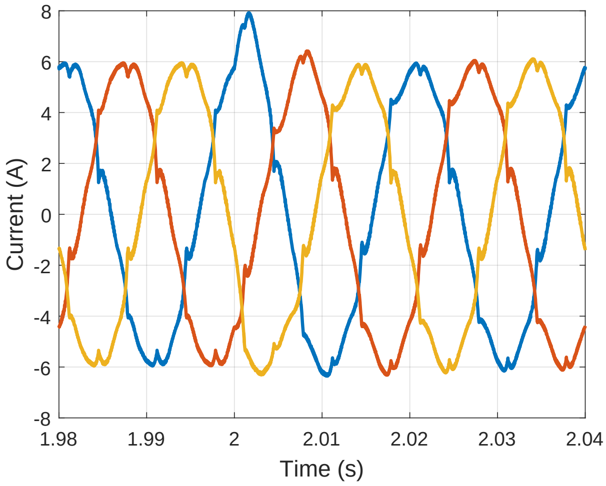

Figure 5.19. Simulated grid current for a DC voltage step from 580 V to 660 V.

As seen the grid current increases when the DC voltage step occurs, but settles back to steady state afterwards, at a DC voltage of 660 V.

Normally the DC capacitor voltage is always constant, so it is mostly during start-up the capacitor should charge to the desired voltage reference. Instead the disturbance rejection capability of the DC voltage loop is important. To test the disturbance rejection capability of the DC voltage loop, the APF is started with harmonic mitigation turned on, and at 1 s the reactive power compensation is turned on to achieve a unity power factor at the grid side. Furthermore, the ASD load is increased from 50 % to 100 % after 2 s. The result of the DC voltage response for the two disturbances is shown in Fig. 5.20.

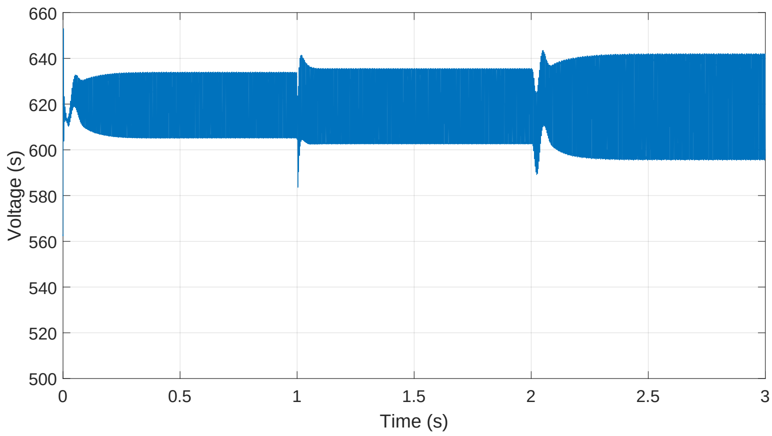

Figure 5.20. Simulated DC voltage for different disturbances. At 1 s reactive power compensation is enabled to achieve a unity power factor, at 2 s the ASD load is increased from 50 % to 100 %.

As seen the overshoot is limited to only a few percent for both disturbances, and furthermore reaches the steady state voltage reference.

5.4.2 Reactive Power Compensation

Since reactive power compensation is a viable option in the Helius CHP and possible with the active power filter, the fundamental PI current controller for i_q is tested by creating a reference to ensure a power factor of 1, and then step up and down to a leading and lagging power factor of 0.95. The simulation is without performing any harmonic mitigation, thus the grid current is highly distorted due to the ASD load. The active and reactive power response when stepping up and down in the reactive power is shown in Fig. 5.21(a).

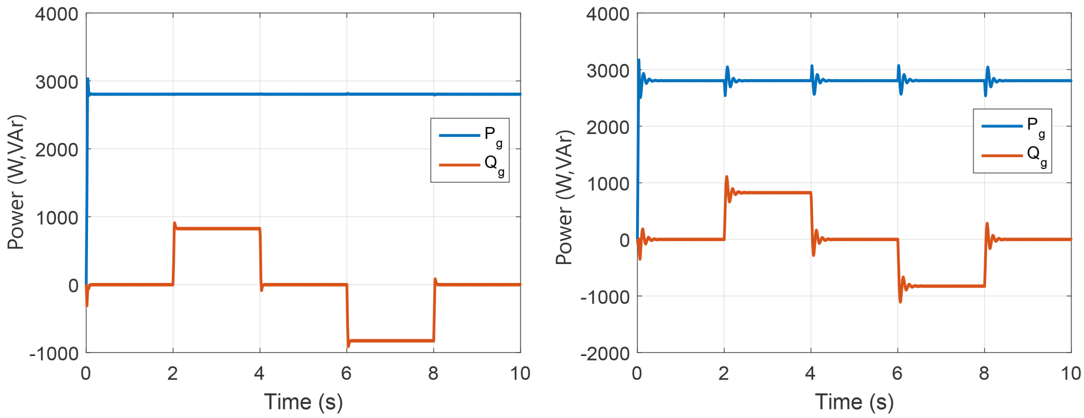

(a) (b)

Figure 5.21. Simulated active and reactive power a) with cross-coupling terms b) without cross-coupling terms.

To improve the controller dynamics the cross-coupling terms was added as feed forward signals, as seen in Fig. 4.6. The effect of not including the cross-coupling terms can be seen in Fig. 5.21(b), compared to Fig. 5.21(a) where the cross-coupling terms are included. As seen the cross-coupling terms improve the transient response of the controllers, when the reactive power reference is changed, and remove coupling from the reactive power loop (i_q PI controller) to the active power loop (i_d PI controller). Using the reactive power compensation to achieve a power factor of one, the grid current and voltage are shown in Fig. 5.22.

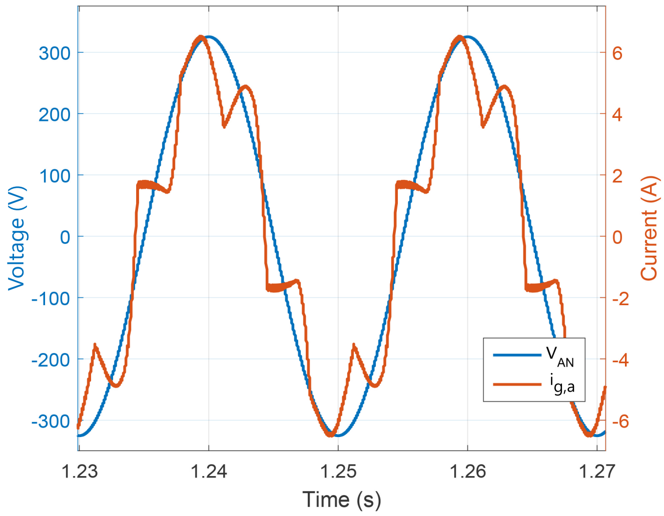

Figure 5.22. Simulated grid current and voltage for a unity power factor.

The grid current and voltage when a lagging power factor of 0.95 is shown in Fig. 5.23(a), while the grid current and voltage when a leading power factor of 0.95 is the reference is shown in Fig. 5.23(b).

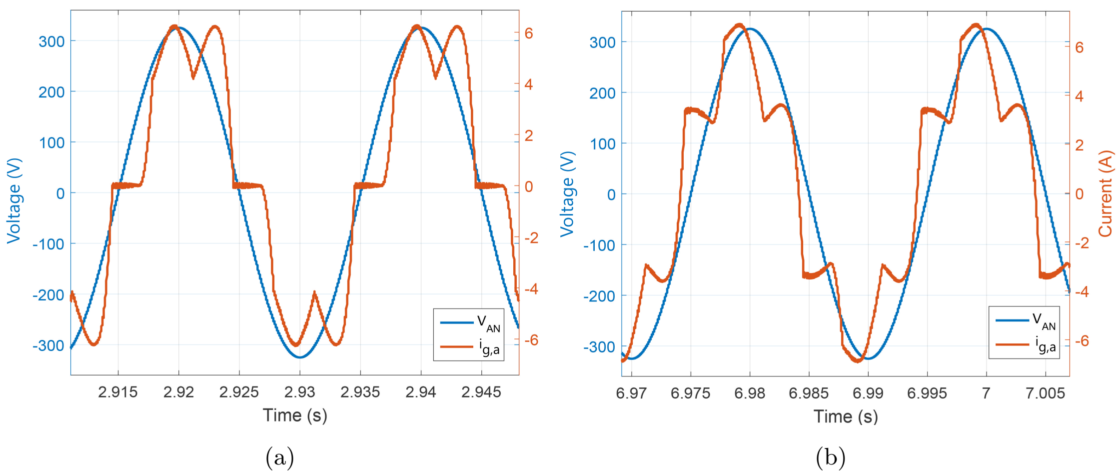

Figure 5.23. Simulated grid current and voltage for a) a lagging power factor of 0.95 b) a leading power factor of 0.95.

As seen the control strategy can achieve the desired reactive power compensation, whether a leading, lagging, or unity power factor is demanded.

5.4.3 Harmonic Mitigation Controller Comparison

In this simulation the harmonic mitigation performance using PR and repetitive controllers is compared. For the PR controller the 17^{th} and 19^{th} harmonics controller is not included, since this causes instability issues in the simulation. Even if the closed loop bandwidth is increased by increasing K_p for the 18^{th} PR controller, it still becomes unstable. The instability issue is therefore caused by aliasing issues since there is $\frac{12000}{19 \cdot 50} = 12.6$ samples per period of the 19^{th} harmonic which is close to the recommended limit of 10 samples per period.

The FFT of the grid current when using a PR or repetitive controller for the harmonic mitigation is shown in Fig. 5.24.

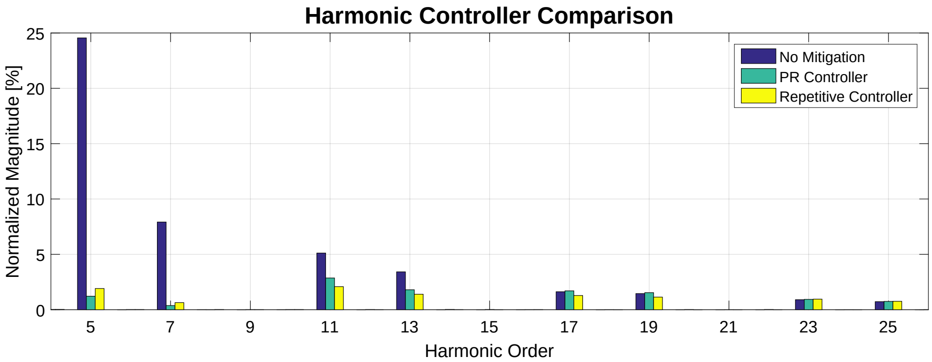

Figure 5.24. Simulated FFT comparison of the grid current using a PR and repetitive controller.

As seen the two controller types have quite similar harmonic compensation performance. The PR controller is slightly better for the 5^{th} and 7^{th} harmonics, while the repetitive controller is better for the 11^{th} and 13^{th} harmonics. The THD of the grid current when using PR controller is 4.69 %, while the repetitive controller achieves a THD of the grid current of 4.16 %, thus the repetitive controller has slightly better harmonic performance. When using the repetitive controller the filter current i_F from the APF is shown in Fig. 5.25(a), and the corresponding grid current is as seen in Fig. 5.25(b).

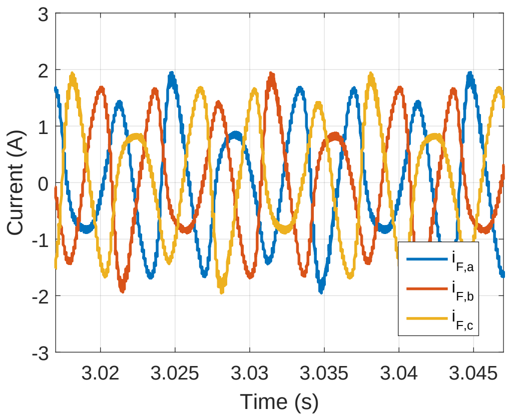

(a)

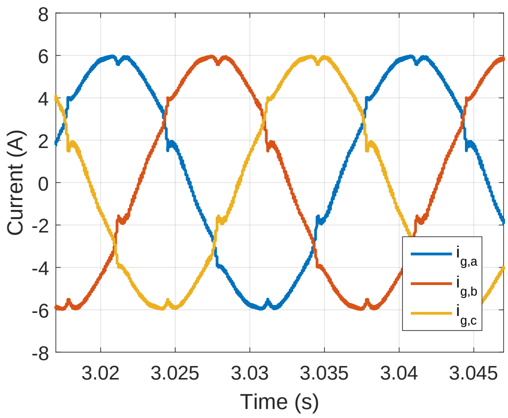

(b)

Figure 5.25. Simulated current using the repetitive controller drawn to a) the APF b) the grid.

In the design of the repetitive controller, a low pass filter was introduced to increase stability. If the low pass filter is not included thus $Q = 1$, the current drawn to the APF has high frequency ripple, which consequently distorts the grid current which is shown in Fig. 5.26.

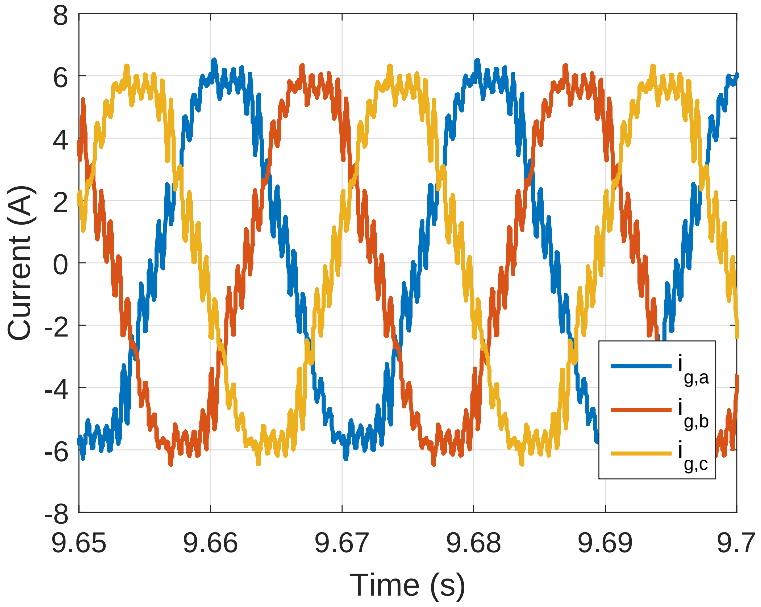

Figure 5.26. Simulated grid current when the low pass filter in the repetitive controller scheme is not included.

When using the repetitive controller to mitigate harmonics from the ASD load, the RMS grid current is reduced from 4.4 A to 4.2 A, which corresponds to a 138 VA reduction in apparent power on the grid side.

Validation of Active Power Filter Performance 6

In this chapter the active power filter and the designed controllers will be tested experimentally. To verify the simulations and controller design, a single non-linear load is connected to the grid through a delta-wye transformer. The control is performed using a dSPACE system, which both includes ADC and DAC boards. The dSPACE system is connected to a computer, where the control algorithm is loaded from a Simulink block diagram simulation. The sampling and switching frequency is chosen to be 12 kHz, as stated in Ch. 5. The schematic of the laboratory setup is shown in Fig. 6.1.

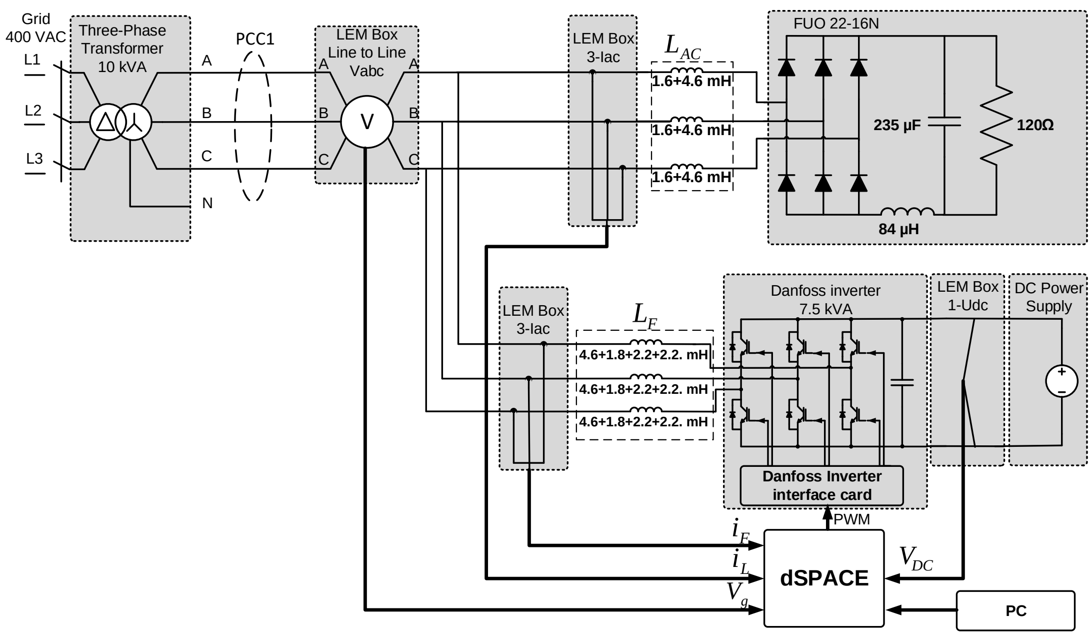

Figure 6.1. Schematic diagram of the laboratory setup.

The resistor in the non linear load is chosen to be 114 Ω, which approximately gives a load of 2.8 kW as in Sec. 3.3. The components used in the experimental setup are listed below:

- 1x Three phase inductor 1.6 mH.
- 1x Three phase inductor 4.6 mH.
- 1x Three phase inductor 10.8 mH (2x2.2 mH + 1x 1.8 mH + 1x 4.6 mH).
- 1x Three phase capacitor 4.7μF.

- 1x 7.5 kVA DANFOSS FC302.
- 1x 8 kW FUO 22-16N Full bridge rectifier.
- 2x Three phase current measurement LEM boxes (LA 55-P).
- 1x Three phase line to line voltage LEM box (LV 25-P).
- 1x 10 kVA DYN11 Transformer.
- 1x Voltech PM300 power analyser.
- 1x dSPACE System incl. ADC and DAC
- 1x Yaskawa D1000 DC Power Supply

A picture of the laboratory setup can be seen in Fig. 6.2.

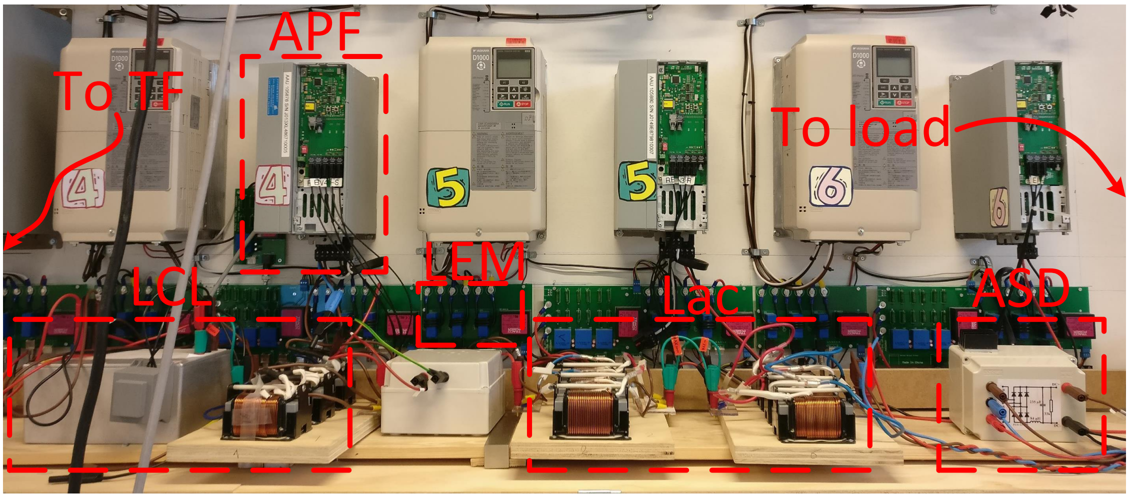

Figure 6.2. Laboratory setup of schematic in Fig. 6.1.

The transformer and the load of the test setup cannot be seen in Fig. 6.2. This is because the components are mounted on a wall, while the transformer and the load are on the ground.

Since the small 84 μH DC inductor (L_{DC}) in the ASD load cannot be changed, more inductance (L_{AC}) is added on the AC side of the ASD load to achieve a load current similar to the simulation case, since this reduce the current THD. The phase-A voltage and current of the grid (PCC1), without any harmonic mitigation, can be seen in Fig. 6.3.

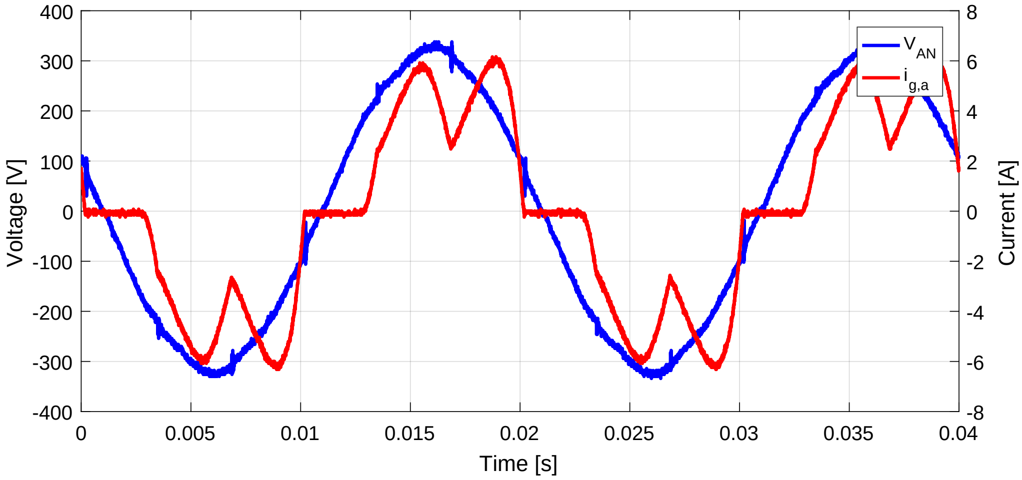

Figure 6.3. Measured grid voltage and current without any harmonic mitigation.

As seen in Fig. 6.1 the grid current is similar to the simulated current from Sec. 5.4, and has a THD of 30 %, while the voltage THD is 0.97 %. The ASD load will be kept constant through all the experiments, thus equal to the current of Fig. 6.3. The background voltage distortion is measured to be 0.8 %.

6.1 PLL Verification

As seen in Fig. 6.1, the Line-to-Line voltage is measured. For the PLL to synchronize to the grid, the measured line to line voltage is converted into the line to neutral voltage by:

$$
\begin{aligned}
V_{AN} &= \frac{V_{AB} - V_{CA}}{3} \\
V_{BN} &= \frac{V_{BC} - V_{AB}}{3} \\
V_{CN} &= \frac{V_{CA} - V_{BC}}{3}
\end{aligned}
$$

Transforming the phase voltage to the synchronized reference frame, the three phase voltage and the angle output of the PLL can be seen in Fig. 6.4.

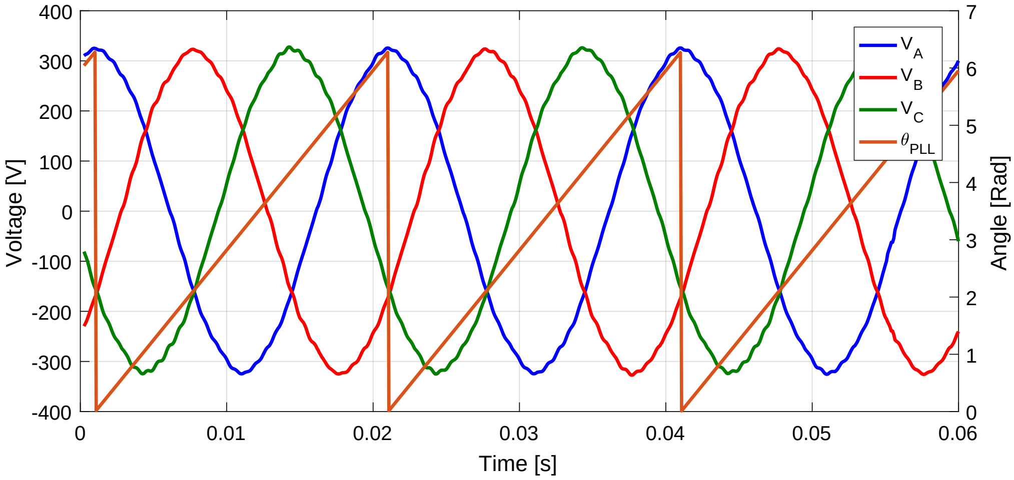

Figure 6.4. Measured phase to neutral voltage and angle output of the PLL.

As it can be seen the PLL is synchronized to the grid phase-A voltage, having 2π (or zero) radians at the peak of phase A. Thereby the phase locked loop system is synchronizing correctly, and it is generating the angle of the phase voltage, which is used in all reference frame transformations, thus enabling control.

6.2 Harmonic Detection

To compare the high pass filter implementations, an experimental verification of these are conducted. The experimental verification is conducted using a single ASD load connected to a low voltage network (400 V), with the load current having a THD of 84 % shown in Fig. 6.5.

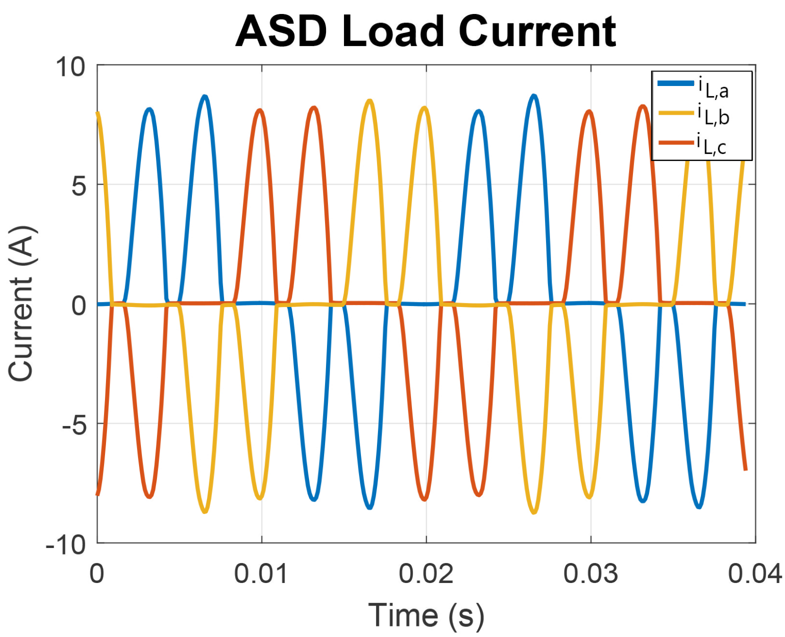

Figure 6.5. Experimental ASD load current used for the harmonic detection verification.

For the test the active filter is not connected since only the harmonic detection is to be proven. The current of Fig. 6.5 is used as input to the high pass filters to extract the current harmonics. The FFT of the output of the two high pass filters, after transforming the output from the dq reference frame to the natural three phase frame, is shown in Fig. 6.6.

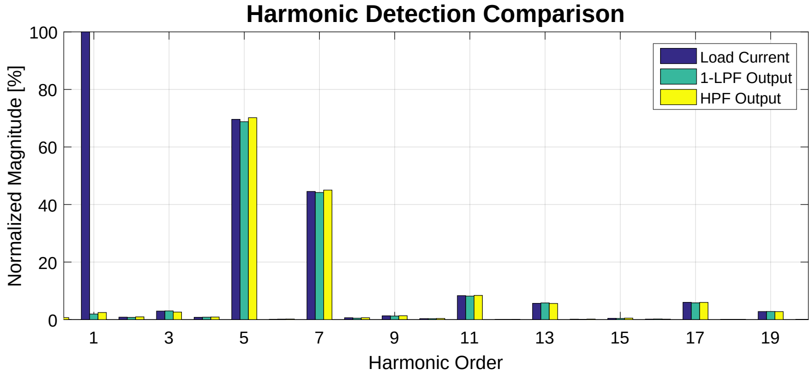

Figure 6.6. FFT of the output of the two high pass filter implementations.

As seen both of the filter implementations rejects the fundamental component, and tracks the harmonic components well. The FFT of both filter outputs are very similar in magnitude. To prove the phase response difference for the two high pass filters, the generated current reference, which is the output of the high pass filters, is subtracted from the measured ASD load current from Fig. 6.5 to generate the theoretical grid current, by assuming that the current controllers can perfectly track the current references. The generated theoretical grid currents using the standard second order high pass filter is shown in Fig. 6.7(a), and the theoretical grid current using the low pass implementation is shown in Fig. 6.7(b).

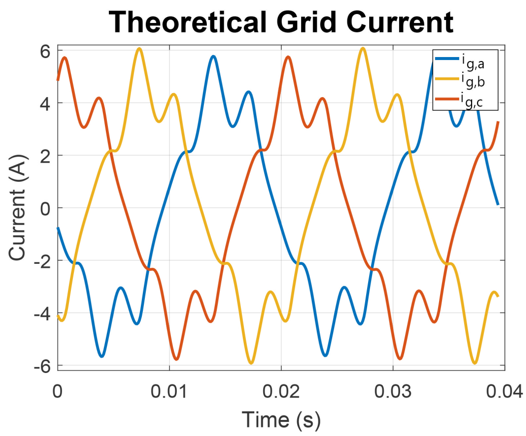

(a)

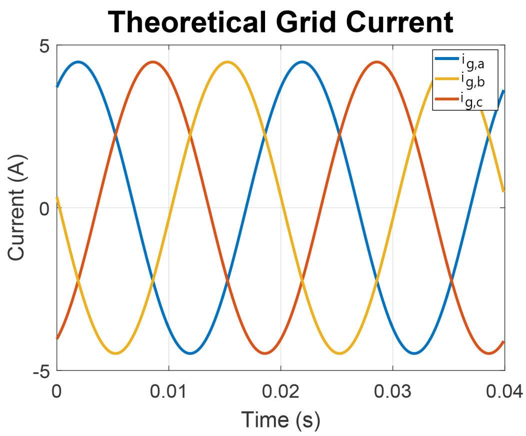

(b)

Figure 6.7. Theoretical grid current using a) a standard second order high pass filter b) a low pass implementation of a second order high pass filter.

It is clearly seen in Fig. 6.7(a) that some of the harmonics are not cancelled even though it tracks the magnitude of the harmonic load current components, when using a standard second order high pass filter. The THD of this theoretical grid current is 16 %. When using the low pass filter implementation the theoretical grid current generated is a smooth sinusoidal waveform with a very low harmonic content. The THD of this generated current is 0.8 %. To compare the harmonic content, the FFT of the theoretical current in Fig. 6.7(a) and Fig. 6.7(b) is plotted in Fig. 6.8.

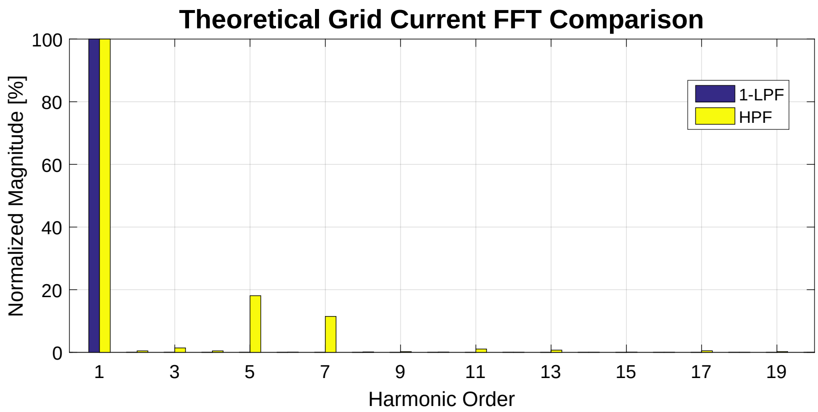

Figure 6.8. FFT of the two theoretical grid currents.

As seen the theoretical generated grid current when using the standard second order high pass filter contains the 5^{th} and 7^{th} order harmonics, but the high order harmonics are cancelled. This concludes that there are some phase shift, which cannot be neglected on the output of the standard second order high pass filter for the 5^{th} and 7^{th} order harmonics, since the magnitudes of the 5^{th} and 7^{th} order harmonics are tracked well.

6.3 Reactive Power Compensation

First step in verifying the control system is to verify the fundamental dq PI controllers. For this test, the load is disconnected, and the APF is connected to PCC1. Firstly a step in the i_q reference is made with a converter filter inductance of 10.8 mH. The result of this test can be seen in Fig. 6.9.

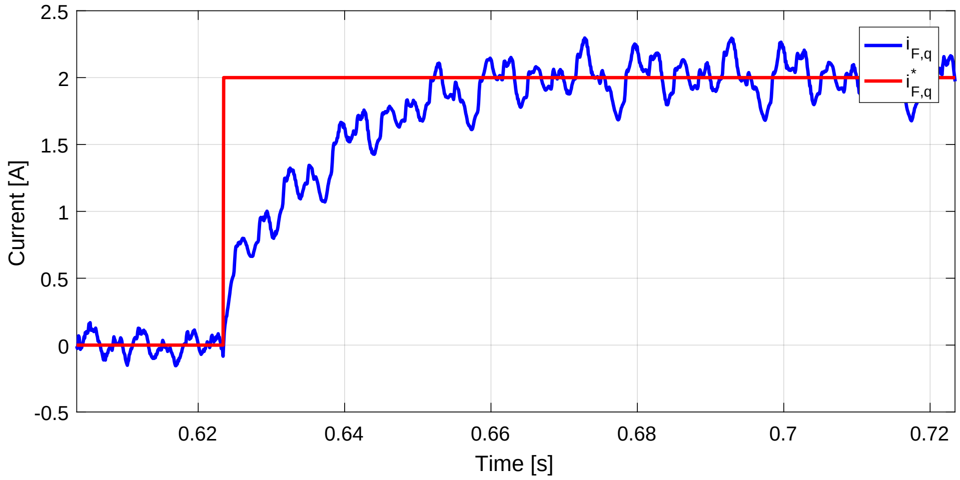

Figure 6.9. Measured i_q step response test with L filter.

As it can be seen, the step response of the q current controller has a settling time of approximate 40 ms. In the laboratory however the single L filter takes too much space, therefore an LCL filter is used instead of a L filter. The LCL filter is designed from the approach in [30] [31], and the design can be seen in App. A.2. This filter uses a 4.6 mH converter side inductance , a 6.4 mH grid side inductance, and a 4.7μF capacitor. The step response with the designed LCL filter is shown in Fig. 6.10.

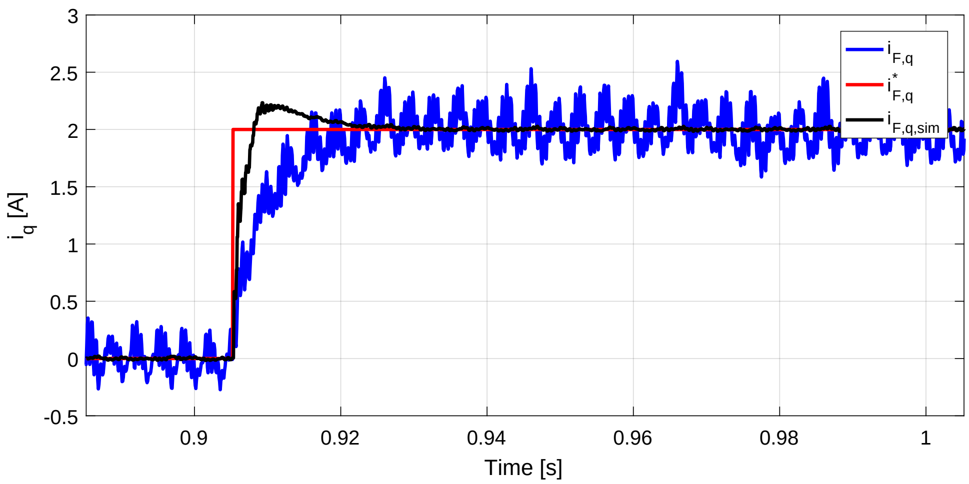

Figure 6.10. Measured i_q step response test with LCL filter with simulation step response also shown.

As seen, the settling time of the step response using an LCL filter is approximately 20 ms, when using the same controller. The simulated step response is conducted by using the same LCL filter as in the laboratory. The settling time of the simulation and measured step response is approximately the same, however the simulated step response has some overshoot. The difference in the two step responses can be caused by parasitic components, or inverter non-idealities which are not modelled in the PLECS simulation.

Now the full bridge rectifier is connected to the grid and the APF is set to compensate the reactive power of the load, by changing i_q. Controlling the q-axis current to achieve a unity power factor at PCC1, the grid voltage and current can be seen in Fig. 6.11.

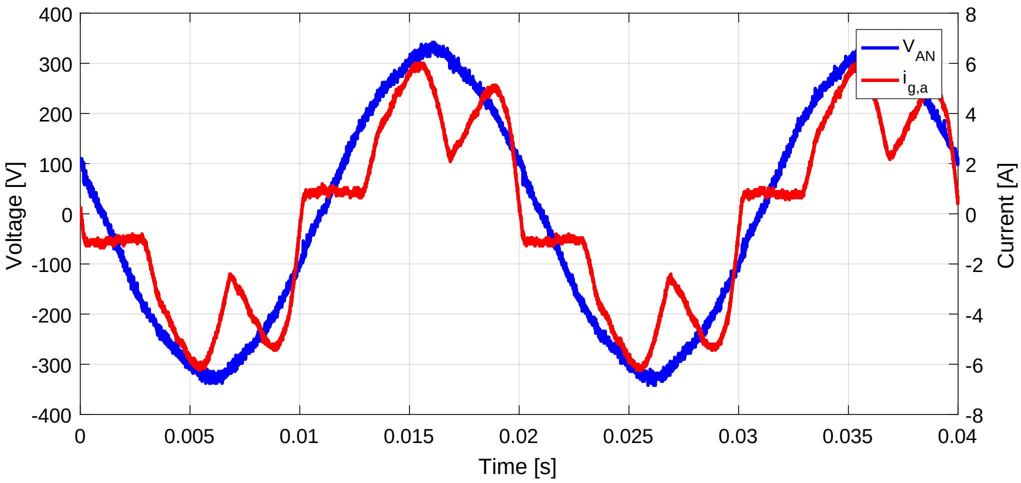

Figure 6.11. Measured grid voltage and current for reactive power compensation for $PF = 1$.

As seen the current waveform matches the simulated grid current in Fig. 5.22 in Sec. 5.4 for a unity power factor. For a 0.95 lagging power factor at PCC1, the resulting grid voltage and current can be seen in Fig. 6.12.

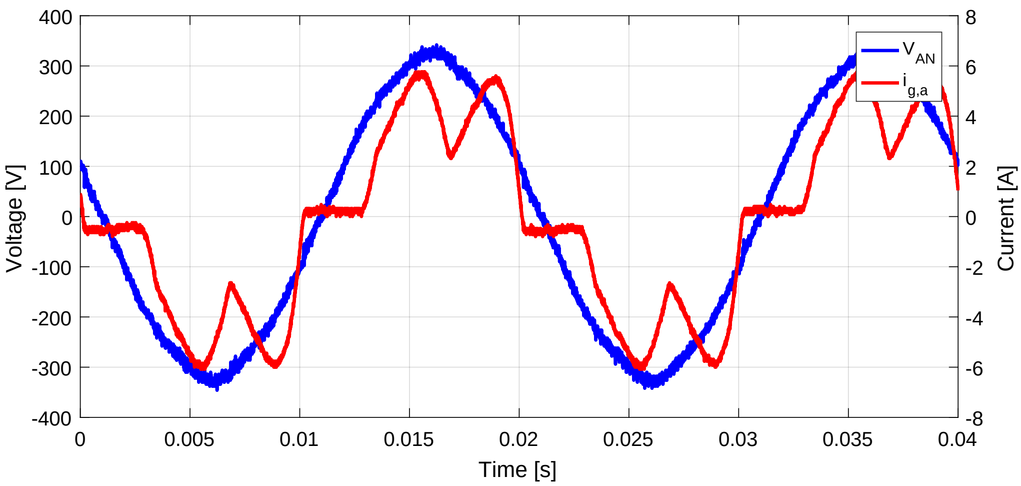

Figure 6.12. Measured grid voltage and current for reactive power compensation for a lagging power factor of 0.95.

This also corresponds to Fig. 5.23(a) in Sec. 5.4. For a 0.95 leading power factor at PCC1, the result can be seen in Fig. 6.12.

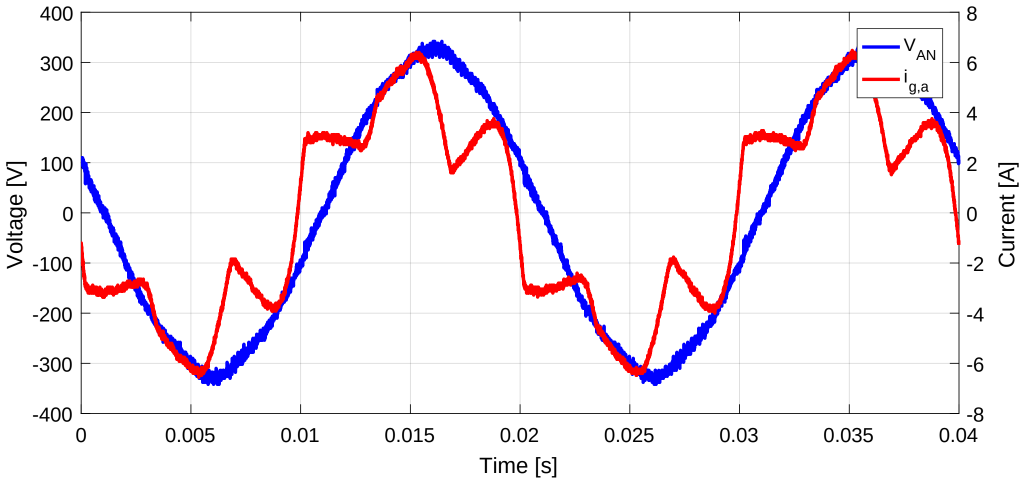

Figure 6.13. Measured grid voltage and current for reactive power compensation for a leading power factor of 0.95.

Comparing to Fig. 5.23(b) in Sec. 5.4, this shows the ability to also achieve a leading power factor. As shown in this section the APF controller can compensate the reactive power as desired, either to unity or a lagging or leading power factor. With the fundamental controller and reactive power compensation verified by matching the simulation, the Harmonic compensation can be tested.

6.4 Harmonic compensation

In order to verify the harmonic controllers the load is connected to the transformer and the APF is connected through the LCL filter. First the PR controller is tested for the 6^{th} and 12^{th} order harmonics. The grid current for this harmonic compensation can be seen in Fig. 6.14.

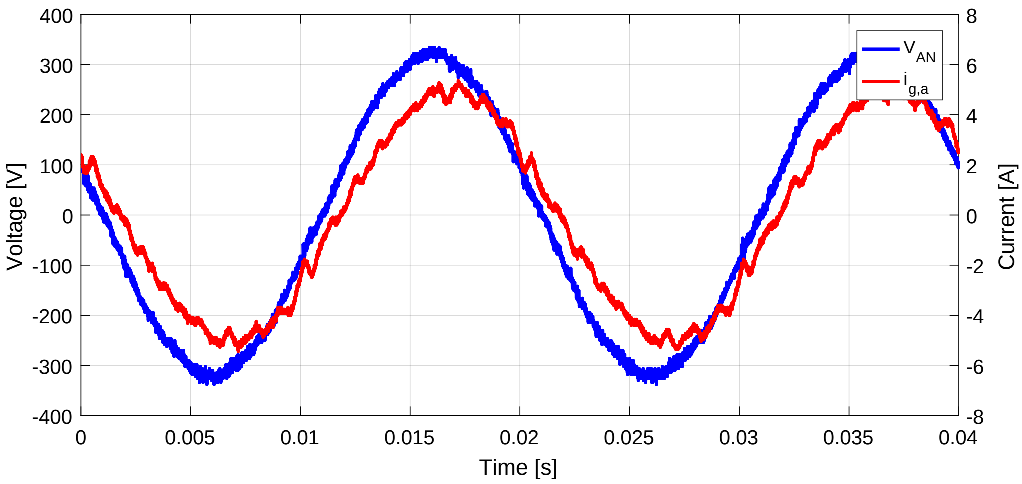

Figure 6.14. Measured grid voltage and current for harmonic compensation using the PR controller.

The THD of the current is measured to be 7.2%. The 18^{th} harmonic PR controller was also tested, but due to under sampling the controller is unstable. With the 12 kHz sampling, the 17^{th} harmonic has 14.1 data points per period and the 19^{th} harmonic has 12.6 samples per period. Next the Repetitive controller is tested as harmonic compensation, this can be seen in Fig. 6.15.

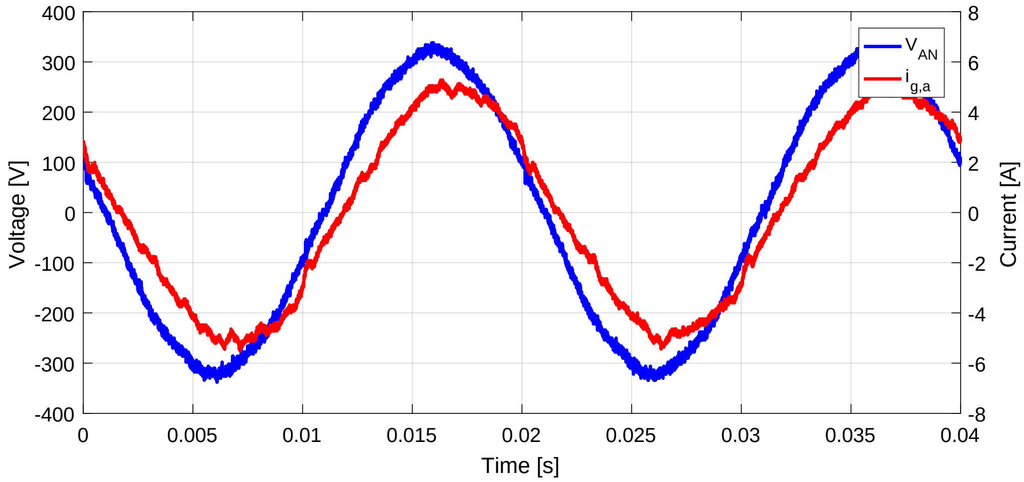

Figure 6.15. Measured grid voltage and current for harmonic compensation using the repetitive controller.

The current THD when using the repetitive controller is measured to be 6.4%. The FFT comparison of the PR and repetitive controller is shown in Fig. 6.16.

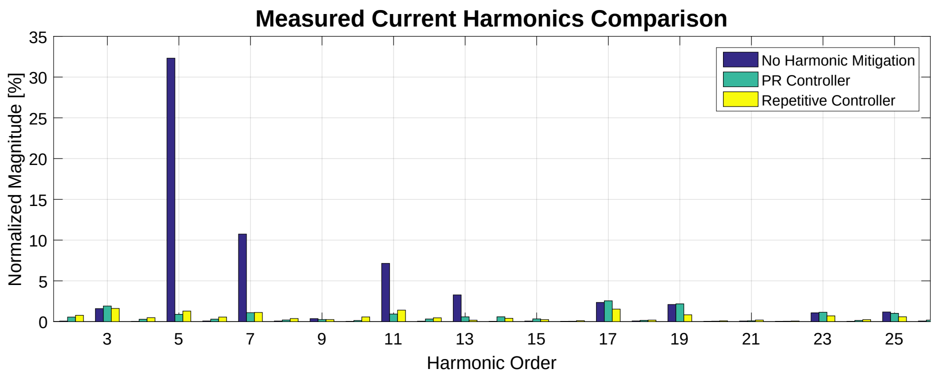

Figure 6.16. FFT comparison of grid current without harmonic compensation, and with PR and repetitive controller as harmonic controller.

The two controllers have similar performance, however the PR controller seems to be slightly better for the 6^{th} and 12^{th} harmonic pair except the 13^{th} harmonic, but the repetitive controller has a lower THD since it also reduces the higher order frequencies, while the PR is unstable when including higher order frequencies than the 6^{th} and 12^{th} harmonic pair.

As stated in Sec. 4.2.4, in order to have an infinite gain at all resonance points of the controller, the low pass filter of the repetitive controller has to be equal to one. This is tested in Fig. 6.17, where $Q = 1$.

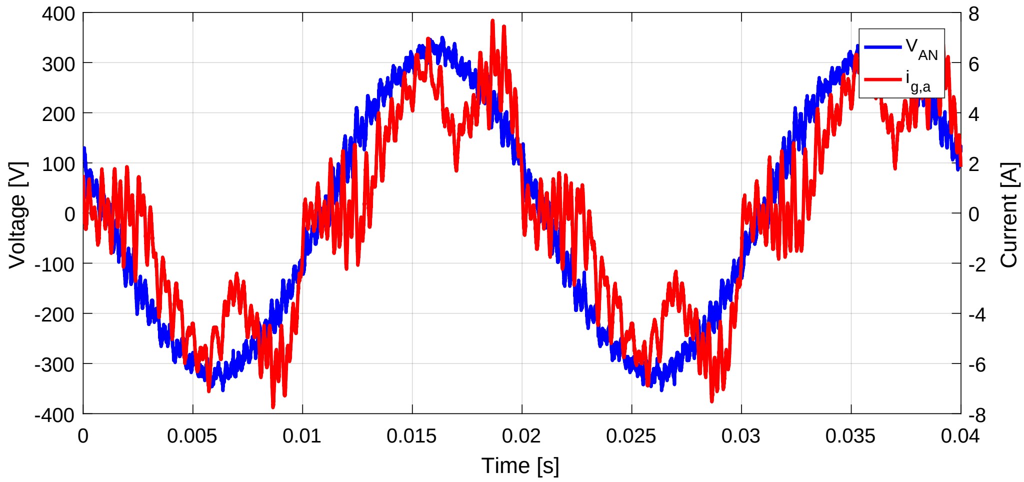

Figure 6.17. Measured grid voltage and current for repetitive controller with Q=1.

As shown the repetitive controller with $Q = 1$ has a lot of noise/ripple, and cannot compensate the harmonics of the load, thus emphasises the need for a low pass filter, as discussed in Sec. 5.3.4. With the PR and repetitive controller tested in steady state, the transient response of the harmonic compensation is tested. The harmonic reference is stepped from 0% to 100%, and the measured dq grid currents for this step is shown in Fig. 6.18(a) and 6.18(b).

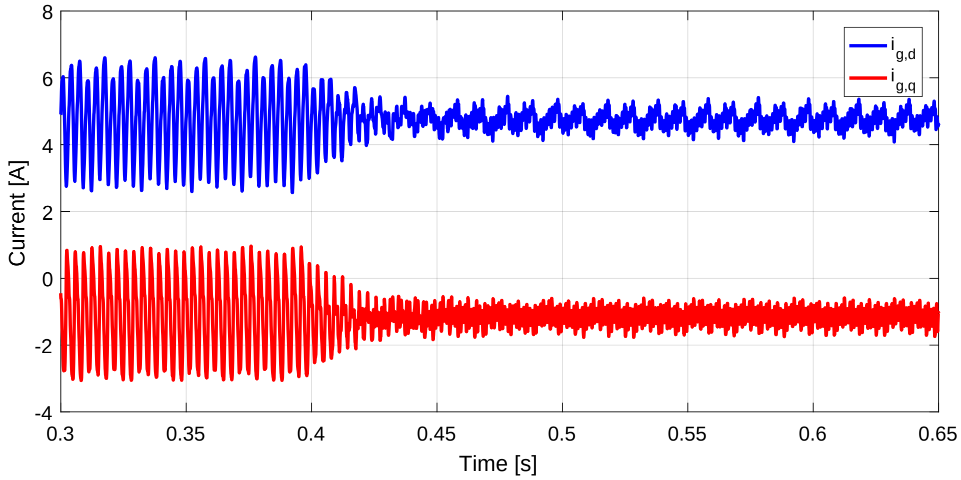

(a)

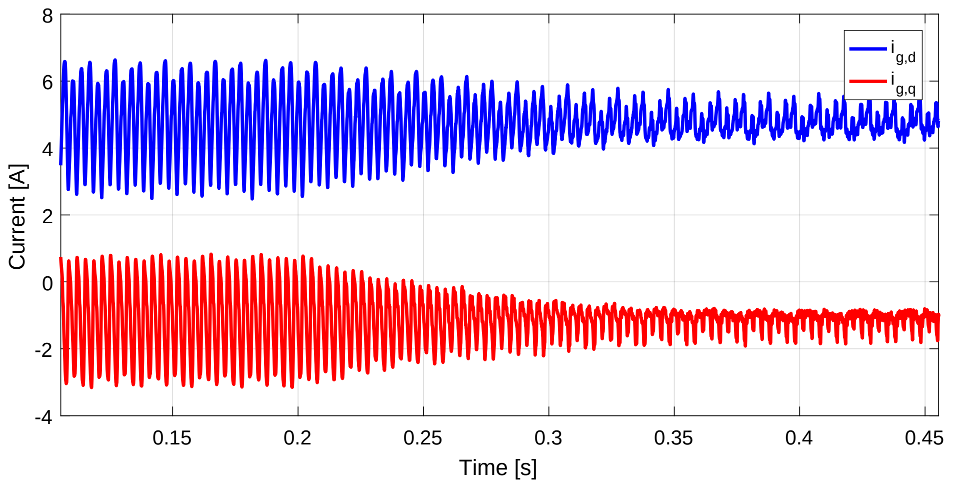

(b)

Figure 6.18. Measured transient behaviour of the grid dq current for a) PR controller b) repetitive controller.

As it can be seen the PR controller has a shorter settling time compared to the repetitive controller. The transient behaviour the APF currents (i_F) are also measured for the harmonic compensation step, this can be seen in Fig. 6.19(a) and 6.19(b).

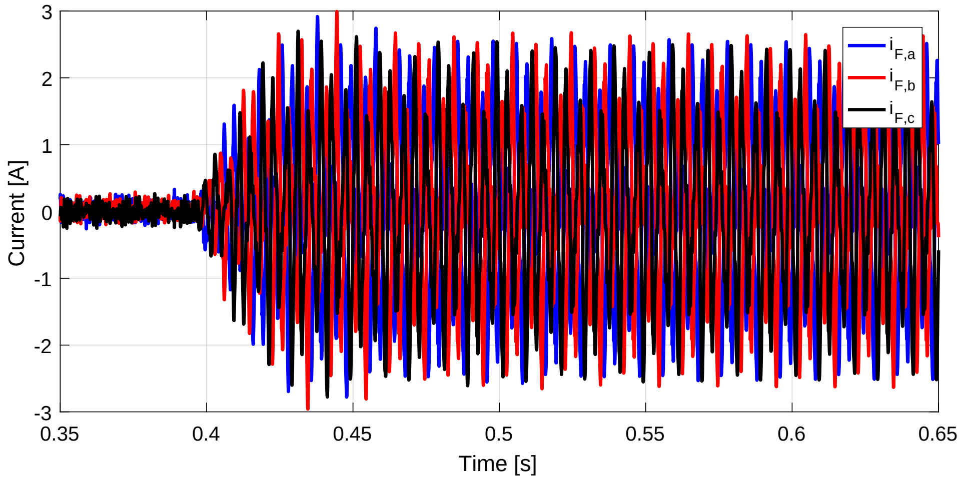

(a)

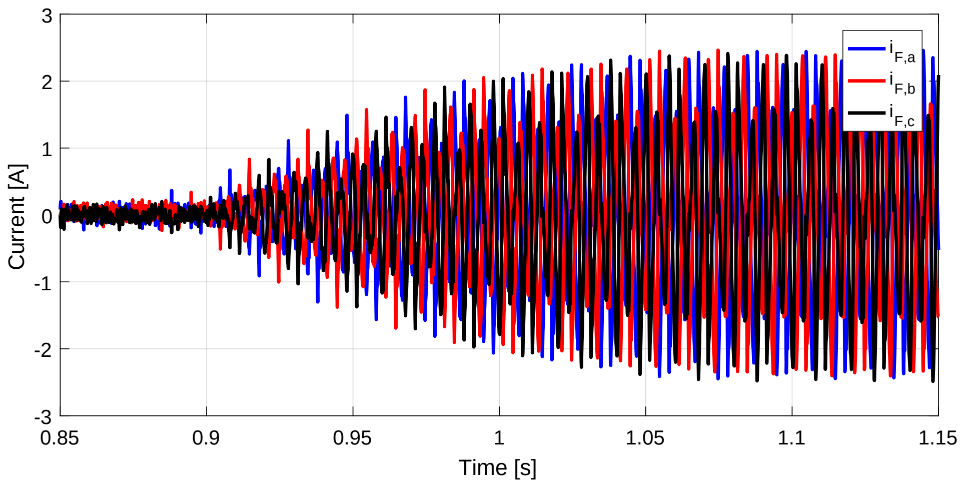

(b)

Figure 6.19. Measured transient behaviour of the APF current for a) PR controller b) repetitive controller.

As seen the PR controller induces an overshoot with lower settling time compared to the repetitive controller.

The last test to be conducted is a full test of the APF. In this test the APF compensates the harmonics using the repetitive controller due to the lower THD, and uses reactive power compensation to achieve a unity power factor. The result is shown in Fig. 6.20.

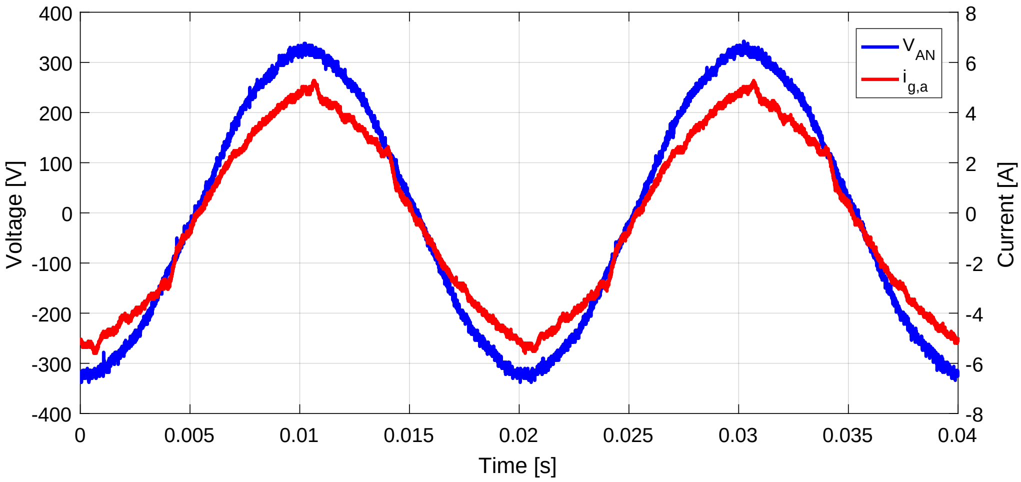

Figure 6.20. Measured grid voltage and current for harmonic and reactive power compensation.

As seen the harmonics are cancelled and the reactive power is compensated, achieving a power factor close to one. Comparing this to the waveform without the reactive compensation, the THD of the current is increased to 6.9%. With the APF connected, and by compensating both harmonics and reactive power, the apparent power at the grid decreases by 9.1 %.

To show that the controller is able to stay stable for different load levels. The ASD load is stepped from 114Ω to 85Ω, which increases the load current from 4.3 A RMS to 6.2 A RMS. The grid dq components can be seen in Fig. 6.21.

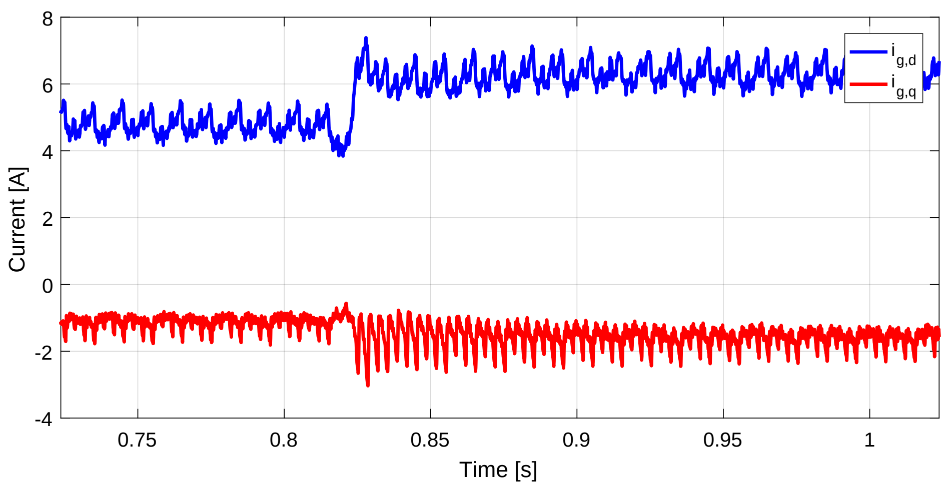

Figure 6.21. Measured dq grid current components when stepping the ASD load power level.

As seen the grid current dq components increases due to the higher ASD load power, and the harmonic current controller can handle changes in the load current, and reach steady state again.

6.5 DC-Link Control

In order to test the DC-link control of the APF, the DC voltage source, seen in Fig. 6.1, is removed. When the converter is connected to the grid, the DC voltage is equal to 540 V, which is the rectified voltage. As seen in Fig. 5.18 in Sec. 5.4, a step from 580 V to 660 V is made. The same step test is made in the laboratory, this can be seen in Fig. 6.22.

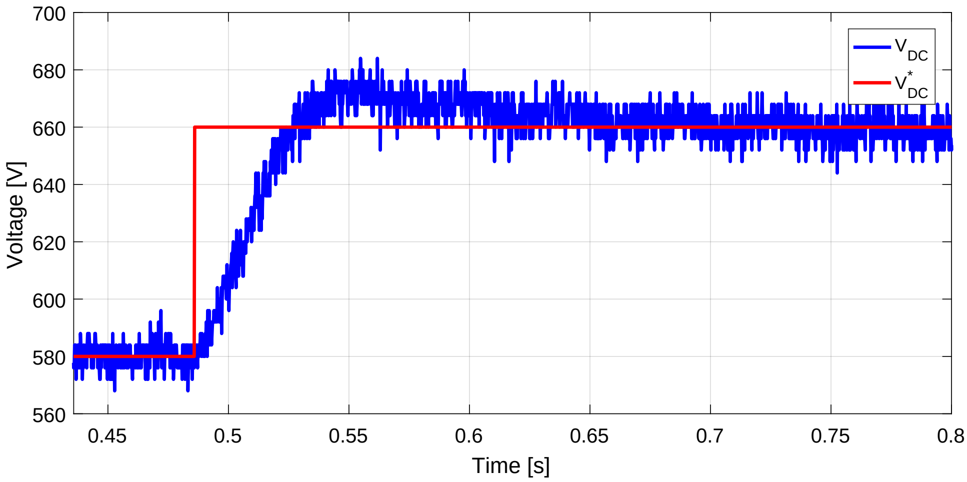

Figure 6.22. Measured DC-link voltage step response.

As it can be seen, the settling time of the DC controller is approximately 170 ms, with an overshoot of 15%. The difference between the measured and simulated step response might be caused by the Danfoss converter, since this converter has a DC current filter. The extra components, which are not simulated, might change the dynamic performance of the DC-link control loop.

The disturbance rejection capability of the DC link controller is tested by running the APF with no reactive power compensation, then enabling reactive power compensation to achieve a unity grid power factor, and then stepping the load power up as in the simulation. This can be seen in Fig. 6.23.

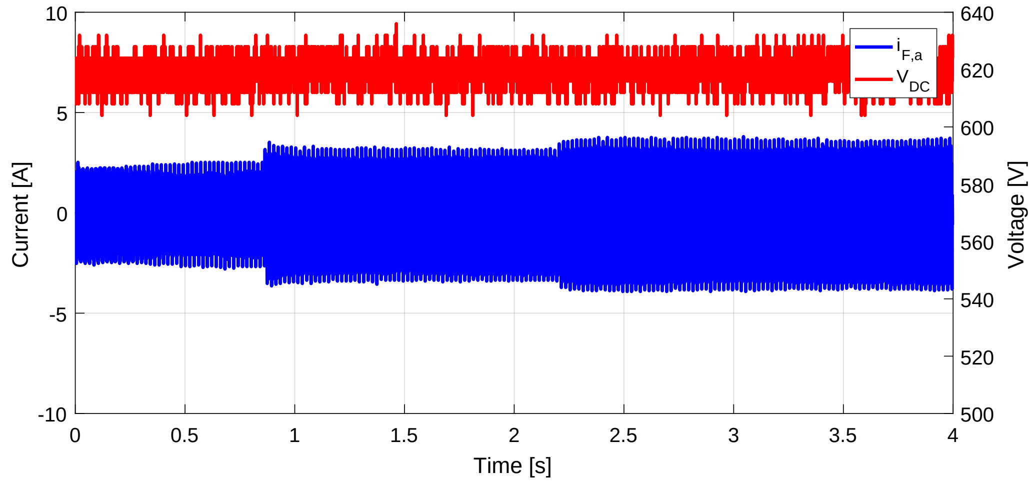

Figure 6.23. Measured DC-link voltage for disturbances of reactive power and load powers steps.

The first disturbance, is activation of reactive power compensation, this is the first increase in $i_{F,a}$, afterwards the load resistance is changed from 114Ω to 85Ω. The simulated disturbance rejection of the DC-link control, seen in Fig. 5.20, show the DC voltage to change slightly when a disturbance is applied, while the measured DC link voltage shows no significant changes/transients when a disturbance is applied.

Assessment of Installing an Active Power Filter 7

In this Chapter the results and findings of previous chapters will be discussed and assessed in terms of benefits, but also drawbacks of installing an APF in the Helius CHP. This will include benefits of installing an APF, a sizing guideline of the APF for the Helius CHP case, brief notes on significance of cost for different harmonic mitigation solutions, simulation of Helius CHP with APF, and controller choice and recommendation.

7.1 Benefits of Installing an APF

If the APF is installed as a centralised option, thus at PCC1 as shown in Fig. 7.1

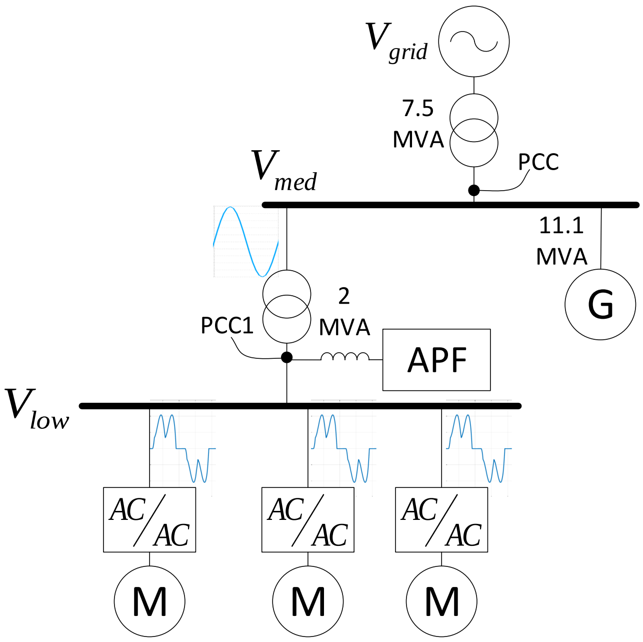

Figure 7.1. Simplified diagram of Helius CHP with centralised APF.

then the power savings will only affect the low to medium voltage transformer and everything connected at the own consumption side of the medium voltage level bus bar. Therefore the benefits of implementing a centralised APF solution are:

Lower Losses

When using harmonic mitigation the losses in the supply transformer, due to the harmonic currents, are reduced according to Eq. 3.3 in Sec 3.2. This saves active power corresponding to the reduced losses, which effectively reduces the operating cost. Furthermore, by installing an APF at PCC1 the lifetime of the transformer might increase due to less thermal stress, because of the lower transformer losses.

Optimized Dimensioning of Components

By using harmonic mitigation, reactive power compensation, or a combination of these two, the apparent power at PCC1 is reduced. In the design of the Helius CHP almost all components are largely over-dimensioned to handle peak load conditions. However, if the APF is considered in the design phase, it is possible to reduce sizing of components, due to the lower apparent power. This can therefore also save money when buying the lower rated components.

Centralised Solution

The APF can be installed as a centralised solution, which for AET is a benefit since many ASD loads are installed in the Helius CHP plant. This ensures less volume and size, compared to the decentralised solutions due to the large number of decentralised solutions needed. Furthermore, the APF can be installed even after the plant has been operating for some time quite easily, which is not the case for decentralised solutions. Another benefit of the APF as a centralised solution is that it is possible to disconnect the APF, and then keep the power plant running but at lower production.

Stringent Current THD Limits

In the Helius CHP the current THD limits from standards are not very stringent. For other countries however, there might be different more strict standards, therefore the standard 6 pulse rectifier solution might exceed the current THD limit, thus demand the use of harmonic mitigation solutions. Furthermore, trends show that the grid codes become more and more strict, like e.g. the wind turbine grid codes [32], [33].

7.2 Sizing and Price Implications

The sizing and price implications will be discussed based on an actual measurement of the Helius CHP on a normal day of operation. The measured data is shown in table 7.1.

Parameter	Value
S_{ASD}	1.174 MVA
P_{ASD}	1.088 MW
Q_{ASD}	0.442 MVAr
$\mathrm{THD_i}$	25.88%
$\mathrm{THD_v}$	4.3 %
PF	0.927

Table 7.1. Measured data from the Helius simulation.

The powers S_{ASD}, P_{ASD}, and Q_{ASD} are the combined powers at the low voltage side of the own consumption 11/0.4 kV transformer. The $\mathrm{THD_i}$, $\mathrm{THD_v}$, and PF are also measured at PCC1.

7.2.1 Sizing of APF

To evaluate the change of converter rating of the APF, for different levels of harmonic mitigation and reactive power compensation, an expression of the APF apparent power is derived. The power due to the harmonic mitigation is given by:

$$D_{APF} = S_{ASD} \cdot \mathrm{THD}_{ASD} \cdot k_c \tag{7.1}$$

$$k_c = 1 - \frac{\mathrm{THD}_{ref}}{\mathrm{THD}_{ASD}} \tag{7.2}$$

where S_{ASD} is the summation of all non linear load apparent powers, THD_{ASD} is the current THD of the combined load current, and THD_{ref} is the reference current THD of the grid. The variable k_c is used to set the amount of current THD to be mitigated by the APF, to reach a given grid THD_{ref}. The reactive power drawn to the APF, when using a PLL thus $V_q = 0$, is given by:

$$Q_{APF} = V_d \cdot i_{APF,q} \tag{7.3}$$

Where V_d is the d-axis voltage at the point of connection of the APF, and $i_{APF,q}$ is the q-axis current drawn to the APF. Alternatively the reactive power drawn to the APF to achieve a given power factor, PF_{ref}, on the grid side, can be expressed as:

$$Q_{APF} = Q_{ASD} - S_{ASD} \cdot sin(cos^{-1}(PF_{ref})) \tag{7.4}$$

When combining the harmonic mitigation and reactive power compensation, the rated power of the APF is given by:

$$S_{APF} = \sqrt{D_{APF}^2 + Q_{APF}^2} \tag{7.5}$$

The power rating of the APF for different power factors of the grid by using reactive power compensation, and for different harmonic mitigation levels thus different grid current THDs, using Eq. 7.5, is shown in Fig. 7.2.

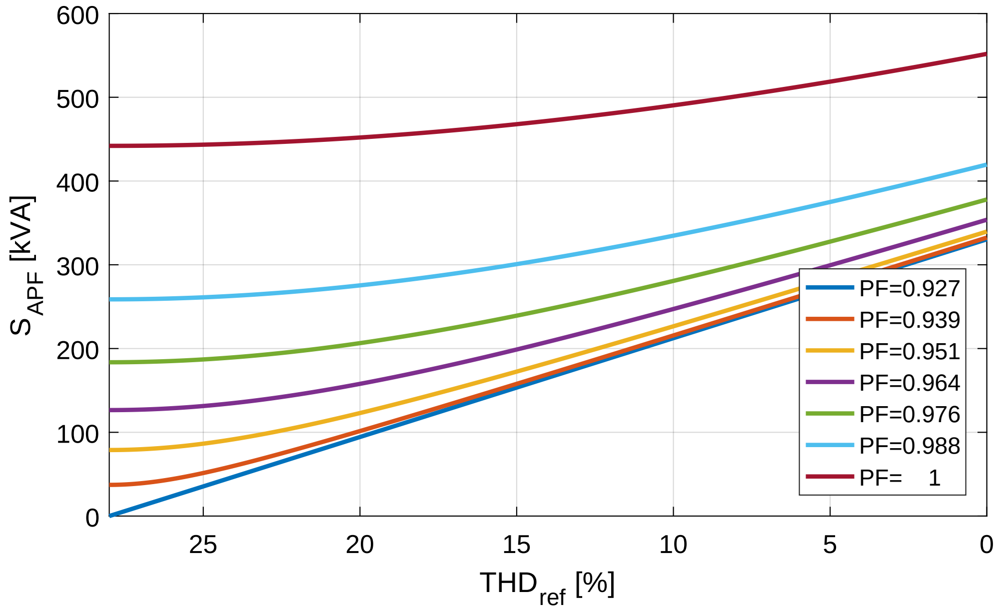

Figure 7.2. APF apparent power rating for different harmonic mitigation and reactive power levels.

A power factor of 0.927 corresponds to not using any reactive power compensation, thus the power rating of the APF has a linear relation with the desired grid THD, and is equal to zero when $\text{THD}_{ref} = \text{THD}_\text{i} = 25.88$ %. From the tendency of the curves it is seen that the power rating has a flat region until a certain THD_{ref} value, and afterwards has an approximately linear tendency with a decreasing THD_{ref}. By assuming the APF controller can remove all harmonic content and achieve a grid side unity power factor, the APF should be rated at $S_{APF} = 550$ kVA, thus approximately rated to half of the ASD load rating. A more realistically option could be to achieve a $\text{THD}_{ref} = 5$ % and a grid side power factor of $PF = 0.95$, in this case the rating of the APF is reduced to $S_{APF} = 290$ kVA, or 25 % of the ASD load rating. It should be noted that the rating is the theoretically minimum rating, since losses of the APF is not taken into account.

This analysis of the APF rating is based on measurements of a normal operation day in the Helius CHP, however this is normally at a $50-70$ % ASD load. If the production increases, thus the ASD load power increases, and the APF is designed for normal operation, then the power drawn to the APF might reach or exceed the rated power of the APF, thus might damage the APF converter. For an increased production the current in the converter will increase, and therefore increase thermal stress on the components. To avoid this situation a current limiter is necessary. The current reference of the APF consist of two contributions, one from the harmonic mitigation, and the reference from the reactive power compensation. The current drawn to the APF can be limited by knowing the maximum current of the APF. The maximum current, $i_{F,max}$, can be expressed as:

$$i_{F,max} \geq \sqrt{i_{F,d}^2 + i_{F,q}^2} \tag{7.6}$$

In the used current control strategy the fundamental PI controllers control the DC components, and the harmonic controllers control the AC components, and these two parts are added together. Therefore the d and q APF current components can be split into a DC and AC part:

$$i_{F,max} \geq \sqrt{\left(i_{F,d}^{DC} + i_{F,d}^{AC}\right)^2 + \left(i_{F,q}^{DC} + i_{F,q}^{AC}\right)^2} \tag{7.7}$$

where $i_{F,d}^{DC}$ is the part of the current from the DC capacitor voltage controller to keep the DC voltage constant, $i_{F,q}^{DC}$ is the part controlling the reactive power flow, and $i_{F,d}^{AC}$ and $i_{F,q}^{AC}$ is the part from the harmonic controllers. How the APF should react if it reaches the rated limit, should be determined primarily by the THD limits in the standard. Therefore after the harmonic mitigation ensures to reach the THD limit, the rest of the current available (if any) can be used to do reactive power compensation. In that case the reactive power compensation reference can be calculated by rearranging Eq. 7.7:

$$i_{F,q}^{DC} \leq \sqrt{i_{F,max}^2 - \left(i_{F,d}^{DC} + i_{F,d}^{AC}\right)^2} - i_{F,q}^{AC} \tag{7.8}$$

In the Helius CHP the current THD limits are not very strict thus this method can also be used to set the desired grid current THD limit, and then use the rest for reactive power compensation. How much reactive power compensation it is possible to achieve after the THD limit is fulfilled, depends on the rating of the APF converter. If the converter is sized for normal production and the transformer is sized according to this, then the transformer might be overloaded when the production is high if the APF reaches the current limit. So there is a trade-off between the APF performance in terms of harmonic compensation and reactive power compensation, and sizing of the APF, but also between sizing of the APF and sizing of the transformer.

7.2.2 General Cost Impact

To compare the cost of installing an active power filter compared to other harmonic mitigation solutions, a cost benefit analysis is shown in Fig. 7.3.

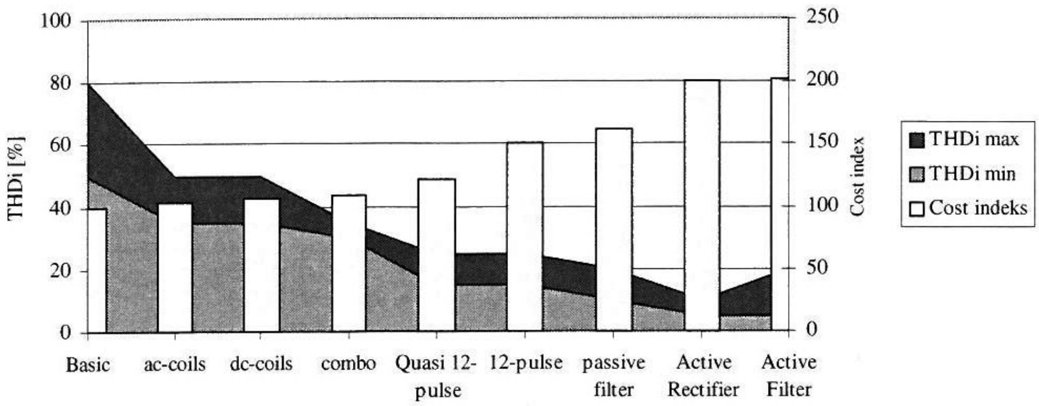

Figure 7.3. Comparison of harmonic mitigation solutions in terms of current THD and cost [11].

The cost benefit analysis in Fig. 7.3, from [11], is based on a market survey from the USA made by Danfoss Drives in 2005. The cost index ("indeks" in figure) is calculated based on the following factors:

- Cost of Device
- Protection, cables, transformers etc.
- Installation and Filters
- Pre-engineering
- Lifetime

The "Basic" mitigation solution in Fig. 7.3 refers to a 6 pulse diode rectifier without any DC or AC inductors, and the "Combo" solution refers to using both DC and AC inductors. The cost benefit analysis is based on a single ASD load, with a single harmonic mitigation solution.

As seen from Fig. 7.3 the lower the resultant current THD is, the higher the price of the solutions is. The APF ("active filter" in figure) is the most expensive solution, but at the same time can be the best in terms of harmonic mitigation performance.

7.3 Simulation of Helius CHP with APF

In this section an APF will be implemented in the Helius Plecs model presented in Sec. 3.4, with the designed component values from Sec. 5.1. The sampling and switching frequency will be the same as the laboratory setup thus 12 kHz. From Sec. 3.4 it was shown that the grid current THD without any APF was 25.88 %. When using the repetitive controller for the Helius CHP the lowest achievable grid current THD is 3.12 %, while it is 3.43 % when using the PR controller for this simulation. When the harmonic mitigation using the repetitive controller is turned on, when the plant is operating without any harmonic mitigation, the grid current response is shown in Fig. 7.4.

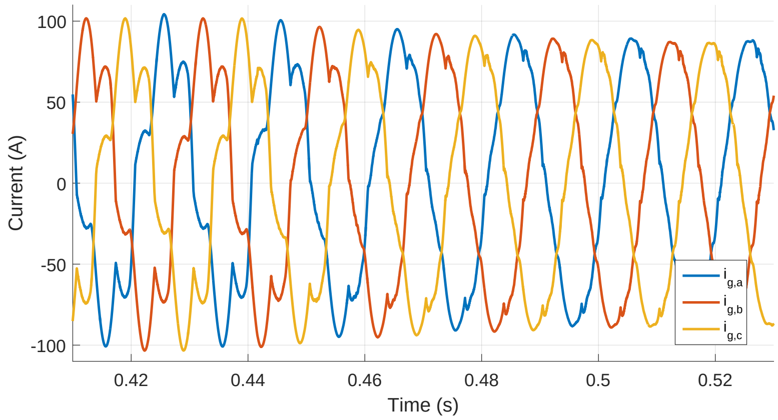

Figure 7.4. Grid current when turning the harmonic mitigation on while the plant is operating without any harmonic mitigation.

As seen there is no overshoot when switching the harmonic mitigation on, and it takes about 60 ms before it reaches steady state. When also enabling the reactive power compensation to achieve a unity grid power factor, the resulting grid current and grid voltage is shown in Fig. 7.5.

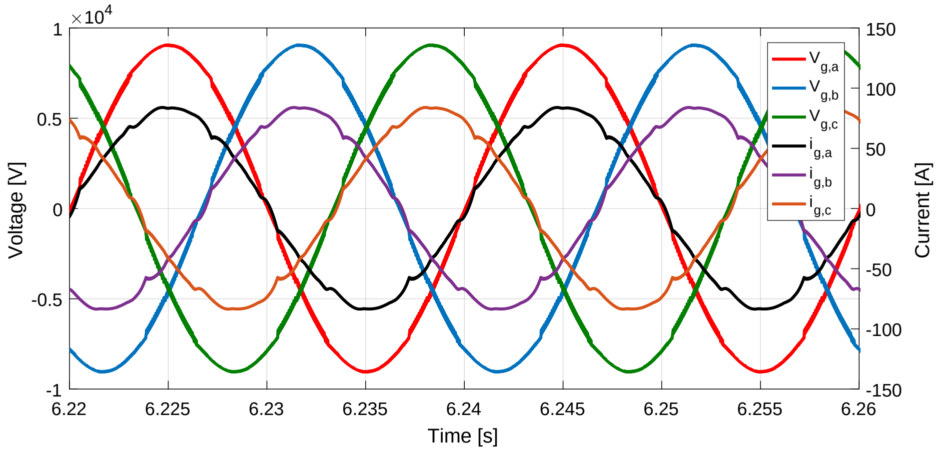

Figure 7.5. Grid current and voltage when using harmonic mitigation and reactive power compensation.

The APF current when the lowest achievable grid current THD is reached, and with a unity grid power factor is shown in Fig. 7.6.

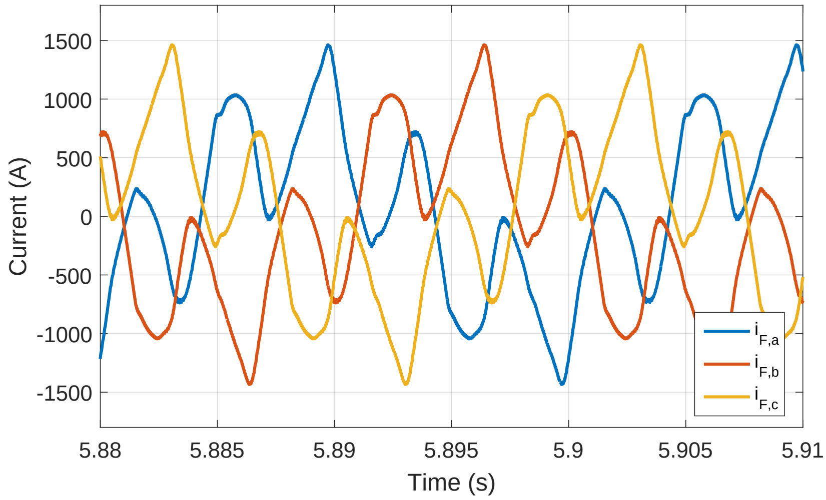

Figure 7.6. APF current for a unity grid power factor and a grid current THD of 3.12 %.

When achieving a unity power factor, and with the lowest achievable grid current THD of 3.12 % the apparent power drawn to the APF is equal to 496.3 kVA. According to Fig. 7.2 the APF minimum rating should be approximately 520 kVA, thus corresponds well to the sizing analysis. The grid apparent power reduction when using this APF size is simulated to be a 6 % reduction, to an apparent grid power of 1.092 MVA.

If the Helius plant is simulated to reach a grid power factor of 0.95 (calculated in simulation to be 0.952) and achieve a grid current THD of 5 % (measured in simulation to be 5.11 %), this results in an APF rating of minimum 287.3 kVA, which also corresponds well to the APF sizing analysis of Fig. 7.2, where the APF minimum rating should be 290 kVA for this operating point. In this case the the apparent grid power is 1.152 MVA thus a 1.88 % reduction.

Another pro when enabling harmonic mitigation, is that even though it is the current harmonics which are controlled to be mitigated, also the voltage THD on the high and low voltage side of the supply transformer reduces. The voltage THD reduces since a current with harmonic content passing through an impedance also induces some harmonics in the voltage. For this simulation case the voltage THD of the low voltage side of the transformer reduces from 6.23 % to 4.95 %, while the voltage THD of the high voltage side of the supply transformer reduces from 2.05 % to 1.69 %.

7.4 Comparison to Danfoss toolbox

To design and size industrial drives and APF solutions in terms of ratings and harmonic performance, Danfoss has made an estimation toolbox called "MCT 31". In the toolbox it is possible to input the parameters and values of the electrical system, which includes transformer, cables, frequency converter parameters including rated power level and normal loading level, direct coupled motor load, power factor correction capacitor, and shunt active power filter parameters. Since the converters used in the Helius CHP is Danfoss FC302 converters, it is directly possible to choose the exact converters used in the CHP in the toolbox. To get an estimation of the rating and harmonic performance when installing an APF in the Helius plant, the Helius CHP is modelled in the toolbox using the same loads and values of Sec. 3.4.

When all the loads, transformer and cables are modelled without adding any APF the output data/results of the toolbox is seen in Fig. 7.7.

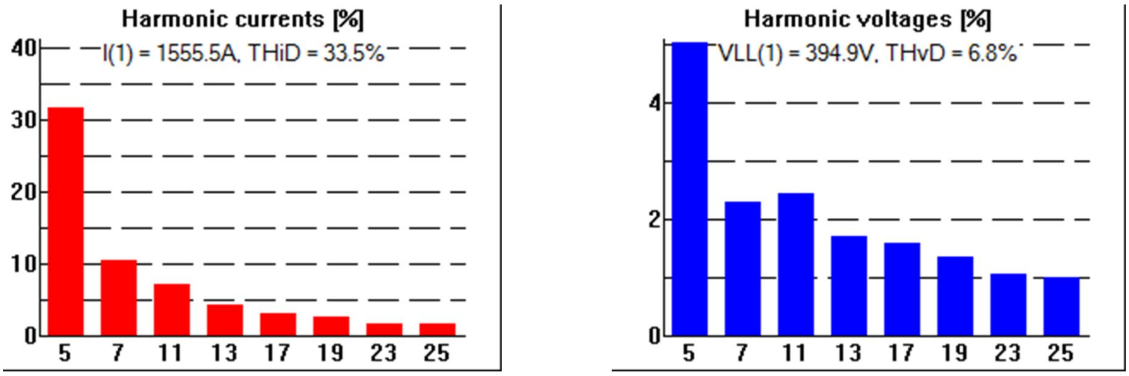

Figure 7.7. Results from Danfoss toolbox without any APF.

The current THD and voltage THD estimation from the toolbox is higher than the actual measurements of the Helius CHP, the current THD is 6 % higher and the voltage THD is 4 %. However, it should be noted that the toolbox results is measured on the low voltage side of the transformer, while the measured data from the actual Helius CHP is measured on the high voltage side. Therefore the current and voltage THD is expected to be lower on the high voltage side in the Danfoss toolbox, due to the transformer filtering effect, but it is not possible to measure at that point in the toolbox. The power factor from the toolbox is 0.93.

To compare to the sizing and simulation sections (Sec 7.2.1 and Sec 7.3), an APF with a desired current THD of 3.12 % and a unity power factor is added. The results of adding two Danfoss 400 A RMS (AAF 400 A T4) shunt active power filters is shown in Fig. 7.8.

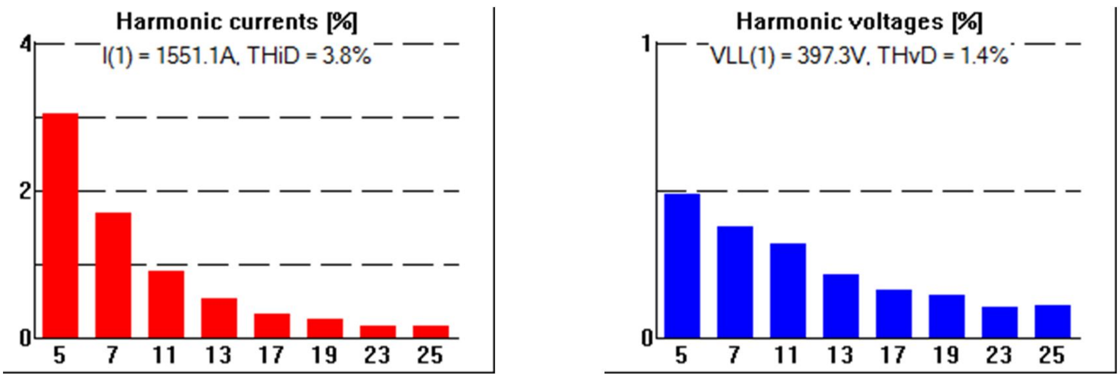

Figure 7.8. Results from Danfoss toolbox with an APF.

As seen not only is the current THD reduced, but the voltage THD is also reduced to

1.5 %. The power factor from the toolbox is 0.999. When using this APF settings, the minimum rating of the APF according to the toolbox is 476.8 kVA. This result corresponds well to the results of the sizing and simulation sections (Sec 7.2.1 and Sec 7.3). According to the Danfoss toolbox, the apparent power is reduced by 5.4 % for this case.

When the data of the electrical system is available, as in the case of the Helius CHP, the toolbox is very simple and fast to give an estimation of the harmonic performance, and estimate how much an APF of a given size can improve the current/voltage THD and power factor. Since the Danfoss toolbox is freely available, it can provide a fast overview when taking a decision about installing an APF for a power plant.

7.5 Controller Strategy Recommendation

To compare and choose the harmonic current control strategy most suitable to use in a large power plant like the Helius CHP, there are different factors which are important to assess. The factors for choosing a controller are listed and discussed below:

Harmonic Mitigation Performance

From the experimental work the repetitive controller was shown to have better harmonic performance compared to the PR controller. The PR controller however, had the best harmonic mitigation performance at the frequencies the PR controller was added for, except the 13^{th} harmonic. Therefore if a much higher sampling frequency was used, and not limited by the dSPACE system, it would be possible to include more harmonics in the PR controller, thus if the PR controller is better at most harmonics it might achieve the same performance or even better than the repetitive controller, since the amplitude of the very high order harmonics, when calculating the THD, can almost be neglected. The PR controller was shown to be faster for load changes, but also had a small overshoot when load changes occurred compared to the repetitive controller.

Design of Controller

The design of the repetitive controller is quite simple, since only care has to be taken when designing the low pass filter Q, and if any gain is added to enhance closed loop bandwidth. When designing the PR controller more care has to taken since it is possible to change the closed loop bandwidth, and it should be assured that non of the resonant frequencies affect each other.

Implementation

In the dSPACE system the repetitive controller is implemented on a transfer function form, since Simulink is used. In a system without dSPACE using only a micro controller, the repetitive controller needs a memory buffer to store the data of the time delay term $z^{-\frac{N}{6}}$ [34]. Compared to the implementation of the PR controller however, the repetitive controller is only a single controller, while the PR controller solution consists of a controller for each harmonic.

Flexibility

In terms of flexibility the PR controller is the best choice since the designer have full control of which frequencies that are desired to track, and it is even possible to include other harmonics than the $6k \cdot 50$Hz frequencies. The repetitive controller is limited to the $6k \cdot 50$Hz frequencies when designed for these frequencies, and the low pass filter Q has to be designed to reduce the tracking capability at frequencies not desired to track. Furthermore, the repetitive controller has the clear disadvantage for changes in grid frequency or for specific choices of sampling frequency, which is not an issue when using the PR controller.

When taking these consideration into account the PR controller would be the desired controller due to the higher flexibility, and for a high sampling frequency the performance of the PR controller should be similar to the repetitive controller.

Conclusion 8

This project has been done in collaboration with Aalborg Energie Technik A/S. As a case study the Helius CHP was chosen. The Helius CHP is a biomass-fired power plant, with an electrical self supply of 1.08 MVA. In the Helius CHP plant all the controlled electrical machines, that drives e.g. pumps and fans, are driven by 6 pulse rectifiers and inverters. Even though this solution is simple and cheap, it has the drawback that the current on the AC side of the diode rectifier is highly distorted. A highly distorted current induces extra losses in cables and in transformers, and might also affect the voltage THD when the distorted current passes an impedance. Due to these reasons AET wants to investigate the benefits of adding an active power filter. The active filter is a viable option for AET due to the following benefits: it can be installed as a centralised solution, reactive power compensation is an option, possibility of reducing rated power of supply transformer, and possibly save power from losses due to high current THD. Therefore the active power filter of the Helius CHP should be capable of achieving harmonic current mitigation and reactive power compensation.

To enable harmonic mitigation and reactive power compensation a control strategy involving a DC link voltage controller, a current controller consisting of 50 Hz fundamental PI controllers, and a harmonic current controller. In this project the PR and repetitive controller was analysed and compared, as the harmonic current controllers. Through simulations and experimental work all the controllers was shown to operate as desired, and according to simulations. It was proven through experimental work that the repetitive controller could achieve a lower grid current THD than the PR controller, for a sampling frequency of 12 kHz. Also, the apparent power at the grid was reduced by 9 %.

For future guidelines to AET when choosing whether or not to install an APF, an assessment of sizing and cost implications was performed. In terms of sizing, simple equations were derived to give a fast overview of the approximate minimum rating of the APF for a given current THD and power factor at PCC1. The equations was shown to be a good estimate when compared to PLECS simulations. Another tool to give an estimate of the minimum required APF rating, is the Danfoss Toolbox. The advantage of using the Danfoss Toolbox is the simple and fast overview/results of adding an APF. The toolbox was shown to corresponds well to both sizing equations and simulations in PLECS. Thus, the Danfoss Toolbox and sizing equations can be used to give a fast estimate of the required APF rating for a desired APF performance. In terms of cost the APF is the most expensive solution, when looking at the day one payment for the customer. However, the APF is also the solution that can save most active power from the THD losses, thus save most money per year from the saved power. Furthermore, if reactive power compensation is used it is possible to reduce the rated power of the supply transformer.

9 Discussion and Future Work

In this project the effect of background voltage distortion was not considered, since the background distortion of the Helius CHP was not available. In practice however this should be considered when designing the power plant since this limits how much more the voltage THD can be. Furthermore, this is also an important part of the PLL design since the PLL performance might be worse when the voltage is distorted as discussed in [20]. For this case different filters can be used to improve the PLL performance, and can even extend the operation points of the PLL to include operation during grid faults.

The conventional plug-in repetitive controller presented and used in this project have disadvantages when $\frac{N}{6}$ is not an integer, thus for certain sampling frequencies or grid frequencies. This problem can however be solved by using frequency adaptive solutions as reported in [35] and [36], but at the cost of worse harmonic mitigation performance when $\frac{N}{6}$ is not an integer. Furthermore, a combination of the repetitive controller and PR controller was used in [36] which allowed for selective harmonic compensation, which gives the repetitive controller more flexibility. The cost of this however, is a more complex control strategy, controller design, and implementation. This could be studied as future work to enhance the performance of the repetitive controller and PR controller.

The assessment of installing an APF in the Helius CHP is performed without considering and modelling the losses in the APF and in the supply transformer. Therefore to give a more precise estimation of the power saved from losses, loss modelling could be investigated. This would also give the option of estimating the money saved per year from reducing the current THD losses, or if the APF losses introduced actually increases losses thus increases price per year instead of saving money. Therefore give an economical estimation of how beneficial the APF is.

Bibliography

[1] Ren21, *RENEWABLES 2016 GLOBAL STATUS REPORT*, Ren21, Ed. Ren21, 2016. [Online]. Available: http://www.ren21.net/status-of-renewables/global-status-report/

[2] Aalborg Energie Technik, "Official aet rothes corde ltd reference." [Online]. Available: http://www.aet-biomass.com/en-GB/Home/References/Biomass-Fired-Plants/Rothes-CoRDe.aspx

[3] K. Scott, "Scotland toasts new whiskey powered bioenergy plant," *The Guardian*, 2011. [Online]. Available: https://www.theguardian.com/environment/2011/may/04/whisky-energy-biomass-scotland-speyside

[4] R. Erickson and D. Maksimovic, *Fundamentals of Power Electronics*, 2nd ed., K. A. Publishers, Ed. Kluwer Acedemic Publishers, 2004.

[5] M. Sørensen, "Interview with Morten Sørensen from Aalborg Energie Technike," Personal Communication, 2016.

[6] H. Akagi, E. H. Watanabe, and M. Aredes, *Instantaneous Power Theory and Applications to Power Conditioning.* Wiley, 2007.

[7] L. Asiminoaei, "Estimation and reduction of currents from power converters," Ph.D. dissertation, Aalborg University, 2006.

[8] J. C. Moreira and T. A. Lipo, "Modelling of saturated ac machines including air gap flux harmonic components," in *Conference Record of the 1990 IEEE Industry Applications Society Annual Meeting*, Oct 1990, pp. 37–44 vol.1.

[9] L. Asiminoaei, F. Blaabjerg, S. Hansen, and P. Thøgersen, "Adaptive compensation of reactive power with shunt active power filters," *IEEE Transactions on Industry Applications*, vol. 44, no. 3, 2008.

[10] *Engineering Recommendation G5/4-1 - Planning Levels For Harmonic Voltage Distortion And The Connection Of Non-linear Loads To Transmission Systems And Public Electricity Supply Systems In The United Kingdom*, Engineering Directorate of the Energy Networks Association Std.

[11] S. Hansen, "Harmonic distortion of rectifier topologies for adjustable speed drives," Ph.D. dissertation, Aalborg University, 2001.

[12] J. S. Subjak and J. S. McQuilkin, "Harmonics-causes, effects, measurements and analysis-update," in *Conference Record. Industrial and Commercial Power Systems Technical Conference*, 1989.

[13] H. Akagi, “Active harmonic filters,” *Proceedings of the IEEE*, vol. 93, no. 12, pp. 2128–2141, Dec 2005.

[14] G. Wakileh, *Power Systems Harmonics: Fundamentals, Analysis and Filter Design*, ser. Engineering online library. Springer, 2001. [Online]. Available: https://books.google.dk/books?id=9lTMmjppOGwC

[15] G. M. Carvajal, G. O. Plata, W. G. Picon, and J. C. C. Velasco, “Investigation of phase shifting transformers in distribution systems for harmonics mitigation,” in *2014 Clemson University Power Systems Conference*, March 2014, pp. 1–5.

[16] J. G. Boudrias, “Harmonic mitigation, power factor correction and energy saving with proper transformer and phase shifting techniques,” in *Canadian Conference on Electrical and Computer Engineering 2004 (IEEE Cat. No.04CH37513)*, vol. 1, May 2004, pp. 133–136 Vol.1.

[17] *Harmonics Mitigation - Requirements and Danfoss Drives' Solutions*, Danfoss.

[18] L. Bede, “Advanced and robust control of grid connected converters,” Ph.D. dissertation, Aalborg University, 2016.

[19] F. Zare, H. Soltani, D. Kumar, P. Davari, H. Delpino, and F. Blaabjerg, “Harmonic emissions of three-phase diode rectifiers in distribution networks,” *IEEE Access*, vol. PP, no. 99, pp. 1–1, 2017.

[20] R. Teodorescu, M. Liserre, and P. Rodriguez, *Grid Converters for Photovoltaic and Wind Power Systems*, J. W. . S. Inc, Ed. John Wiley & Sons Inc, 2011.

[21] S. Corsi, *Voltage Control and Protection in Electrical Power Systems*. Springer, 2015.

[22] M. Liserre, A. Dell'Aquila, and F. Blaabjerg, “Design and control of a three-phase active rectifier under non-ideal operating conditions,” in *Conference Record of the 2002 IEEE Industry Applications Conference. 37th IAS Annual Meeting (Cat. No.02CH37344)*, vol. 2, Oct 2002, pp. 1181–1188 vol.2.

[23] R. Costa-Castello, J. Nebot, and R. Grino, “Demonstration of the internal model principle by digital repetitive control of an educational laboratory plant,” *IEEE Transactions on Education*, vol. 48, no. 1, pp. 73–80, Feb 2005.

[24] G. A. Ramos, J. M. Olm, and R. Costa-Castello, *Digital Repetitive Control under Varying Frequency Conditions*. Springer, 2013.

[25] Z. Zeng, J.-Q. Yang, S.-L. Chen, and J. Huang, “Fast-transient repetitive control strategy for a three-phase lcl filter-based shunt active power filter,” *Journal of Power Electronics, Vol 14, No. 2, pp. 392-401*, 2014.

[26] L. Lanfang, M. Hui, X. Xiaogang, C. Xiaoke, S. Biaoguang, and X. Yunxiang, “Repetitive control implementation with frequency adaptive algorithm for shunt active power filter,” in *2016 IEEE 8th International Power Electronics and Motion Control Conference (IPEMC-ECCE Asia)*, May 2016, pp. 1328–1332.

[27] L. Asimmoaei, E. Aeloiza, J. H. Kim, P. Enjeti, F. Blaabjerg, L. T. Moran, and S. K. Sul, "An interleaved active power filter with reduced size of passive components," in *Twenty-First Annual IEEE Applied Power Electronics Conference and Exposition, 2006. APEC '06.*, March 2006, pp. 8 pp.–.

[28] C. L. Phillips and J. M. Parr, *Feedback Control Systems.* Pearson, 2011.

[29] K. Sharifabadi, L. Harnefors, H. Nee, R. Teodorescu, and S. Norrga, *Design, Control and Application of Modular Multilevel Converters for HVDC Transmission Systems*, ser. Wiley - IEEE. Wiley, 2016. [Online]. Available: https://books.google.dk/books?id=d57LDAAAQBAJ

[30] M. Liserre, F. Blaabjerg, and S. Hansen, "Design and control of an lcl-filter-based three-phase active rectifier," *IEEE Transactions on Industry Applications , VOL. 41*, 2005.

[31] M. Liserre, F. Blaabjerg, and S. Hansen, "Design and control of an lcl-filter-based three-phase active rectifier," *IEEE Transactions on Industry Applications*, vol. 41, no. 5, pp. 1281–1291, Sept 2005.

[32] M. Tsili and S. Papathanassiou, "A review of grid code technical requirements for wind farms," *IET Renewable Power Generation*, vol. 3, no. 3, pp. 308–332, Sept 2009.

[33] K. Ma, *Power Electronics for Next Generation Wind Turbine System.* Springer, 2015.

[34] G. Escobar, M. Hernandez-Gomez, A. A. Valdez-Fernandez, M. J. Lopez-Sanchez, and G. A. Catzin-Contreras, "Implementation of a $6n \pm 1$ repetitive controller subject to fractional delays," *IEEE Transactions on Industrial Electronics*, vol. 62, no. 1, pp. 444–452, Jan 2015.

[35] Y. Yang, K. Zhou, and F. Blaabjerg, "Enhancing the frequency adaptability of periodic current controllers with a fixed sampling rate for grid-connected power converters," *IEEE Transactions on Power Electronics*, vol. 31, no. 10, pp. 7273–7285, Oct 2016.

[36] Y. Yang, K. Zhou, H. Wang, F. Blaabjerg, D. Wang, and B. Zhang, "Frequency adaptive selective harmonic control for grid-connected inverters," *IEEE Transactions on Power Electronics*, vol. 30, no. 7, pp. 3912–3924, July 2015.

[37] Nexans, *FXQJ EMC 1 kV 3X95/50 Cable datasheet.* [Online]. Available: https://www.nexans.dk/eservice/Denmark-da_DK/pdf-product_540326434/FXQJ_EMC_1_kV_3X95_50.pdf

[38] Nexans, *FXQJ EMC 1 kV 3X120/70 Cable datasheet.* [Online]. Available: https://www.nexans.dk/eservice/Denmark-da_DK/pdf-product_540326443/FXQJ_EMC_1_kV_3X120_70.pdf

[39] Nexans, *FXQJ EMC 1 kV 3X150/70 Cable datasheet.* [Online]. Available: https://www.nexans.dk/eservice/Denmark-da_DK/pdf-product_540326444/FXQJ_EMC_1_kV_3X150_70.pdf

[40] Nexans, *FXQJ EMC 1 kV 3X185/95 Cable datasheet*. [Online]. Available: https://www.nexans.dk/eservice/Denmark-da_DK/pdf-product_540326446/FXQJ_EMC_1_kV_3x185_95.pdf

Appendix A

A.1 Cable Data

The Cable data has been provided by Morten Sørensen from Aalborg Energie Technik's database and can be seen below:

Name	Resistance	Inductance	Length
3x95/50 [37]	$0.193\,\Omega/\mathrm{km}$	$0.17\,\mathrm{mH}/\mathrm{km}$	15 m
3x120/70 [38]	$0.153\,\Omega/\mathrm{km}$	$0.15\,\mathrm{mH}/\mathrm{km}$	15 m
3x150/70 [39]	$0.124\,\Omega/\mathrm{km}$	$0.17\,\mathrm{mH}/\mathrm{km}$	15 m
3x185/95 [40]	$0.0991\,\Omega/\mathrm{km}$	$0.14\,\mathrm{mH}/\mathrm{km}$	15 m
KTC3200 [5]	0.025Ω	$0.6\mu\mathrm{H}$	

These cables connect the adjustable speed drives to the low voltage bus bar, the different cables are used for different power ratings. The cable configurations can be seen below:

Power Rating	Cable configuration
315 kW	$2 \cdot 3x150/70$
250 kW	$2 \cdot 3x120/70$
160 kW	$1 \cdot 3x185/70$
110 kW	$1 \cdot 3x95/50$

A.2 Design of LCL filter

In this appendix the LCL filter used in the laboratory setup will be designed. The LCL configuration is shown in Fig. A.1.

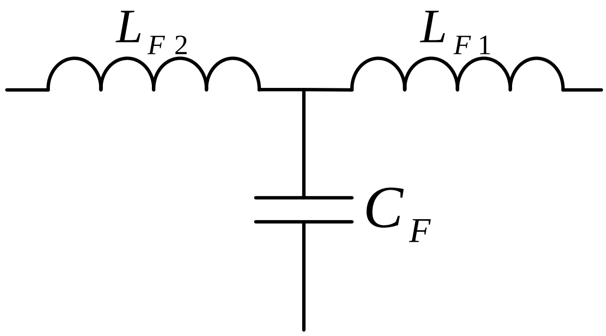

Figure A.1. LCL filter for a single phase.

The LCL filter consist of two inductors, L_{F1} which is the converter side inductor, and L_{F2} which is the grid side inductor or the inductor closest to the PCC. To design the LCL filter for the laboratory setup the parameters of table A.1 is used.

Parameter	Value
Filter power - S_b	1.39 kW
Line voltage - V_{LL}	400 V
DC voltage - V_{DC}	620 V
Grid frequency - f_g	50 Hz
Grid velocity - ω_g	314 $\frac{\text{rad}}{\text{s}}$
Filter current - i_F	4.24 A
Maximum current ripple - Δi_F	1.5 A
Switching number - n	12
Switching Frequency - f_s	12 kHz

Table A.1. Relevant parameters to the design of the LCL filter.

The LCL filter is designed based on the approach suggested in [30] and [20]. The first step is to design the converter side inductor L_{F1}. The converter side inductor is chosen based on the maximum allowed current ripple. The inductance can be calculated from:

$$L_{F1} = \frac{V_{DC}}{n \cdot f_s \cdot \Delta i_F} \tag{A.1}$$

Where V_{DC} is the DC voltage, n is the switching number set by [20], f_s is the switching frequency, and Δi_F is the maximum allowed ripple in the filter current. The maximum allowed current ripple is set to 20 %, which gives a converter side inductance of $L_{F1} = 10.7$ mH.

Since the LCL filter consists of a capacitor, the capacitance cannot be too large, since this can cause a large reactive power flow to the capacitor, which might cause a poor power factor. Therefore the reactive power of the capacitor should be limited. In [30] it is suggested to limit the reactive power to 5 % of the rated power of the converter. The capacitance can be calculated from by:

$$X_c = \frac{V_c^2}{Q_c} \tag{A.2}$$

Where Q_c is the maximum allowed reactive power consumed by the filter capacitor, V_c is the voltage across the LCL filter capacitor, and X_c is the capacitor reactance. In the design V_c can be approximated by the voltage at the PCC, if the voltage across the grid side inductor L_{F2} is neglected. By using this approximation and by limiting the reactive power the capacitance can be estimated by:

$$\frac{1}{C_F \cdot \omega_g} = \frac{V_{PCC}^2}{0.05 \cdot S_{APF}} \tag{A.3}$$

Using this gives a capacitance of $C_F = 1.38\ \mu$F.

The grid side inductor L_{F2} can be chosen based on frequency limits of the resonant frequency. The resonant frequency of the LCL filter is given by:

$$f_{res} = \frac{\sqrt{\frac{L_{F1}+L_{F2}}{L_{F1} \cdot C_F \cdot L_{F2}}}}{2\pi} \tag{A.4}$$

Care should be taking when placing the resonant frequency. The resonant frequency should not be close to the frequency of the grid, but also far from the switching frequency, to not amplify any of these frequencies. Furthermore, the resonant frequency should not interfere with any of the harmonics desired to mitigate in the APF. Therefore to ensure this does not happen the resonant frequency should be chosen based on the limits:

$$h \cdot f_g < f_{res} < \frac{f_s}{2} \tag{A.5}$$

Where h is the highest harmonic order which is compensated in the APF [31]. In the control of the APF the highest order harmonic desired to compensate is 19^{th}. Choosing a resonant frequency at the 39^{th} harmonic, thus 1950 Hz, is between two $6k \cdot 50$ Hz frequencies, and is within the limit defined in Eq. A.4, equals a grid side inductance of $L_{F2} = 10.7$ mH. When using this design approach the frequency response of the LCL filter is shown in Fig.

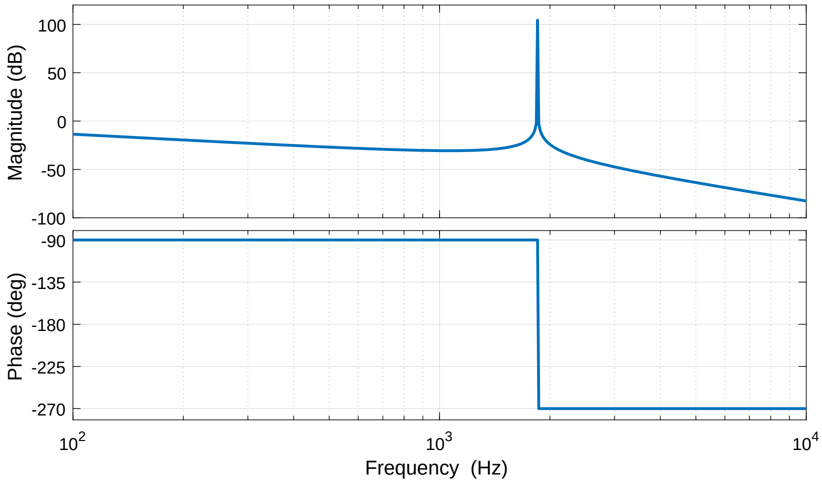

Figure A.2. Frequency response of LCL designed LCL filter.

In the laboratory however the available inductors and capacitor are $L_{F1} = 4.6$ mH, $L_{F2} = 6.4$ mH, and $C_F = 4.7\mu$F. The resonant frequency using these values is equal to 1419 Hz, which complies with the frequency limits.

Although the resonant frequency is placed far from any dominant frequencies in the system, it can still have an influence on stability. If a resistor is added in series with the LCL capacitor it is possible to dampen the resonance magnitude. A series resistor is however not added in the laboratory setup.